

# We are IntechOpen, the world's leading publisher of Open Access books Built by scientists, for scientists

6,300

Open access books available

171,000

International authors and editors

190M

Downloads

Our authors are among the

154

Countries delivered to

TOP 1%

most cited scientists

12.2%

Contributors from top 500 universities



WEB OF SCIENCE™

Selection of our books indexed in the Book Citation Index  
in Web of Science™ Core Collection (BKCI)

Interested in publishing with us?  
Contact [book.department@intechopen.com](mailto:book.department@intechopen.com)

Numbers displayed above are based on latest data collected.  
For more information visit [www.intechopen.com](http://www.intechopen.com)



# Introductory Chapter: Cement Industry

*Abeer M. El-Sayed, Abeer A. Faheim, Aida A. Salman  
and Hosam M. Saleh*

Cement is a capital-intensive, energy-consuming and critical sector for the construction of nation-wide infrastructure. The international cement industry, while constituting a limited share of the world's output has been rising at an increasing pace compared to the local demand in recent years. Attempts to protect the environment in developing countries, particularly Europe have forced cement manufacturing plants to migrate to countries with less strict environmental regulations. Along with consistently rising real prices, this has provided a trend for economic performance and environmental enforcement [1].

It is worth noting that cement is known to be one of the most important construction materials in the world. It is primarily used in the manufacture of concrete. Concrete is a combination of inert mineral aggregates such as sand, gravel, crushed stones and cement. Consumption and production of cement are directly connected to the building sector and thus to the general economic activity. Cement is one of the most developed goods in the world, due to its importance as a building material and the geographical availability of the main raw materials, i.e. limestone, cement is manufactured in almost all countries. The widespread development is also due to the comparatively low price and high density of cement, which, due to the relatively high costs, decreases ground transport. Export trade (excluding border-based plants) is typically limited relative to global production.

Cement-based materials, such as concrete and mortars, are used in very significant amounts. For example, concrete production amounted to more than 10 billion tonnes in 2009. Cement plays an important role in terms of economic and social importance as it is necessary to develop and enhance infrastructure. This sector, on the other hand, is also a strong polluter. Cement processing emits 5–6% of the carbon dioxide emitted by human activity, accounting for around 4% of global warming. It may emit vast quantities of chronic chemical contaminants, such as dioxins and heavy metals and particulate matter. Energy use is also important. Cement production accounts for about 0.6% of all electricity generated in the United States. In the other hand, the chemistry driving the manufacture of cement and its applications can be very beneficial in solving these environmental concerns.

Cement manufacturing is an extremely energy-intensive method of processing. The energy consumption is measured at around 2% of global primary energy consumption, or approximately 5% of total manufacturing energy consumption [2], regarding to the prevalent use of carbon-intensive fuels, e.g. coal, in the manufacture of clinkers. In addition to energy consumption, the clinker process also releases CO<sub>2</sub> as a result of the calcination process. Ecofys Energy and Climate and Berkeley National Laboratory therefore carried out an appraisal for the IEA Greenhouse Gas R&D Program on the role of the cement industry in the development of CO<sub>2</sub> and the options for lowering carbon dioxide emissions. This discuss the historical development and global distribution of cement production [3].

Moreover, the cement industry needs raw materials, fuel and chemical additives, and these activities generate emissions which have a negative effect on the quality of the atmosphere. The gas emissions emitted are CO<sub>2</sub>, CH<sub>4</sub>, NO<sub>x</sub>, SO<sub>x</sub>, N<sub>2</sub>O and particulate matter.

These emissions have an effect on the rise in global warming and the decrease in atmospheric air quality, which has an impact on human health and the atmosphere [4].

However, cement is the second primary source of anthropogenic pollution, source for about 7% of global CO<sub>2</sub> emissions. The technology for carbon dioxide capture and storage (CCS) is considered by the International Energy Agency (IEA) to be a crucial technology capable of lowering CO<sub>2</sub> emissions in the cement sector by 56% by 2050. CO<sub>2</sub> capture technologies for the cement production process and analyses economic and financial problems relevant to carbon dioxide capture in the cement production has an important trend for study [5].

The overall CO<sub>2</sub> emissions from cement manufacturing, including process and energy-related emissions has a significant interest. Actually, much of the relevant evidence only covers process pollution. CO<sub>2</sub> pollution control solutions for the cement industry are also discussed. In 1994, the projected gross carbon emissions from cement manufacturing is 307 million metric tonnes of carbon (MtC), 160 MtC from process carbon emissions and 147 MtC from electricity usage. Overall, the top 10 cement-producing countries accounted for 63% of the total carbon emissions from cement manufacturing in 1994. The estimated strength of carbon dioxide emissions from global cement output is 222 kg of C/t of cement. Emissions reduction solutions include enhancing energy quality, new methods, transitioning to low-carbon oil, using waste oils, the use of additives in cement processing, and gradually eliminating substitute cements and CO<sub>2</sub> from flue gas in clinker kilns [6].

Contamination of the atmosphere in the area of cement factories, e.g. some cement emissions around it, it may be claimed that CaO percentages were found to be higher (37.7%) particularly in surface soil samples taken near the cement factory. Based on the geo-accumulation index, soils in the study area could be graded as moderately to highly contaminate with (As, Cd, Pb and Ni) and highly contaminated with Cr, whereas soils in the study region were moderately polluted with Zn. On the other hand, the soils of the sample region are considerably polluted with As, Cd and Cu ( $5 > EF > 20$ ) on the basis of the Enrichment Factor (EF). The most hazardous areas are clustered within 0 to 2 km of the cement plant [7].

As the health history of factory employees and certain inhabitants of nearby areas indicates a high incidence of respiratory and skin infections. Regulation of the regulations on pollution enforcement and the establishment of a buffer zone around the cement factory can protect the atmosphere and public health [8].

Egypt increased cement production from 4 million tonnes in 1975 to 46 million tonnes in 2009 and now accounts for about 1.5 percent of global cement supply. Dust emissions account for around 6% of PM<sub>10</sub> in Greater Cairo, hitting as much as 30% in areas near cement plants. New regulatory requirements, due to be approved in 2010, would-the emissions of dust from 300 to 100 mg/m<sup>3</sup> for existing plants and from 100 to 50 mg/m<sup>3</sup> for new plants. Online tracking of the 72 main stacks in the 16 cement plants by the Egyptian Environmental Affairs Agency (EEAA) offers real-time details on the emissions of carbon. New plants are 98% compliant and older plants are 92% compliant with pollution standards. No manual monitoring of SO<sub>x</sub> and NO<sub>x</sub> pollution is performed. Cleaner development and pollution control prospects for the cement sector include: i) the use of alternative fuels in cement kilns; ii) the reduction of NO<sub>x</sub>; iii) the removal of dust emissions; iv) the use of silica waste to manufacture new cement products; v) the reuse of bypass dust; and vi) the disposal of radioactive waste [9].

As far as processing is concerned, there are many alternate products that can be used to mitigate carbon dioxide emissions and limit energy consumption, such as calcium sulfoaluminate and b-Ca<sub>2</sub>SiO<sub>4</sub>-rich cements. The use of residues from other manufacturing industries will also increase the sustainability of the cement industry. Under suitable conditions, waste materials such as tires, fuels, urban solid waste and solvents can be used as additional fuel in cement plants. Concrete can be used to encapsulate discarded products such as rubber, plastics and glasses. In this manner, certain aspects of the cement industry related to environmental science are explored. Other problems, such as economic considerations, the chemistry of cement manufacturing and its properties, are also addressed. Special attention is paid to the role that cement chemistry can play in terms of sustainability. The most important elements, such as the use of substitute products, are outlined; fresh opportunities as well as the recycling of products. It is also argued that the role of research and development required to boost the sustainability of cement is a significant feature [10].

### **Author details**

Abeer M. El-Sayed<sup>1</sup>, Abeer A. Faheim<sup>1</sup>, Aida A. Salman<sup>1</sup> and Hosam M. Saleh<sup>2\*</sup>

<sup>1</sup> Chemistry Department, Faculty of Science, Al Azhar University, Egypt

<sup>2</sup> Radioisotope Department, Nuclear Research Center, Atomic Energy Authority, Giza, Egypt

\*Address all correspondence to: [hosam.saleh@eaea.org.eg](mailto:hosam.saleh@eaea.org.eg);  
[hosamsaleh70@yahoo.com](mailto:hosamsaleh70@yahoo.com)

### **IntechOpen**

© 2020 The Author(s). Licensee IntechOpen. This chapter is distributed under the terms of the Creative Commons Attribution License (<http://creativecommons.org/licenses/by/3.0>), which permits unrestricted use, distribution, and reproduction in any medium, provided the original work is properly cited. 

## References

- [1] T. Selim and A. Salem, "Global cement industry: Competitive and institutional dimensions," 2010.
- [2] N. Martin, M. D. Levine, L. Price, and E. Worrell, "Efficient use of energy utilizing high technology: An assessment of energy use in industry and buildings," *London World Energy Council*, 1995.
- [3] C. A. Hendriks, E. Worrell, D. De Jager, K. Blok, and P. Riemer, "Emission reduction of greenhouse gases from the cement industry," in *Proceedings of the fourth international conference on greenhouse gas control technologies*, 1998, pp. 939-944.
- [4] C. Chen, G. Habert, Y. Bouzidi, and A. Jullien, "Environmental impact of cement production: detail of the different processes and cement plant variability evaluation," *J. Clean. Prod.*, vol. 18, no. 5, pp. 478-485, 2010.
- [5] J. Li, P. Tharakan, D. Macdonald, and X. Liang, "Technological, economic and financial prospects of carbon dioxide capture in the cement industry," *Energy Policy*, vol. 61, pp. 1377-1387, 2013.
- [6] E. Worrell, L. Price, N. Martin, C. Hendriks, and L. O. Meida, "Carbon dioxide emissions from the global cement industry," *Annu. Rev. energy Environ.*, vol. 26, no. 1, pp. 303-329, 2001.
- [7] A. M. Al-Omran, S. E. El-Maghraby, E. A. Nadeem, A. M. El-Eter, and S. M. I. Al-Qahtani, "Impact of cement dust on some soil properties around the cement factory in Al-Hasa Oasis, Saudi Arabia," *Am. J Agric Env. Sci*, vol. 11, no. 6, pp. 840-846, 2011.
- [8] O. Oguntoke, A. E. Awanu, and H. J. Annegarn, "Impact of cement factory operations on air quality and human health in Ewekoro Local Government Area, South-Western Nigeria," *Int. J. Environ. Stud.*, vol. 69, no. 6, pp. 934-945, 2012.
- [9] Y. Askar, P. Jago, M. M. Mourad, and D. Huisingh, "The cement industry in Egypt: Challenges and innovative cleaner production solutions," in *Knowledge Collaboration & Learning for Sustainable Innovation: 14th European Roundtable on Sustainable Consumption and Production (ERSCP) conference and the 6th Environmental Management for Sustainable Universities (EMSU) conference, Delft, The Netherland*, 2010.
- [10] F. A. Rodrigues and I. Joekes, "Cement industry: sustainability, challenges and perspectives," *Environ. Chem. Lett.*, vol. 9, no. 2, pp. 151-166, 2011.

# We are IntechOpen, the world's leading publisher of Open Access books Built by scientists, for scientists

6,300

Open access books available

171,000

International authors and editors

190M

Downloads

Our authors are among the

154

Countries delivered to

TOP 1%

most cited scientists

12.2%

Contributors from top 500 universities



WEB OF SCIENCE™

Selection of our books indexed in the Book Citation Index  
in Web of Science™ Core Collection (BKCI)

Interested in publishing with us?  
Contact [book.department@intechopen.com](mailto:book.department@intechopen.com)

Numbers displayed above are based on latest data collected.  
For more information visit [www.intechopen.com](http://www.intechopen.com)



# Compressive Strength of Concrete with Nano Cement

*Jemimah Carmichael Milton and Prince Arulraj Gnanaraj*

## Abstract

Nano technology plays a very vital role in all the areas of research. The incorporation of nano materials in concrete offers many advantages and improves the workability, the strength and durability properties of concrete. In this study an attempt has been made to carry out an experimental investigation on concrete in which cement was replaced with nano sized cement. Ordinary Portland cement of 53 grade was ground in a ball grinding mill to produce nano cement. The characterization of nano cement was studied using Scanning Electron Microscope (SEM), Brunauer Emmett–Teller (BET), Energy Dispersive X ray microanalysis (EDAX) and Fourier Transform Infrared Spectroscopy (FTIR). From the characterization studies, it was confirmed that particles were converted to nano size, the specific surface area increased and the chemical composition remained almost the same. The properties of cement paste with and without nano cement were found. For the experimental study, cement was replaced with 10%, 20%, 30%, 40% and 50% of nano cement. Cement mortar of ratio 1:3 and concrete of grades M20, M30, M40 and M50 were used. Compressive strength of cement mortar and concrete with different percentages of nano cement was found. The cement mortar was also subjected to micro structural study. It was found that the strength increased even up to the replacement level of 50%. Further increase in the replacement is not possible since the addition of nano cement reduces the initial and final setting time of cement paste. At 50% replacement level, the initial setting time got reduced to 30 minutes which the least permitted value as per IS 12269: 2013. The increase in strength was due to the fact that nano cement acts not only as a filler material but also the reactivity increased due to the higher specific surface area. The SEM image shows the formation of additional C-S-H gel. The percentage increase in compressive strength was found to increase up to 32%. The workability of concrete with nano cement was found to be significantly more than that of the normal cement concrete.

**Keywords:** compressive strength, nano cement, normal cement concrete, scanning electron microscope (SEM), energy dispersive X ray microanalysis (EDAX), Fourier transform infrared spectroscopy (FTIR)

## 1. Introduction

Nano technology is a new emerging area in field of engineering. Development of nanotechnology in the field of material science and evolution of advanced instrumentation have paved way for application of nanotechnology in the construction field. Incorporation of nano sized particles in cement composites makes a significant

change in structural and nonstructural properties of cement paste, mortar and concrete. The particles converted from micron size to nano size results in more specific surface area. The increase in surface area leads to changes in morphology, increase in the chemical reactivity, structural modification of cement hydrates and enhancement of the properties of concrete. Nano particles are produced by two approaches. In “top down” approach, larger particles are reduced to smaller particles without altering the original properties and in “bottom down” approach very small nanoscopic molecules and atoms combine together to form bigger structures wherein the particles properties can be altered. The nano scale particles can result in vividly improved properties from conventional grain size materials of the same composition. Nano materials show unique physical and chemical properties that can lead to the development of more effective materials than the ones which are currently available. The use of nano materials in concrete, results in stronger and more durable concrete with desired stress-strain behaviour.

The structure of nano materials can be studied using the various sophisticated non-destructive techniques. The scaled down particles are to be checked for their size and some of the equipment available to determine particle size are scanning electron microscope, atomic force microscope and transmission electron microscope. Many techniques like Energy dispersive X-ray analysis, X-ray diffraction, X-ray absorption spectroscopy, Fourier transform infrared spectroscopy, Nuclear magnetic resonance *spectroscopy*, Thermal gravimetric analysis, Low-energy ion scattering spectroscopy, UV-V's spectroscopy, Photoluminescence spectroscopy, Dynamic light scattering are available for the surface chemical analysis and characterization of nano materials.

Nowadays application of nanotechnology can be widely seen in medical, car manufacturing, pharmaceutical, chemical and other industries. Nano particles are used for the manufacturing of medicines, bio medical instruments, paints, coatings, glass, plastics and rubber. In the construction field, nano titanium oxide, nano silica, nano aluminum oxide, nano zirconium oxide, carbon nano tubes, carbon nano fibers and nano fly ash are commonly used nano materials. According to Konstantin Sobolev [1], nano particles improve the ductility, thermal resistance and hence can be used in refractory concrete. Hanus [2] reported that nano particles produce anti-microbial surfaces and can be adopted in hospital buildings. It was also suggested that nano particles can be used in pavement as it possess high thermal resistance and abrasion property. According to Gann [3], shells and bones contain crystals of calcium and can be used in nano form to arrest crack and to dissipate energy.

Nano particles are added to concrete to improve its material properties. Perumalsamy Balaguru and Ken Chong [4] expressed that particle size upto 500 nm can be used in concrete whereas Surinder Mann [5], Florence Sanchez and Konstanin Sobolev [6] Bhuvaneshwari et al., [7], reported that the size of nano particles used in concrete has to be restricted to 200 nm. Hui li et al., [8], Maile Aiu and Huang [9] studied the effect of nano materials on the compressive strength of cement mortar. Tao Ji [10] and Ali Nazari and Shadi Riahi [11] studied the permeability and microstructure of concrete containing nano particles. Thomas.K.paul et al., [12] reported that nano materials can be produced using different techniques and gave an outline of producing nano fly ash. Research proves that there will be considerable changes in the chemical reactivity and mechanical properties, when the particles are converted to nano size. When the size is reduced, more atoms will be found at the surface of particle which significantly imparts a change in the morphology and energy at the surface. The changes in the chemical reactivity will improve the catalytic ability in paints and pigments which impart self-cleaning and self-healing properties. Nano titanium oxide is used as a self-cleaning material in

glass and as anti-corrosive element in steel. Carbon nano tubes (both single walled and multi walled) and carbon nano fibers are used in concrete to prevent cracks and to improve ductility. Nano ferric oxide due to its super para magnetic property can improve the strength property of concrete. Nano aluminum oxide is used to resist abrasion of concrete in pavements. Nano fly ash acts as a promoter to enhance the pozzolanic property. Nano silica with different quality and properties are used as an additive material in concrete. It can be seen from literature that addition of nano particles significantly improves the strength and durability of concrete. In common, nano particles are used to enhance mechanical and durability properties of concrete and to develop sustainable concrete materials and structures.

## **2. Review of literature**

The review of literature on the behaviour of mortar and concrete with nano materials is reported to understand the behaviour of cement mortar and concrete with nano particles, According to Hanus and Andrew T. Harris [13], Silvestre et al. [14] and Elzbieta Horszczaruk [15], nano silica, nano titanium oxide, nano zirconium oxide, carbon nano tubes and carbon nano fibers are commonly used materials for making nano concrete. These nano materials are not cost effective and also not available in abundance compared to the supplementary cementitious materials. Balaguru Perumalsamy and Chong Ken [4] reported that nano silica in colloidal state was more efficient than the micron sized silica in improving the durability of concrete. It was also reported that nano cement and nano carbon tubes can enhance the properties of concrete compared to nano carbon fibers. Konstantin Sobolev and Miguel Ferrada Gutierrez [16], Surinder Mann [5], Zhi Ge and Zhili Gao [17] reported that introduction of nanotechnology may bring major changes in the field of concrete technology. The concept of nanotechnology can be applied to concrete, steel and glass to produce new products with new properties. It was highlighted that the structure and behaviour of concrete should be understood at micro and nano scale. Bhuvaneshwari et al. [7] reported that efforts were taken to evolve new nano material towards a green and sustainable solution in the area of cement based materials and their composites for the construction applications. It was reported that the study of cement based material at nano level will result in a new generation construction materials with enhanced strength and durability properties. Sanchez Florence and Sobolev Konstantin [6] reported that the measurement and characterization of nano structure of cement and concrete materials is nano science and use of nano materials in cement and concrete composite is nano engineering. The nano structure study of nano materials was done by atomic force microscope, nano indentation technique, nuclear techniques, neutron and X ray scattering technique. Experimental study and micro structural study on nano materials is essential to study the effect of nano particles in concrete. They reported that mechanical properties of concrete can be enhanced with incorporation of nano particles in concrete. Laila Raki et al. [18] reported that nano-sized particles modify and improve the durability of concrete.

Jafarbeglou et al. [19] reviewed the current state of nano technology in enhancing the performance of concrete by producing new sustainable advanced cement based composites. The advance instruments like Atomic Force Microscope (AFM), Transmission Electron Microscope (TEM) were used to understand the role of nano particles and to predict the life of concrete with nano materials. It was discussed that the uniform proper dispersion and compatibility of nano materials should be taken care while incorporating the nano sized materials in concrete. Guillermo Bastos et al. [20] stated that it is necessary to have a unique synthesis

method to produce nano materials in a large scale Standards should be adopted to mix efficiently nano particles in cement composites. High quality standards in production, common codes and identical terminology are needed to transfer the knowledge of research findings to global market. Implementation of concept of nano technology in construction field is difficult due to the cost involved in synthesis and dispersion of nano materials. Muhd Norhasri Muhd Sidek et al. [21] reported that particle size less than 500 nm can be used in concrete which enhances the properties of concrete. It was also stated that ultrafine particles less than 200 nm helps to reduce cement content and helps in the reduction of micro pores by acting as a filler agent and increase the density of concrete. Hosam M. Saleh et al. [22] discussed the formation of stabilized radioactive waste immobilization and construction materials from hazardous cement kiln dust. Portland cement with slag, silica fume, kiln dust along with 0.1% of nano materials were mixed and solidified. Compressive strength and porosity of the cement composite were found. It was reported that the performance with 0.1% nano silica increased the mechanical integrity by four fold. Hosam M. Saleh et al. [23] explored the possibility of improving the properties of cement by adding iron slag and titanate nano fibers to stabilize the radio active waste. The mechanical and physical characterization of the cement was enhanced. It was reported that it captured radionuclides from the contaminated aqueous solution before the immobilization process. Hosam M. Saleh et al. [24] studied the performance of cement-slag-titanate nano fibers composite immobilized radioactive waste solution. It was observed that cement nano composite was created by mixing iron slag with Portland cement which was hydrated with aqueous titanate nano fibers. SEM, FT-IR and X-ray diffraction analysis was performed to confirm the calcium silicate hydrate formation. It was observed that nano composite enhanced the mechanical and durability properties of cement and cement based materials. The chemical stability of cement-slag-titanate nano fibers composite was studied by monitoring leaching of  $^{137}\text{Cs}$  which confirms immobilization radioactive waste and other hazardous waste. Hosam M. Saleh et al. [25] studied the influence of severe climatic variability on the structural, mechanical and chemical stability of cement kiln dust slag nano silica composite. The dust from cement kiln dust was mixed with 20% of iron slag and 0.1% nano silica, to produce modified cementitious composites which are suitable for construction and waste stabilization applications. The leachability studies showed that the impact of flooding can be reduced. Further freezing and thawing studies showed that the immobilization of radioactive waste can be enhanced.

Maile Aiu and Huang [9] synthesized the components of portland cement type I nano particles using sol gel process and compared the properties with that of commercial cement. Scanning Electron Microscope study revealed that nano cement particles were of size between 40 nm to 100 nm and appeared to be conglomerated and spherical. Energy Dispersive X-Ray Analysis test showed that the calcium to silica ratio was 3:1 or 2:1 and X-ray powder diffraction (XRD) result showed that nano cement contains  $\text{C}_3\text{S}$ ,  $\text{C}_2\text{S}$  and copper oxide. Thomas Paul et al. [12] explained about the preparation, characterization of nano structured fly ash. The class F fly ash was ground in a high energy ball milling and converted into nano structured material. The nano structured fly ash was characterized for its particle size using particle size analyzer. Specific surface area was found using Brunauer-Emmet-Teller (BET) surface area apparatus. Fourier Transform Infrared Raman analysis (FTIR), SEM and TEM were used to study the particle aggregation and shape of the particles. On ball milling, the particle size got reduced from 60  $\mu\text{m}$  to 148 nm i.e., by 405 times and the surface area increased from 0.249  $\text{m}^2/\text{g}$  to 25.53  $\text{m}^2/\text{g}$  i.e. by more than 100%. Surface of the nano structured fly ash was

found to be more active as was evident from the FTIR studies. Morphological studies revealed that the surface of the nano structured fly ash was more uneven and rough and shape is irregular as compared to fresh fly ashes which are mostly spherical in shape. Narasimha Murthy Inampudi et al. [26] studied the crystallite size and lattice strain using XRD when micro sized fly ash was converted to nano sized fly ash using high energy ball milling process. The characterization was done after every 5 hours and at the end of 30 hours, the size of nano fly ash was found to be 83 nm. It was observed that the crystallite size was decreased and lattice strain was increased. It was also observed that the spherical shaped fly ash was converted to irregular shaped nano fly ash particle. The nano fly ash particles increased the hardness of composite and improved the compressive strength of cement composite. Gujjala Raghavendra et al. [27] presented the method of converting uneven micro size fly ash in to smooth glassy nano sized fly ash by planetary ball milling. From BET and XRD studies, it was noted that after 16 hours of milling, the surface area increased from  $0.31\text{m}^2/\text{g}$  to  $24.65\text{m}^2/\text{g}$ , the crystalline structure reduced from 59–26% and the particle size converted from  $11\ \mu\text{m}$  to  $148\ \text{nm}$ . Sada Abdal khaliq Hasan Alyasri et al. [28] investigated the economic feasibility of producing nano cement in a large scale through the cement factories. The mineral admixtures such as fly ash and slag should be added with crushed clinker where the moisture content should be maintained below 3%. The mixture was ground for 30 to 40 min to get nano cement. The specific gravity of nano cement was found to be 2.11 and specific surface area was  $3,582,400\text{cm}^2/\text{g}$ . Bickbau and Shykun [29] explained that the Russian federal agency on technical regulating and metrology formulated the national standard on nano modified portland cement. Nano cement was produced by grinding process in ball mills of the clinker. Silicate minerals and gypsum were also added. The properties of nano cement were checked for its consistency. The specific surface area found by Blaine's apparatus should be below  $400\text{m}^2/\text{kg}$  and grain size should be 10-100 nm. The mineral supplements were added in clinker to get economical nano cement, to reduce cost of fuel, reduce  $\text{CO}_2$  emissions and to improve the quality of concrete with nano cement.

Parang Sabdono et al. [30] studied the effect of nano cement on the compressive strength of cement mortar. It was proved that use of nano cement in mortar helps in the reduction of the micro voids present in cement mortar, enhances the pozzolanic activity and increase the hydration rate of cement. Ordinary Portland Cement (OPC) and Portland Pozzolana Cement (PPC) were converted to nano particles of size 50 nm and 47 nm size. The experimental result showed that the initial setting time reduced from 138 min to 75 min with nano OPC and 123 min to 45 min with nano PPC. The compression test was conducted on 28 days cement mortar specimens of size 50 mm x 50 mm x 50mm. The compressive strengths of mortar with nano OPC and nano PPC were found to be  $68.493\ \text{N}/\text{mm}^2$  and  $65.286\ \text{N}/\text{mm}^2$  respectively. It was reported that the nano cement improved the hydration reaction, lowered the initial setting time and increased the compressive strength. Ikhlef Bualem [31] studied the properties of cement and cement mortar with two combination of nano particles. First combination used was grinding 100% OPC to nano size without mineral additives and the second combination was grinding 50% of OPC together with 50% of silica sand (it is equal parts of granulated blast furnace slag and quartz sand) to nano size. It was found that the specific surface area of nano cement without mineral additive was  $4900\ \text{cm}^2/\text{g}$  and nano cement with 50% of mineral additive, the specific surface area was found to be  $5000\ \text{cm}^2/\text{g}$ . It was also found that the 90th day compressive strength of nano cement mortar was 51.4 MPa. for cement mortar with 100% nano cement, the strength was 114.3 MPa and for mortar with nano cement and mineral additive the strength was 77.8 MPa.

Gengying Li [32] compared the properties of normal cement concrete, high-volume fly ash high-strength concrete (SHFAC) incorporating nano silica and high-volume fly ash high-strength concrete (HFAC). Compressive strength was found from 3 days to 2 years. It was found that HFAC showed a 10% less compressive strength upto 56 days compared to normal cement concrete but increased to 21% higher than that of normal cement concrete at 2 years. The compressive strength of SHFAC showed that addition of 4% nano silica helped to gain early age strength by about 81% and also helped in gaining later strength upto 47% compared with normal cement concrete. The pore size of SHFAC was found to be less than that of NCC and HFAC. Zaki and KhaledRagab [33] studied the influence of nano silica on the properties of fresh and hardened normal cement concrete. In this study 18% of silica fume and 0.5%, 0.7% and 1% of nano silica were used. It was found that the workability of concrete improved with addition of super plasticizers when nano silica was added. It was reported that concrete with nano silica had a higher compressive strength, since nano silica not only acts as filler but helps in rapid formation of C-S-H gel. It was also reported that the efficiency of nano silica depends on its morphology, size and method of production. It was stated that 0.5% nano silica was found to perform better with and without silica fume compared to normal cement concrete. Nili et al. [34] discussed the performance of concrete with using nano silica and micro silica. It was reported that due to the high pozzolanic property, the compressive strength of concrete with 1.5, 3, and 4.5% of nano silica and 3, 4.5, 6 and 7.5% of micro silica gave a higher value than the normal cement concrete. It was found that the compressive strength of concrete with 1.5% nano silica and 6% of micro silica gave optimum values. Praveen and Janagan [35] experimentally studied the strength of concrete with nano particles. In this study, cement was replaced with 30% nano fly ash along with 3% nano Ground Granulated Blast Furnace slag (GGBS), 40% nano fly ash along with 4% nano GGBS and 50% nano fly ash along with 5% nano GGBS. The compressive strength and tensile strength of concrete were investigated on 7th and 28th day. It was reported that the strength was more when cement was replaced with 30% of nano fly ash along with 3% nano GGBS. Harihanandh and Sivaraja [36] experimentally studied the compressive strength, tensile strength and flexural strength of M20 grade concrete with nano fly ash. In this study class F calcium fly ash was converted into nano size in a ball grinding mill and its size was confirmed by SEM analysis. It was found that concrete with cement replaced with 23% nano fly ash gave 34% more compressive strength, 58.57% more tensile strength and 33.07% more flexural strength than the normal cement concrete. It was reported that the nano fly ash filled the pores and made the concrete denser.

It is obvious from the review of literature, that the application of nanotechnology in concrete is one of the promising areas of research. Studies were done on cement paste, cement mortar and cement concrete with incorporation of small percentage of nano materials. Nano particles of silicon dioxide, cement, fly ash, clay, metakaolin, iron oxide, aluminum oxide, zirconium oxide, carbon nano tubes, carbon nano fibers and nano carbonates are considered by many researchers in which nano silica was commonly used. Syntheses of nano materials were done by various methods and the properties of the nano materials were found to be dependent on the method of production. Characterization is done to understand the property of nano materials. Since the particle is of nano size with high specific surface area, the behaviour of cement paste, mortar and concrete with nano materials may be different from that of the normal cement paste, mortar and concrete. Normal consistency and setting time tests are usually carried out with cement paste, strength and durability studies are done with mortar and concrete. Few studies were also carried out with the addition of admixtures.

The special focus of the present investigation intends to highlight the replacement of cement with nano cement in larger percentages. Though many methods of production of nano materials are given in literature, ball milling method is adopted by which a large amount of nano materials can be produced economically without chemical change. Hence an attempt has been made to study the properties of nano cement, properties of cement paste with nano cement, properties of cement mortar with nano cement and compressive strength of concrete with nano cement.

### 3. Properties of materials

Concrete is considered to be a composite material containing a binder medium within which aggregate particles are embedded. The properties of materials used in the experimental investigation are cement, fine aggregate, coarse aggregate, and water. The properties are presented in this session.

#### 3.1 Cement

Ordinary Portland Cement (OPC) of 53 grade conforming to IS: 12269-2013 [37] and procured from a single source was used for this investigation. The chemical and physical properties of the cement used are given in **Table 1**.

| Particulars                               | Results (%) | Requirements of IS:12269 |
|---|-------------|--------------------------|
| SiO <sub>2</sub>                          | 21.8        | —                        |
| Al <sub>2</sub> O <sub>3</sub>            | 4.8         | —                        |
| Fe <sub>2</sub> O <sub>3</sub>            | 3.8         | —                        |
| CaO                                       | 63.3        | —                        |
| SO <sub>3</sub>                           | 2.2         | —                        |
| MgO                                       | 0.9         | Maximum6                 |
| Na <sub>2</sub> O                         | 0.21        | —                        |
| K <sub>2</sub> O                          | 0.46        | —                        |
| Cl  | 0.04        | Maximum0.1               |
| P <sub>2</sub> O <sub>5</sub>             | <0.04       | —                        |
| Loss of ignition                          | 2.0         | Maximum4                 |
| Insoluble residue                         | 0.4         | Maximum3                 |
| Specific surface area, m <sup>2</sup> /kg | 370         | Minimum225               |
| Initial setting time, minutes             | 50          | Minimum30                |
| Final setting time, minutes               | 510         | Maximum600               |
| Standard consistency, %                   | 34          | —                        |
| Soundness, Le-chatelier, mm               | 1.0         | Maximum10                |
| Compressive strength, MPa                 |             |                          |
| 3-days                                    | 42.5        | Minimum27                |
| 7-days                                    | 48.0        | Minimum37                |
| 28-days                                   | 63.5        | Minimum53                |
| Specific gravity                          | 3.15        | —                        |

**Table 1.**  
 Chemical and physical properties of 53 grade OPC.

### 3.2 Fine aggregate

The locally available clean and dry natural sand from Cauvery river basin, Karur, India free from debris was used as fine aggregate. The specific gravity of fine aggregate was found to be 2.65. From sieve analysis, it was confirmed that the sand belongs to Zone II grading. Bulk density of fine aggregate was found to be 1520 kg/m<sup>3</sup>. Fineness modulus of sand was found to be 2.32. The properties of fine aggregate were found to confirm with IS: 383-2016 [38].

### 3.3 Coarse aggregate

The coarse aggregate used was natural hard broken granite stones. Crushed granite metals of size 20 mm were used. The specific gravity of coarse aggregate was 2.79 and it was confirming to IS: 383-2016 [38].

### 3.4 Water

Potable water available in laboratory was used for casting and curing all specimens in this investigation. The quality of water was found to satisfy the requirements of IS: 456-2000 [39].

## 4. Synthesis and characterization of nano cement

### 4.1 Production of nano cement

Nano cement was produced by grinding ordinary Portland cement of 53grade in a high intensity ball grinder for 12 hours. In high energy ball grinding milling machine, high impact collisions were used to reduce microcrystalline materials down to nano crystalline structure without chemical change. Care was taken to avoid balling effect and agglomeration.

### 4.2 Microstructure analysis of nano cement

The particles size of the nano cement were found by surface morphology studies, the specific surface area was found by Brunauer Emmett Teller theory, and the elemental compositions were found by X-ray spectroscopic method.

#### 4.2.1 Particle size determination of nano particles

Surface morphology studies were carried out using a Scanning Electron Microscope (JEOL, JSM 35 CF, Japan) shown in **Figure 1**.

53grade OPC was ground in the ball grinder mill for 12 hours to produce nano cement which was taken for morphological study using SEM. The SEM images of cement and nano cement are shown in **Figures 2 and 3** respectively.

From the SEM image, it can be seen that the cement particles have been ground to nano size. The size varies between 45 nm to 86 nm. It was also found that the shape of the particles was not altered due to grinding and agglomeration of cement particles did not take place.

#### 4.2.2 Specific surface area of nano materials

The specific surface area is the total surface area of the exposed surface in square centimeter per unit mass. It was found by Brunauer, Emmett and Teller



**Figure 1.**  
*Scanning electron microscope.*

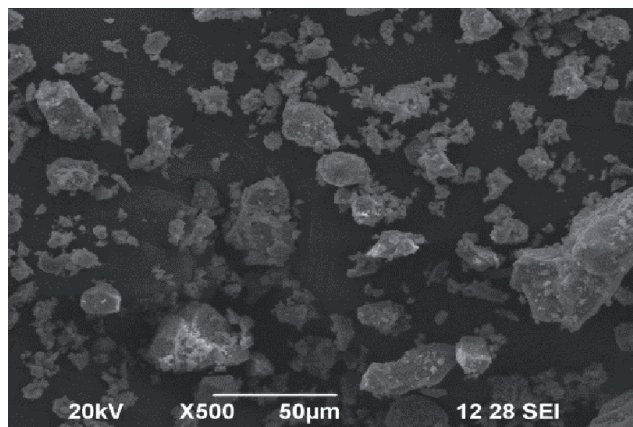


**Figure 2.**  
*SEM image of cement.*

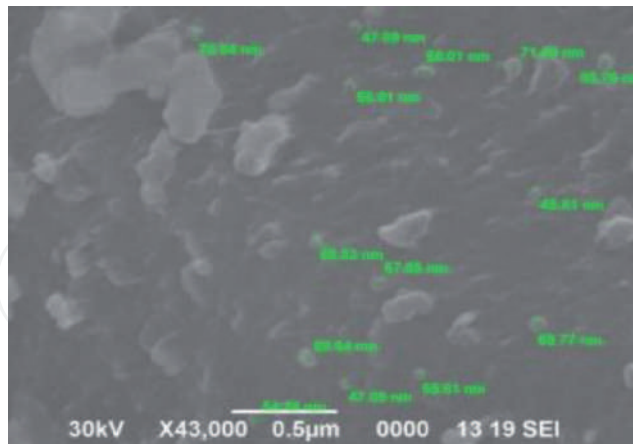


**Figure 3.**  
*SEM image of nano cement.*

method for cement and nano cement. The specific surface area of cement was found to be  $3700 \text{ cm}^2/\text{g}$  and for nano cement, the specific surface area was found to be  $485,000 \text{ cm}^2/\text{g}$ . It can be seen that the particles in nano size have much higher specific surface area compared to particles in micro size.

#### 4.2.3 Energy dispersive X-ray analysis of materials

EDAX is an x-ray spectroscopic method for determining elemental compositions. EDAX studies were carried out using a Scanning Electron Microscope. EDAX analysis

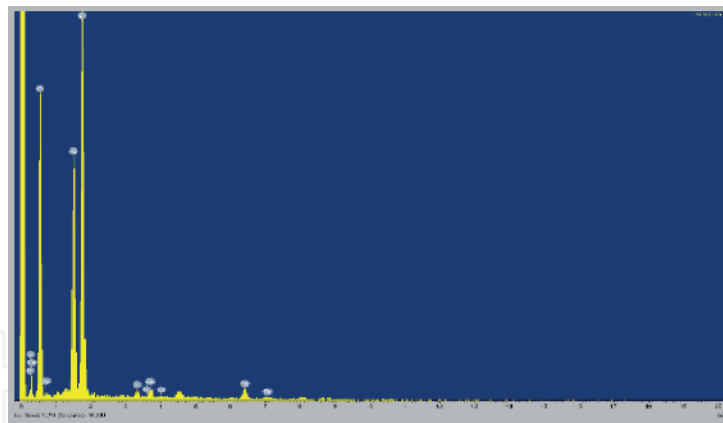


**Figure 4.**  
EDAX of cement.

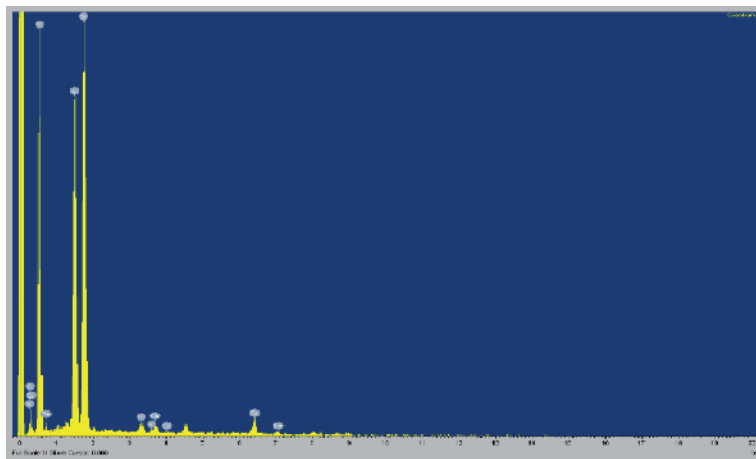


**Figure 5.**  
EDAX of nano cement.

| Element     | Atomic weight percentage of chemical elements (%) |       |      |       |      |      |      |
|-------------|---|-------|------|-------|------|------|------|
|             | C   | O     | Al   | Si    | K    | Ca   | Fe   |
| Cement      | 21.55   | 58.27 | 6.84 | 12.17 | 0.20 | 0.28 | 0.69 |
| Nano Cement | 19.80   | 59.95 | 8.00 | 11.07 | 0.24 | 0.19 | 0.75 |

**Table 2.**  
EDAX analysis of particles.

was done in conjunction with SEM analysis. In EDAX analysis, X rays are emitted from the sample due to bombardment of electron beam from a spot, an area, a line profile or a 2D map. These X-rays are detected to characterize the elemental composition. In the EDAX images, the X axis represents energy and Y axis represents intensity. EDAX of cement and nano cement are shown in **Figures 4** and **5** respectively.

The details of EDAX analysis are given in **Table 2**.

From the EDAX study it was noted that the chemical composition of elements does not vary much when ground to nano particles.

## 5. Tests on cement paste with nano cement: normal consistency and setting time

The consistency test and setting time test on cement mortar with nano cement were carried out using the Vicat's apparatus conforming to IS: 5513-1996 [40].

| Particulars          | % Replacement of Cement with Nano Cement |    |    |    |    |    |
|----------------------|--|----|----|----|----|----|
|                      | 0  | 10 | 20 | 30 | 40 | 50 |
| Normal Consistency   | 34                                       | 33 | 33 | 34 | 35 | 33 |
| Initial setting time | 50                                       | 45 | 40 | 38 | 35 | 30 |

**Table 3.**  
 Normal consistency and setting time of cement paste with nano cement.

The values of consistency, initial setting time and final setting time of the cement paste with 0%, 10%, 20%, 30%, 40% and 50% of nano cement are given in **Table 3**.

From **Table 3**, it can be seen that the consistency of cement pastes with nano cement was almost the same but the initial and final setting times of are found to decrease as the replacement percentage increases.

The initial setting time of cement paste with nano cement was found to decrease to 30 minutes with 50% replacement whereas the initial setting time of normal cement paste is found to be 50 minutes. As per the IS 12269-2013 [37], the initial setting time of cement should not be less than 30mins. Hence the replacement level of cement with nano cement should not exceed 50%. The final setting time of cement paste with nano cement was found to decrease to 245 minutes at a replacement level of 50%.

## 6. Tests on cement mortar with nano materials

The compressive strength of cement mortar was determined on the 3rd, 7th, 21st and 28th days. After the 28th day test, the powder of the tested cement mortar cubes was taken for micro structural studies. The properties were evaluated by SEM, EDAX and FTIR test.

### 6.1 Compressive strength of cement mortar by experiment

The compressive strength of hardened mortar cubes of size 70.6 mm x 70.6 mm x 70.6 mm with and without nano cement were found using a compression testing machine of capacity 2000kN. The load was applied with a uniform rate of 35 N/mm<sup>2</sup>/min after the specimen had been centered in the testing machine. The compressive strengths of cement mortar cubes are shown in **Table 4**.

The compressive strength of cement mortar was found to increase upto 50% replacement of cement with nano cement. The percentage increase in strength was found to vary between 34.36 and 77.85 for nano cement.

| % replacement of cement with nano cement | Average Compressive Strength of Cement mortar (N/mm <sup>2</sup> ) |                     |                      |                      |
|--|--|---------------------|----------------------|----------------------|
|  | 3 <sup>rd</sup> day  | 7 <sup>th</sup> day | 21 <sup>st</sup> day | 28 <sup>th</sup> day |
| 0  | 42.50  | 48.00               | 57.00                | 63.50                |
| 10                                       | 58.98  | 74.48               | 83.23                | 85.32                |
| 20                                       | 62.98  | 79.50               | 88.42                | 90.66                |
| 30                                       | 65.50  | 81.20               | 90.96                | 93.24                |
| 40                                       | 67.88  | 85.37               | 92.44                | 95.68                |
| 50                                       | 70.00  | 75.53               | 94.00                | 98.00                |

**Table 4.**  
 Compressive strength of cement mortar with nano cement.

## 6.2 Microstructure of cement mortar with nano cement

Scanning Electron Microscope image of the crushed cement mortar particles cured for 28th days is shown in **Figure 6**.

It can be seen from **Figure 6** that the textures of particles consists of standalone clusters which indicates less formation of C-S-H gel. Hence the strength will be less than the mortar containing nano cement.

SEM images of cement mortar cubes in which cement was replaced with 10%, 20%, 30%, 40% and 50% of nano cement are shown in **Figure 7**.

From **Figure 7**, it can be seen that with 10% nano cement, the texture of hydrate particles are standalone clusters and with 50% nano cement, the texture of particles are colloidal due to the formation of C-S-H gel and hence the strength of mortar cubes with 50% nano cement is higher.

## 6.3 Energy dispersive X-ray spectroscopy study on cement mortar with nano materials

The EDAX study was carried out using the same sample used for SEM study. The EDAX of crushed cement mortar is shown in **Figure 8**.

The EDAX images of cement mortar in which cement was replaced with NC are shown in **Figure 9**.

From the EDAX analysis, the chemical elements present in the mortar with nano cement were found and the details are given in **Table 5**.

From the chemical composition, Ca/Si ratio was found. The strength of the mortar depends on Ca/Si ratio. Wolfgang Kunther et al. [41] reported that the strength of mortar cubes decreases as the Ca/Si ratio increases. It can be seen from **Table 5** that the ratio of Ca/Si decreases for replacement levels and hence maximum strength is obtained at 50% replacement level.

## 6.4 FTIR Spectrum for 28 days cement mortar with nano materials

Fourier transform infrared spectroscopy is a technique used to obtain an infrared spectrum of absorption or emission of a solid, liquid or gas. an Fourier transform infrared spectroscopy spectrometer simultaneously collects

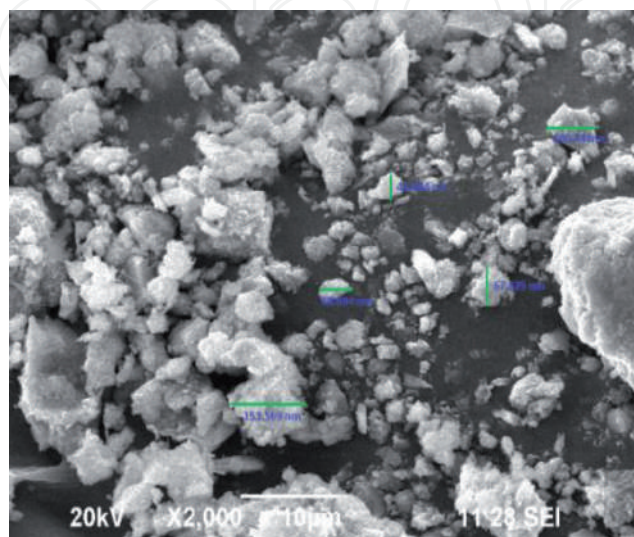


**Figure 6.**  
SEM image of cement mortar cured for 28<sup>th</sup> days.

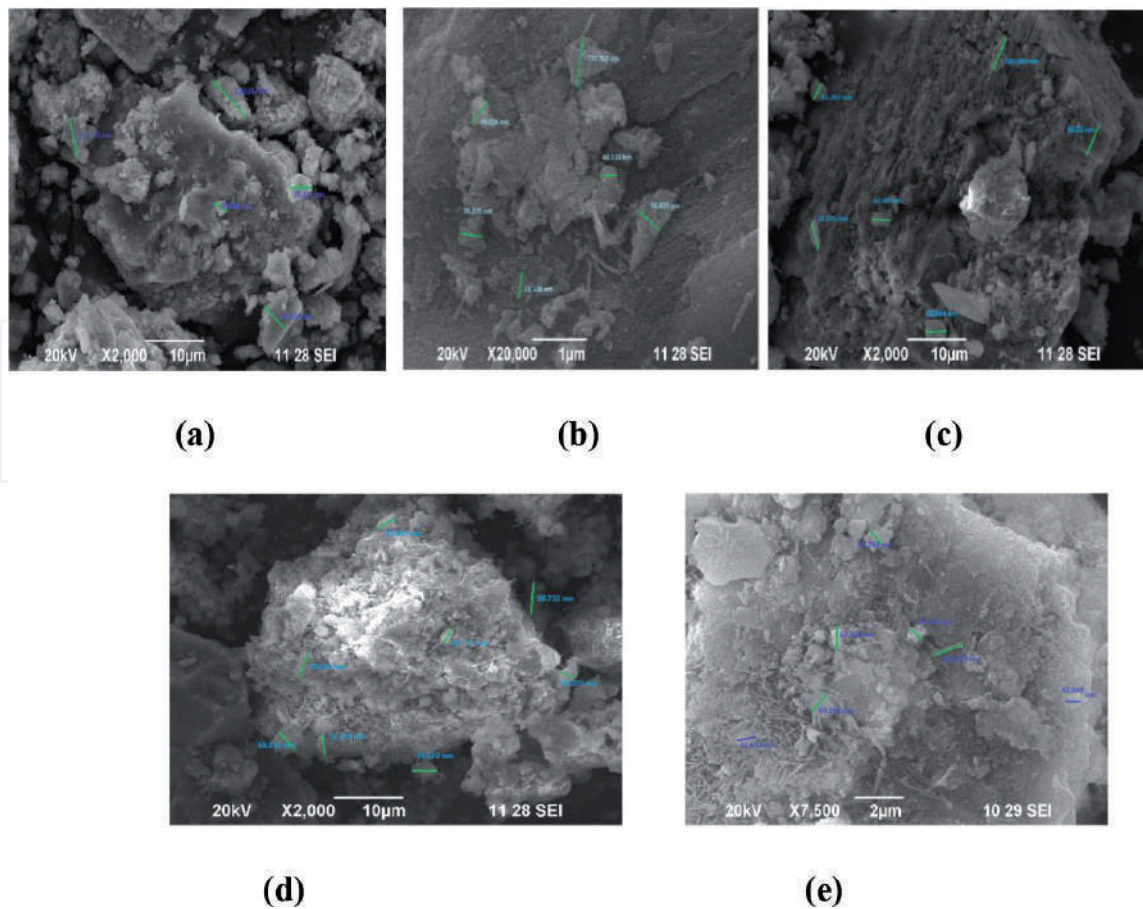


**Figure 7.** SEM images of cement mortar cubes with nano cement cured for 28<sup>th</sup> days (a) 10% replacement (b) 20% replacement (c) 30% replacement (d) 40% replacement (e) 50% replacement.

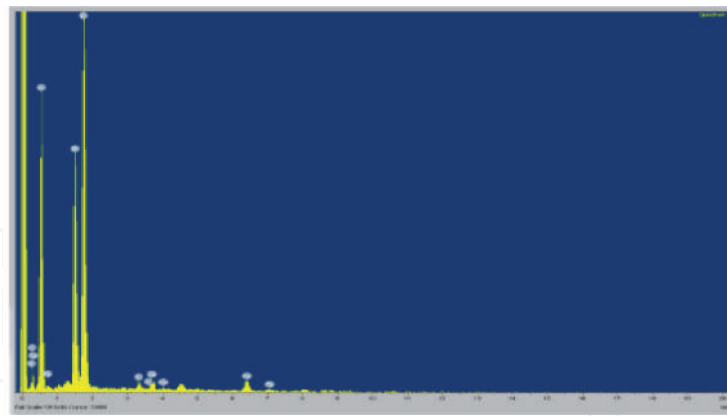


**Figure 8.** EDAX image of cement mortar cube cured for 28<sup>th</sup> days.

high-spectral-resolution data over a wide spectral range. The an Fourier transform infrared spectroscopy spectrum was recorded on IR PRESTIGE 21, SHIMADZU spectrophotometer at ambient temperature using a KBr disk method. The resulting spectrum creates a molecular fingerprint of the sample representing the molecular absorption and transmission. The changes in the molecular groups in the cement mortar before and after addition of nano particles were made by a Fourier transform infrared spectroscopy analysis. In an Fourier transform infrared spectroscopy test, the X-axis of an IR spectrum is labeled as Wave number ( $1/\text{cm}$ ) and ranges from  $400 \text{ cm}^{-1}$  on the far right to  $4000 \text{ cm}^{-1}$  on the far left.

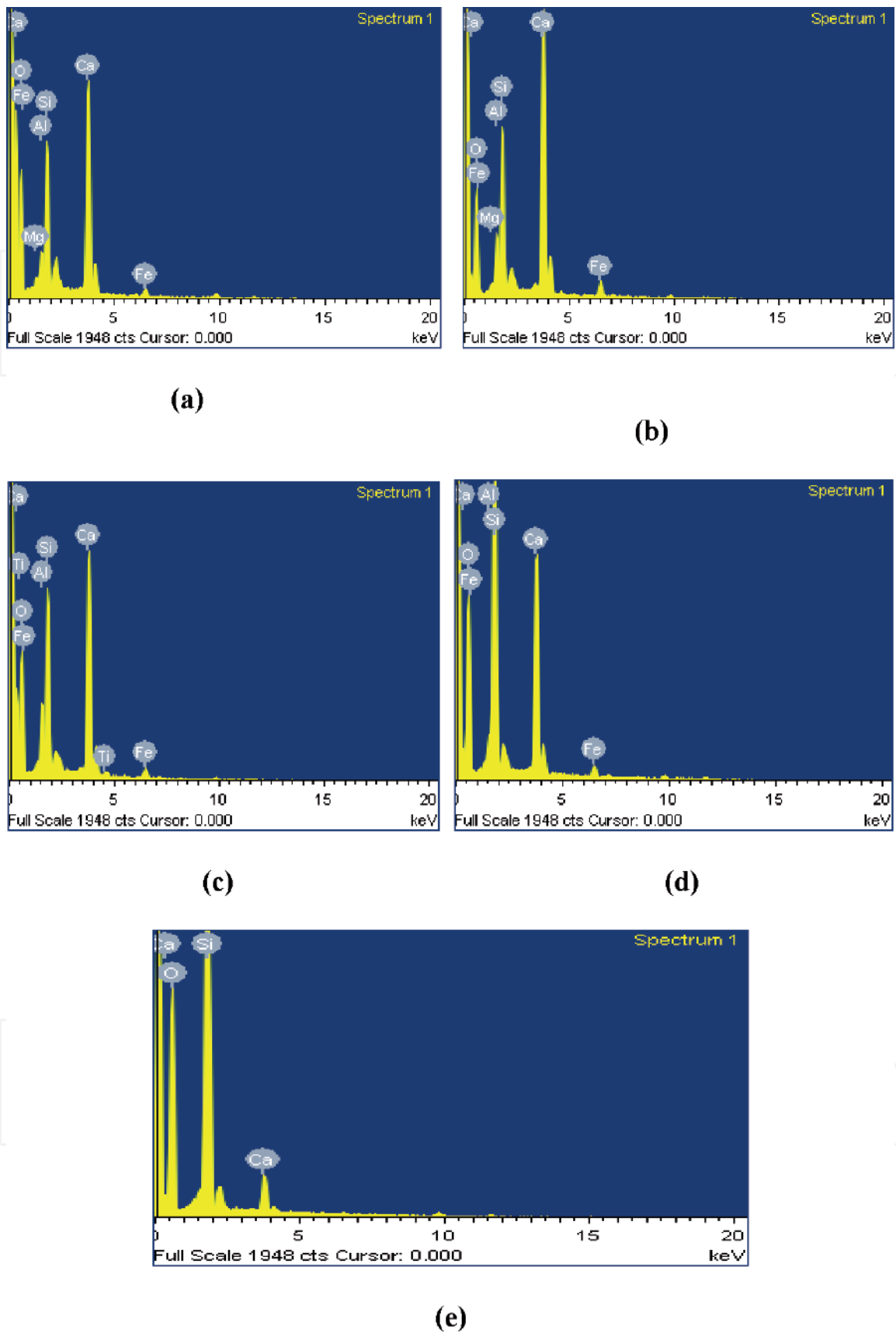


**Figure 9.** EDAX images of cement mortar cubes with nano cement cured for 28<sup>th</sup> days (a) 10% replacement (b) 20% replacement (c) 30% replacement (d) 40% replacement (e) 50% replacement.

The Y-axis is labeled as Transmittance in % and ranges from 0 at the bottom to 100 at the top. The characteristic peaks in the infrared spectrum were determined. All infra-red spectra contain many peaks. However, the large peaks on the spectrum will provide the data necessary to read the spectrum. The regions of the spectrum

in which the characteristic peaks exist were determined. The characteristic peak is compared to IR spectrum and the compounds were identified. an Fourier transform infrared spectroscopy transmission spectrum of the normal cement mortar is shown in **Figure 10**.

According to Hasan Biricika and Nihal Sarierb [42], Xu et al. [43] and Varas et al. [44], the band of the spectra between  $3640\text{ cm}^{-1}$  to  $3400\text{ cm}^{-1}$  corresponds to the structural -OH group formed during the hydration of  $\text{C}_2\text{S}$  and  $\text{C}_3\text{S}$  and free -OH group from water molecules present in the mixture. The spectral band between  $2500\text{ cm}^{-1}$  and  $1500\text{ cm}^{-1}$  corresponds to the H-O-H absorbed water molecule group which indicates the decrease in the free water and between  $1500\text{ cm}^{-1}$  to  $400\text{ cm}^{-1}$  and it corresponds to Si-O and Si-O-Si silicate group which indicate the formation C-S-H.

The FTIR transmission spectra of cement mortar in which cement was replaced with nano cement are shown in **Figure 11**. From the FTIR transmission spectra, the peaks attained by the mortar with nano cement are given in **Table 6**.

From **Figure 10** and **Table 6**, it can be seen that the band value of  $3429.43\text{ cm}^{-1}$  diminishes to  $462.92\text{ cm}^{-1}$  which implies the formation of C-S-H gel.

**Figure 11** and **Table 6**, it can be seen that the band value between  $3635.74\text{ cm}^{-1}$  and  $3410.28\text{ cm}^{-1}$  diminishes to  $488.34\text{ cm}^{-1}$  and  $455.87\text{ cm}^{-1}$  which implies that strength has been achieved. It can be seen that the lowest band value is seen in 50% replacement of cement with nano cement and the decrease in the band value implies a decrease in free water and increase in strength.

| S.No | Element | Atomic percentage of elements            |      |      |      |      |      |
|------|---------|--|------|------|------|------|------|
|      |         | % Replacement of cement with nano cement |      |      |      |      |      |
|      |         | 0%                                       | 10%  | 20%  | 30%  | 40%  | 50%  |
| 1    | O       | 53.9                                     | 78.3 | 71.7 | 73.7 | 71.7 | 69.1 |
| 2    | Al      | 5.80                                     | 2    | 3.3  | 3.9  | 1.5  | 0.43 |
| 3    | Si      | 12.7                                     | 7.9  | 9.1  | 10.2 | 17.9 | 29.4 |
| 4    | Ca      | 26.9                                     | 10.3 | 14.1 | 11.3 | 8.3  | 1.5  |
| 5    | Fe      | 0.70                                     | 0.6  | 1    | 0.7  | 0.6  | 0.12 |
| 6    | Ca/Si   | 2.12                                     | 1.3  | 1.5  | 1.1  | 0.5  | 0.1  |

**Table 5.**  
 Results of EDAX analysis of cement mortar with nano cement.

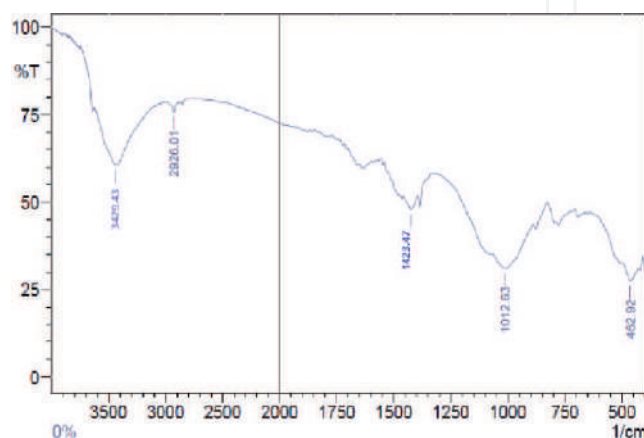


**Figure 10.**  
 FTIR transmission spectrum of cement mortar cured for 28<sup>th</sup> days.

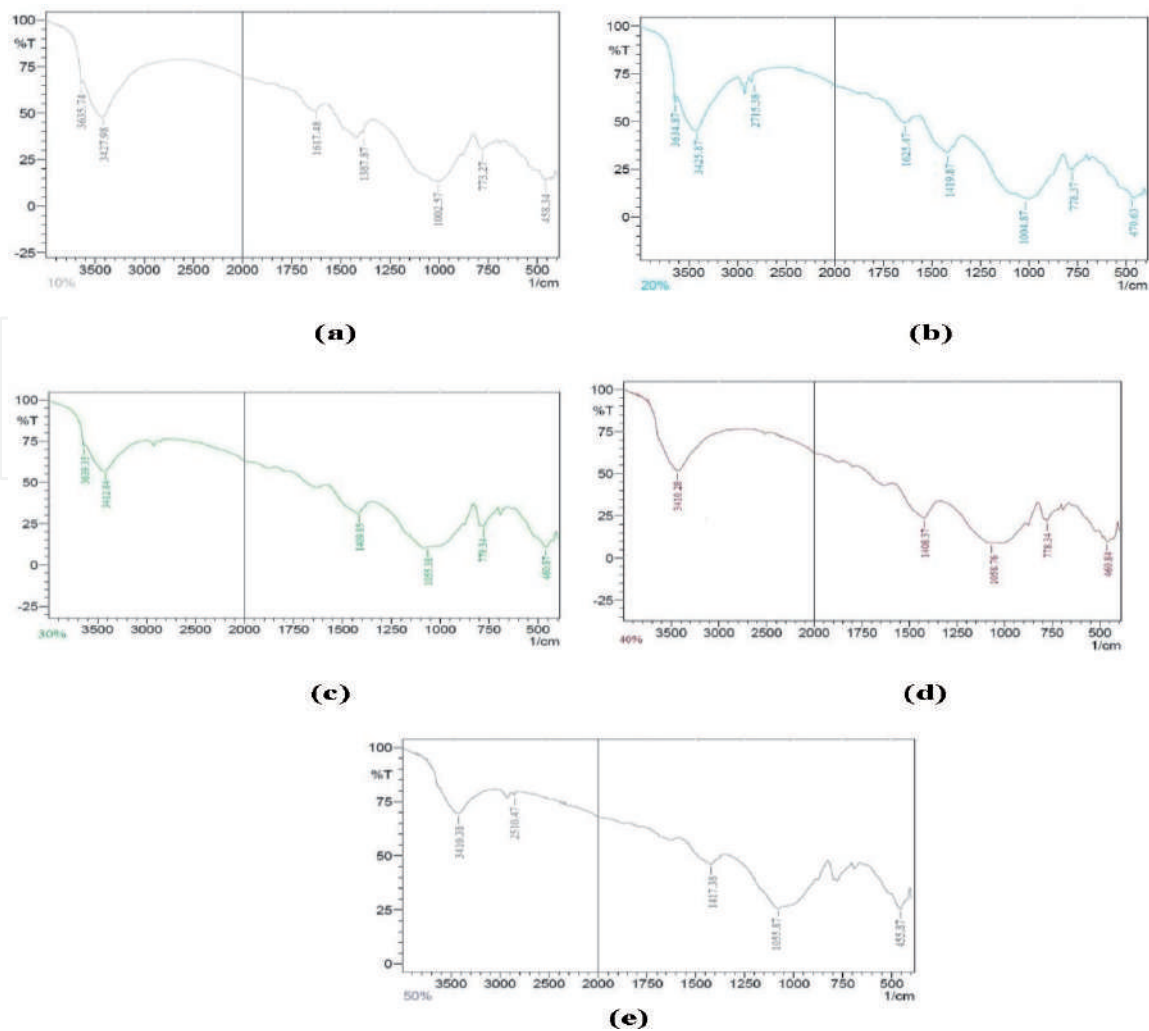


**Figure 11.** FTIR transmission spectra of cement mortar on 28<sup>th</sup> day with nano cement (a) 10% replacement (b) 20% replacement (c) 30% replacement (d) 40% replacement (e) 50% replacement.

| FTIR spectra peak of mortar with NC in cm <sup>-1</sup> |         |         |         |         |         |
|---|---------|---------|---------|---------|---------|
| %RCNP   |         |         |         |         |         |
| 0   | 10      | 20      | 30      | 40      | 50      |
| 3429.43   | 3635.74 | 3634.87 | 3639.35 | 3410.28 | 3410.28 |
| 2626.61   | 3427.98 | 3425.87 | 3412.84 | 1408.37 | 2510.47 |
| 1423.47   | 1617.48 | 2715.38 | 1409.85 | 1058.76 | 1417.38 |
| 1012.63   | 1387.87 | 1625.47 | 1055.38 | 778.24  | 1055.87 |
| 462.92  | 1002.57 | 1419.87 | 779.34  | 460.84  | 455.87  |
|   | 773.27  | 1004.87 | 460.87  |         |         |
|   | 488.34  | 778.37  |         |         |         |
|   |         | 470.63  |         |         |         |

**Table 6.** FTIR transmission spectrum peak of cement mortar with nano cement.

From both the experimental and micro structural studies, it was noted that the compressive strength of cement mortar increases as the replacement level of cement with nano cement increases. From the SEM analysis, it was seen that the nano particles filled the pores and made the concrete denser. Additional formation

of C-S-H gel can be seen from SEM analysis, reduction of Ca/Si ratio from EDAX analysis and the reduction of band spectra values from FTIR analysis which indicate the increase in strength of cement mortar with nano particles.

## 7. Compressive strength of concrete with nano materials

The compressive strength of M20, M30, M40 and M50 grades of concrete with and without nano cement are presented in **Table 7**.

**Figure 12** shows the compressive strength of concrete with respect to the percentage replacement of cement with NC.

From the **Table 7** and **Figure 12**, it can be seen that the compressive strength increases with the increase in percentage replacement of cement with nano cement. It can be seen that the compressive strength increases up to 50% replacement of cement with nano cement. The correlation coefficient between the compressive strength and percentage replacement of cement with nano cement were found to be 0.9971, 0.9946, 0.9717 and 0.9928 for M20, M30, M40 and M50 grades of concrete respectively.

It can be seen that the compressive strength increases as the replacement of cement with nano materials, curing days and grade of concrete increase. The increase in compressive strength was found to range between 0.71% and 31.5%. The percentage increase in the compressive strength of M20 grade was found to be more than that of M50 grade of concrete. Saloma et al. [45] reported that the rapid development of the compressive strength of concrete with nano materials is due to the fact that nano materials serve as a filler to increase the density and as an activator

| Average compressive strength of concrete with nano cement N/mm <sup>2</sup> |                      |                      |                      |                      |                      |                      |
|---|----------------------|----------------------|----------------------|----------------------|----------------------|----------------------|
| GC  | M20                  |                      |                      | M30                  |                      |                      |
| %RCNC   | 28 <sup>th</sup> day | 56 <sup>th</sup> day | 90 <sup>th</sup> day | 28 <sup>th</sup> day | 56 <sup>th</sup> day | 90 <sup>th</sup> day |
| 0   | 25                   | 27.3                 | 33.1                 | 32                   | 34.7                 | 42                   |
| 10  | 26.1                 | 28.7                 | 36.5                 | 32.6                 | 35.6                 | 43.4                 |
| 20  | 27.6                 | 29.9                 | 37.3                 | 33.7                 | 36.7                 | 44.6                 |
| 30  | 28.4                 | 32.2                 | 38.9                 | 35.1                 | 37.9                 | 46.3                 |
| 40  | 29.5                 | 34                   | 41.1                 | 36.4                 | 38.9                 | 47.7                 |
| 50  | 31                   | 35.9                 | 42.8                 | 37.4                 | 39.7                 | 48.8                 |
| GC  | M40                  |                      |                      | M50                  |                      |                      |
| %RCNC   | 28 <sup>th</sup> day | 56 <sup>th</sup> day | 90 <sup>th</sup> day | 28 <sup>th</sup> day | 56 <sup>th</sup> day | 90 <sup>th</sup> day |
| 0   | 42                   | 44.3                 | 48                   | 49.9                 | 51.4                 | 59.3                 |
| 10  | 44.3                 | 46.6                 | 49.6                 | 52.3                 | 55.1                 | 62.6                 |
| 20  | 46                   | 47.6                 | 52.7                 | 53.2                 | 56.7                 | 64.2                 |
| 30  | 45.7                 | 48.3                 | 54                   | 55.3                 | 58.6                 | 66.8                 |
| 40  | 47.8                 | 49.8                 | 55.5                 | 57.2                 | 60.9                 | 69.4                 |
| 50  | 49.2                 | 50.8                 | 56.6                 | 59.9                 | 63.9                 | 70.9                 |

GC is grade of concrete.  
 %RCNC is percentage replacement of cement with nano cement.

**Table 7.**  
 Compressive strength of concrete with nano cement.

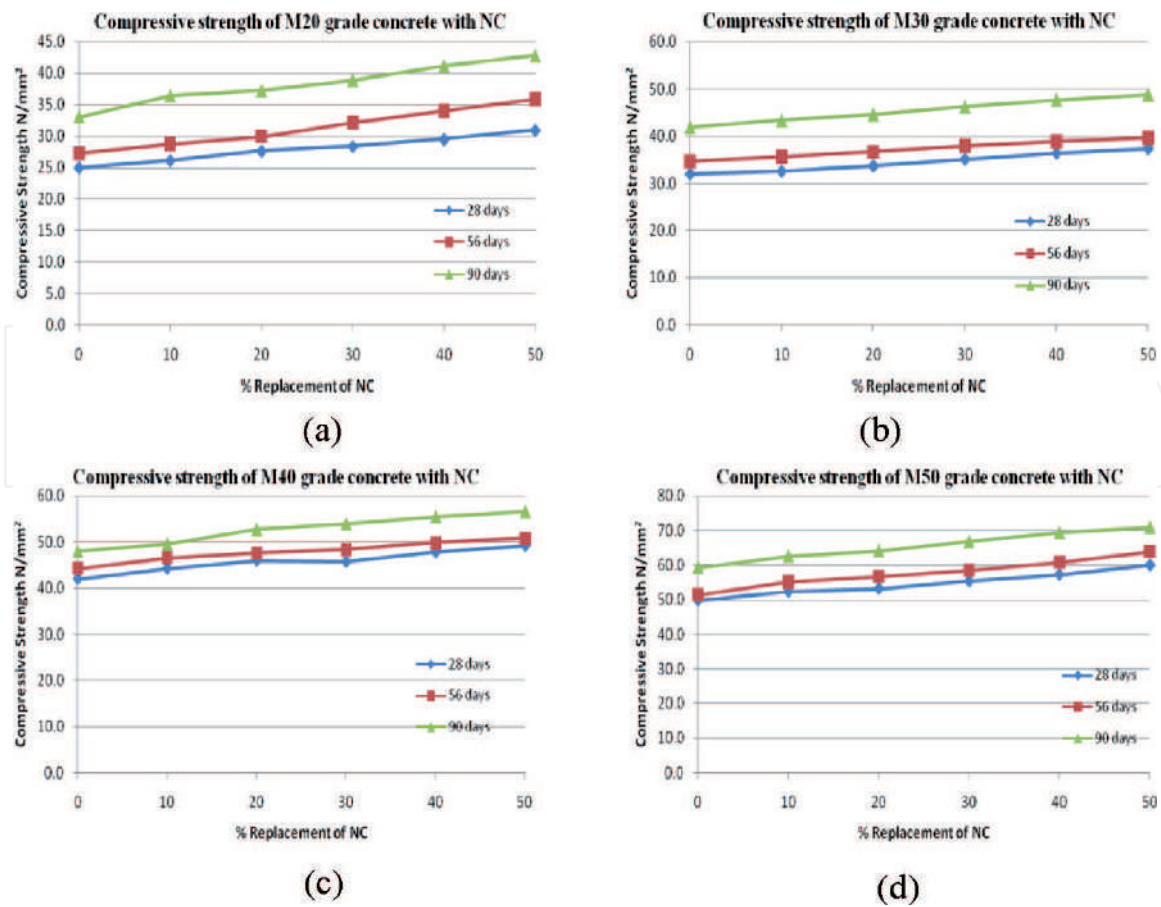


**Figure 12.** Compressive strength of concrete with nano cement (a) M 20 grade of concrete (b) M 30 grade of concrete (c) M 40 grade of concrete (d) M 50 grade of concrete.

| NP | Particulars | Variations in compressive strength |               |               |               |
|----|-------------|------------------------------------|---------------|---------------|---------------|
|    |             | M 20                               | M30           | M40           | M50           |
| NC | %           | 4.4 to 31.5                        | 1.88 to 16.88 | 3.33 to 17.92 | 4.81 to 24.32 |
|    | ratio       | 1.04 to 1.32                       | 1.02 to 1.17  | 1.03 to 1.18  | 1.06 to 1.24  |

**Table 8.** Range in the variations in compressive strength for different grades.

in the hydration reaction and reacts with free  $\text{Ca}(\text{OH})_2$  resulting in concrete with higher compressive strength. The ranges in the variations of compressive strength are given in **Table 8**.

From the **Table 8**, it can be seen that the nano cement is very effective in increasing the compressive strength of concrete.

## 8. Conclusions

### 8.1 Effect of grinding on materials

The micro-sized cement was converted to nano size by grinding it in a ball grinding mill for 12 hours and the particle size was found to range from 45 nm to 86 nm.

The specific surface areas of nano cement, increased by 13008.11%, when compared with that of ordinary portland cement.

The chemical properties of nano sized particles were found to be the same as the particles before grinding.

## 8.2 Effect of nano materials on properties of cement paste and cement mortar

The normal consistency of cement paste with nano cement was found to range between 33% and 35%.

The initial setting time of cement paste with nano cement, was found to decrease to 30 minutes at 50% replacement level when compared to the initial setting time was 50 minutes for the normal cement paste.

The final setting time of cement paste with NC, was found to decrease to 245 minutes at 50% replacement level when compared with the final setting time of 510 minutes for the normal cement paste.

The percentage increase in compressive strength of cement mortar with nano cement was found to range between 23.76 and 64.91 when compared with the compressive strength of the normal cement mortar.

The optimum replacement level of nano cement is 50%. Replacement level beyond 50% will result in the rapid setting which is not desirable.

## 8.3 Effect on compressive strength of concrete

The compressive strength of concrete was found to increase as the replacement level of cement with nano cement increases for all grades of concrete and for all curing days considered. The percentage increase in strength was found to vary between 2% and 29.3% for nano cement. The lower percentage of 2% was obtained for M30 mix cured for 28 days at a replacement percentage of 10%. The higher percentage of 29.3% was obtained for M20 mix cured for 90 days at a replacement percentage of 50%.

## Conflict of interest

The authors declare no conflict of interest.

## Author details

Jemimah Carmichael Milton<sup>1\*</sup> and Prince Arulraj Gnanaraj<sup>2</sup>

1 Department of Civil Engineering, Vignan's Lara Institute of Technology and Sciences, Vadlamudi, Guntur, Andra Pradesh, India

2 School of Engineering and Technology, Karunya Institute of Technology and Sciences, Coimbatore, Tamil Nadu, India

\*Address all correspondence to: [jemimahcarmichael@gmail.com](mailto:jemimahcarmichael@gmail.com)

## IntechOpen

© 2020 The Author(s). Licensee IntechOpen. This chapter is distributed under the terms of the Creative Commons Attribution License (<http://creativecommons.org/licenses/by/3.0>), which permits unrestricted use, distribution, and reproduction in any medium, provided the original work is properly cited. 

## References

- [1] Konstantin Sobolev. Modern developments related to nanotechnology and nanoengineering of concrete. *Frontiers of Structural and Civil Engineering*. 2016;**10**(2):131-141
- [2] Hanus MJ. Nanotechnology innovations for the construction industry. *Progress in materials science*. 2008
- [3] Gann D. A Review of Nanotechnology and its Potential Applications for Construction. SPRU, University of Sussex. 2002
- [4] Perumalsamy B, Ken C. Nanotechnology of concrete: Recent developments and future perspectives, *Nanotechnology and Concrete: Proceedings of ACI Session*; 2006:15-28
- [5] Surinder M. Nanotechnology and construction. *European Nanotechnology Gateway-Nanoforum Report*, Institute of Nanotechnology; 2006:2-10
- [6] Florence S, Konstantin S. Nanotechnology in concrete—a review. *Construction and building materials*; 2010;**24**:2060-2071
- [7] Bhuvaneshwari. B, Saptarshi S, Nagesh RI. Nanoscience to Nanotechnology for Civil Engineering - Proof of Concepts. *Proceedings of the 4th WSEAS International conference on Energy and development-environment-biomedicine*, Corfu Island, Greece. 2011:230-235
- [8] Hui L, Hui-gang X, Jie Y, Jinping O. Microstructure of cement mortar with nano-particles. *Composites Part B Engineering*; 2004;**35**:185-189
- [9] Maile A, Huang CP. The chemistry and physics of nano-cement. Report submitted to NSF REU University of Delaware; 2006:1-28
- [10] Tao J. Preliminary study on the water permeability and microstructure of concrete incorporating nano-SiO<sub>2</sub>. *Cement and concrete research*; 2005;**35**(10):1943-1947
- [11] Ali N, Shadi R. The effects of SiO<sub>2</sub> nano particles on physical and mechanical properties of high strength compacting concrete. *Composites Part B: Engineering*; 2011;**42**(3):570-578
- [12] Thomas PK, Satpathy SK, Manna I, Chakraborty KK, Nando GB. Preparation and characterization of nano structured materials from fly ash. *Nanoscale Research Letters*; 2007;**2**(8):397-404
- [13] Hanus MJ, Andrew TH. Nanotechnology innovations for the construction industry. *Progress in materials science*; 2013;**58**(7):1056-1102
- [14] Silverstre J, Silvestre N, Brito JD. Review on concrete nanotechnology. *European Journal of Environmental and Civil Engineering*; 2016;**20**(4):455-485
- [15] Elzbieta H. Properties of cement-based composite modified with magnetic nanoparticles: A review *Materials*; 2019:1-34
- [16] Konstantain S, Miguel FG. How nanotechnology can change the concrete world. *American ceramic Society Bulletin*; 2005;**84**:16-20
- [17] Zhi G, Zhili G. Applications of nanotechnology and nanomaterials in construction. *First International Conference on Construction in Developing Countries (ICCIDC-I), Advancing and Integrating Construction Education, Research & Practice*, Karachi, Pakistan; 2008:235-240

- [18] Laila R, James B, Rouhollah A, Jon M, Taijiro S. Cement and concrete nanoscience and nanotechnology. *Materials*; 2010;**3**:918-942
- [19] Jafarbeglou M, Abdouss M, Ramezaniyanpour AA. Nanoscience and nano engineering in concrete advances a review. *International journal of nano science and nanotechnology*; 2015;**11**(4):263-273
- [20] Guillermo B, Faustino P, Faustino P, Julia A. Nano-inclusions applied in cement-matrix composites: A review. *Materials*; 2016;**9**(12):10-15
- [21] Muhd NMS, Hamidah MS, Mohd FA. Applications of using nano materials in concrete: A review, *Construction and Building Materials*; 2017;**133**:91-97
- [22] Hosam MS, Fathy A El-Saied, Taher AS, Aya AH. Macro-and nanomaterials for improvement of mechanical and physical properties of cement kiln dust-based composite materials. *Journal of Cleaner Production*; 2018a-1;**204**:532-541
- [23] Hosam M, El-Sheikh SM, Elshereafy EE, Essa AK. Mechanical and physical characterization of cement reinforced by iron slag and titanate nano fibers to produce advanced containment for radioactive waste. *Construction and Building Materials*; 2018b -2; **200**:135-145
- [24] Hosam MS, El-Saied FA, Salaheldin TA, Hezo AA. Influence of severe climatic variability on the structural, mechanical and chemical stability of cement kiln dust-slag-nanosilica composite used for radwaste solidification. *Construction and Building Materials*; 2019a -1;**218**:556-567
- [25] Hosam MS, El-Sheikh SM, Elshereafy EE, Essa AK. Performance of cement-slag-titanate nanofibers composite immobilized radioactive waste solution through frost and flooding events. *Construction and Building Materials*; 2019b -2; **223**:221-232
- [26] Narasimha MI, Venkata RD, Babu Rao J. Microstructure and mechanical properties of aluminum-fly ash nano composites made by ultrasonic method. *Materials and design*; 2011;**25**:55-65
- [27] Gujjala R, Shakuntala O, Samir KA, Pal Sk. Fabrication and characterization of nano fly ash by planetary ball milling. *International journal of material science innovations*; 2014;**2**(3):59-68
- [28] Sada AKHA, Iyad SA, Prabir KS. Feasibility of producing nano cement in a traditional cement factory in Iraq. *Case studies in construction materials*. 2017;**7**:91-101
- [29] Bickbau MY, Shykun VN. Nanocements future of world cement industry and concrete technology. Program International conference, seminar, Dubai; 2017:3-33
- [30] Parang S, Frisky S, Dion AF. The effect of nano-cement content to the compressive strength of mortar. 2nd International Conference on Sustainable Civil Engineering Structures and Construction Materials 2014 (SCESCM 2014), *Procedia Engineering*; 2014:386-395
- [31] Ikhlef B. Test on nano cement mortar and concrete. Program International conference, Dubai; 2017:38-55
- [32] Gengying L. Properties of high-volume fly ash concrete incorporating nano-SiO<sub>2</sub>. *Cement and Concrete Composites*; 2004;**34**(6):1043-1049
- [33] Zaki SI, Khaled SR. How nano technology can change the concrete industry. SBEIDCOH International conference on sustainable Built Environment Infrastructures in

developing countries, Oran, Algeria; 2009:407-414

[34] Nili M, Ehsani A, Shabani K. Influence of nano-SiO<sub>2</sub> and microsilica on concrete performance. *Construction Materials and Technologies*; 2010:1-7

[35] Praveen S, Janagan SS. Partial replacement of cement with nano flyash(class c) and nano GGBS. *International research journal of engineering and technology*; 2015;2(8):979-983

[36] Harihanandh M, Sivaraja M. Strength and mechanical properties of nano fly ash concrete. *International Journal of Advanced Engineering Technology*; 2016;7(2):596-598

[37] IS: 12269-2013. Indian Standard Specification for 53 Grade Ordinary Portland Cement. Bureau of Indian Standards, New Delhi, India

[38] IS: 383-2016. Indian Standard Specification for Coarse and Fine Aggregates from Natural Sources for Concrete. Bureau of Indian Standards, New Delhi, India

[39] IS: 456-2000. Indian Standard Code of Practice for Plain and Reinforced Concrete. Bureau of Indian Standards, New Delhi, India

[40] IS: 5513-1996. Vicat Apparatus – Specification. Bureau of Indian Standards, New Delhi, India

[41] Wolfgang K, Sergio F, Jorgen S. Influence of the Ca/Si ratio on the compressive strength of cementitious calcium–silicate– hydrate binders. *Journal of Materials Chemistry*; 2017;33:17401-17412

[42] Hasan B, Nihal S. Comparative study of the characteristics of nano silica, silica fume and fly ash incorporated cement mortars. *Materials Research*; 2014;17(3):570-582

[43] Xu P, Kikpatrick RJ, Poe B, McMillan PF, Cong X. Structure of calcium silicate hydrate (C-S-H): Near-, mid-, and far-infrared spectroscopy. *Journal of the American Ceramic Society*; 1999;82(3):742-748

[44] Varas MJ, Alvarez de Buergo M, Fort R. Natural cement as the precursor of Portland cement: Methodology for its identification. *Cement and Concrete Research*; 2005;35:2055-2065

[45] Saloma AN, Iswandi I, Mikrajuddin A. Improvement of concrete durability by nanomaterials. *Procedia Engineering*; 2015;125:608-612

# The Resistance of New Kind of High-Strength Cement after 5 Years Exposure to Sulfate Solution

*Michal Bačuvčík, Pavel Martauz, Ivan Janotka and Branislav Cvopa*

## Abstract

This article deals with the determination of technically important properties, the recognition of microstructure and pore structure, and the mortar resistance of a new cement kind NONRIVAL CEM I 52.5 N containing 7.94% wt. of  $C_3A$  to 5% sodium sulfate solution. Both reference types of cement were industrially manufactured: 1) ordinary Portland cement CEM I 42.5 R and 2) Portland cement CEM I 42.5 R – SR 0, declared as sulfate resistant because of  $C_3A = 0\%$ . The research was carried out at standardized mortars. The used sodium sulfate solution, which contained 33802.8 mg of aggressive  $SO_4^{2-}$  per liter, exceeded approximately 5 to 10 times the concentration of the third degree of aggressiveness of the XA chemical environment according to STN EN 206 + A1. The reference medium was drinking water. The 5-year results of non-destructive and destructive physical-mechanical tests as well as the formed microstructure and pore structure in both liquid media were evaluated. The cause of the NONRIVAL CEM I 52.5 N sulfate resistance was explained, despite the manufacturer's declared  $C_3A$  content of up to 8% by weight. Sulfate resistance of NONRIVAL CEM I 52.5 N is found comparable to that of sulfate resistant CEM I 42.5 R – SR 0.

**Keywords:** high-strength cement, sulfate resistance, durability

## 1. Introduction

A sulfate attack represents one of the most aggressive ways of acting on concrete, which worsens the durability of the structures. There is a large number of civil engineering structures, such as the foundations of pillars, bridges or concrete canals, etc., which could be exposed to aggressive sulfates throughout their lifetime [1–3]. The resistance of concrete is increased by using durable types of cement compared to Portland, such as pozzolanic cement when natural or industrial pozzolans are added. Považská cementáreň a. s., Ladce has developed a new type Portland cement, designated as NONRIVAL CEM I 52.5 N, which does not meet the criteria for sulfate-resistant cement according to the requirements of STN EN 197–1 [4]. NONRIVAL CEM I 52.5 N is considered to

be an innovative new generation cement [5] with a content of up to 5% wt. of industrially produced submicron-sized pozzolanic addition with minimum of 50% SiO<sub>2</sub>. Studies show that the response of a cement-based material to sulfate attack varies in many cases and is influenced by many factors. Most experiments took place on a macroscopic scale, but it should be noted that the essence of the resulting attack lies in changes in the microstructure and pore structure of the cement matrix. Therefore, it is necessary to study the sulfate attack on cement-based mortar not only by assessing its physical properties but also by analyzing a microstructure and pore structure [6]. The condition of the pore structure of concrete is an important criterion for assessing sulfate resistance as its strength, as it determines the permeability for the penetration of aggressive solution into the interior of the microstructure formed over time.

According to the source of sulfate ions, sulfate attack is divided into two main types by secondary ettringite formation: external and internal. External sulfate attack occurs when the source of sulfates comes from the external environment when sulfates penetrate the concrete structure. Internal sulfate attack is caused by internal sulfate sources in an environment without external sulfate sources, such as coming from aggregates or by the thermal decomposition of ettringite [7].

External sulfate attack, also referred to as traditional, is characterized by the chemical interaction of sulfate-rich soil or water with the hydrated cement matrix. Soils containing sodium, potassium, magnesium, and calcium sulfates are the main sources of sulfate ions in groundwater. Another source of sulfates is industrial wastewater, e. g. from the chemical or agricultural industry [8–10].

External sulfate attack occurs if the following three factors coexist:

- a. high permeability of the cement composite/concrete structure;
- b. sulfate-rich environment;
- c. the presence of water.

The first step of the external sulfate attack is the penetration of sulfate ions from the outer environment into the concrete. Consequently, the transformation of calcium hydroxide and/or calcium silicate hydrate (C-S-H) to gypsum takes place according to specific reactions [11]. This process causes the hydrated cement matrix to expand, crack, and peel. Gypsum is prevalingly formed by the reaction of sulfate ions with Ca(OH)<sub>2</sub> or calcium silicate hydrate (C-S-H). However, a more important manifestation of sulfate attack is the reduction of the strength and cohesiveness of the developed cement matrix by the decalcination of C-S-H.

The STN EN 197–1 [4] defines sulfate-resistant cement for general use as a cement whose properties meet the requirements for sulfate resistance. Additional requirements for sulfate-resistant cement are the sulfate content (as SO<sub>3</sub>) in cement, the C<sub>3</sub>A content in clinker, and the pozzolanicity of cement. The seven sulfate-resistant cements for general use are divided into 3 main types as follows:

1. Sulfate-resistant Portland cement with different C<sub>3</sub>A content in clinker:
  - C<sub>3</sub>A content in the clinker = 0% by weight, designated as CEM I-SR 0
  - C<sub>3</sub>A content in the clinker ≤3% by weight, designated CEM I-SR 3
  - C<sub>3</sub>A content in the clinker ≤5% by weight designated CEM I-SR 5;

2. Sulfate-resistant blast furnace cement without the requirement for  $C_3A$  content in clinker: either designated CEM III/B-SR or CEM III/C-SR;
3. Sulfate-resistant pozzolanic cement with  $C_3A$  content in a clinker  $\leq 9\%$  by weight: designated either CEM IV/A-SR or CEM IV/B-SR.

Sulfate-resistant types of cement, defined by the European standards [12, 13] must therefore meet the criteria for  $C_3A$ ,  $SO_3$ , and pozzolan content, without additional requirements for verifying their resistance. The standards discriminate “new generation cements”, which, despite not meeting the criteria in the defined standards, can show high sulfate resistance. Other ways to increase sulfate resistance are “innovative cement kinds” either hybrid cement [14] or as in this case, high-fine pozzolanic addition present in the cement. Such a cementitious composition with active submicron-sized pozzolanic particles forms a dense microstructure, poor in  $Ca(OH)_2$  but rich in gel hydration products that are specified by low-permeable pore structure.

There are various ways to verify chemical resistance; a) long-term, multi-year exposures to aggressive media [15, 16] and b) accelerated [17, 18]. However, there is no known, unified and universally valid testing methodology worldwide. Therefore, the efficiencies of determinations are not mutually comparable; in addition, the same material systems and exposure conditions are not always tested. The final output of each method is a knowledge on the increased chemical (e. g. sulfate) resistance of the verified cement system compared to the reference. It is still problematic to determine the coherence between the laboratory test results (a or b) and the actual resistance time of concrete used in the field for decades of years either in aggressive soil or groundwater.

The objective of this chapter is to characterize the sulfate resistance of submicron-sized pozzolan containing NONRIVAL CEM I 52,5 N with up to 8% wt.  $C_3A$  and to explain the cause for its comparability with sulfate-resistant CEM I 42.5 SR 0 with none of  $C_3A$ .

## 2. Experimental procedure

### 2.1 Materials

Ordinary Portland cement (CEM I 42.5 N) as a reference cement 1 (PC), sulfate-resistant CEM I 42.5 R - SR 0 as a reference cement 2 (SR) and NONRIVAL CEM I 52.5 N as experimental cement (N), were used. Both reference types of cement were produced according to STN EN 197-1 [4] and NONRIVAL CEM I 52.5 N was prepared according to the internal cement plant's standard and SK technical assessment.

### 2.2 Casting and curing

Mortar specimens of size (40 × 40 × 160) mm with the cement to standard sand weight ratio of 1: 3 and water to cement ratio of 0.5, were prepared. The mortars were cured 24 hours at 20°C/95% R.H.-air in a climate chamber. After demolding, they were kept 27 days in water at (20 ± 1) °C (basic curing – BC), and then either in water (reference medium) and aggressive 5% sodium sulfate solution (33,800 mg  $SO_3$  per liter) for 5-year exposure, respectively.

The tests of chemical resistance were conducted by the own methodology of “partially accelerated tests” [14] based on keeping the mortars in strongly

over-concentrated aggressive solutions for a sufficiently long time. The aggressive environment was specified in the following way: every 1 cm<sup>2</sup> of the exposed area of prism must be in permanent contact with at least 10 cm<sup>3</sup> of 5% wt. Na<sub>2</sub>SO<sub>4</sub>. A sulfate solution and reference water were refreshed every 30 days within 90 days of testing, every 45 days between 90 and 365 days, and every 60 days up to 5 years of exposure, respectively.

### **2.3 Testing procedures for cement**

All types of cement were tested for chemical composition by STN EN 196–2 [19]; consequently, the Bogue mineral composition was determined. Standard consistency, initial and final set, and soundness were verified by STN EN 196–3 [20]. After 2- and 28-day cure, flexural and compressive strengths of the mortars were obtained according to STN EN 196–1 [21].

### **2.4 Testing procedures for mortars conducted to sulfate attack**

The consistency according to STN EN 1015–3 [22] represents the value of the degree of pouring of the formed fresh mortar after 15 strokes of the compaction table. The bulk density was determined in one-liter container according to STN EN 1015–6 [23]. Based on the consistency results, all mortars fall into the category of plastic mortar, according to STN EN 1015–6. Air content in the mortar was determined by the pressure method according to STN EN 1015–7 [24].

The hardened mortars were during 5 years of sulfate exposure continuously tested for length changes [25], dynamic modulus of elasticity (DME) [26], and periodically for flexural and compressive strength [21]. After destructive tests, the microstructure and pore structure were identified by X-ray diffraction analysis (XRD), thermal analysis (TG-DTA), mercury intrusion porosimetry (MIP), and scanning electron microscopy (SEM) techniques. The grounded mortars were sieved through a 0.063 mm mesh to receive the powder suitable for testing. For the XRD, the Philips diffractometer was used in a 2 $\Theta$  range of 5–65°. CuK $\alpha$  radiation and Ni - filter was applied. Thermal analysis was performed on the Netzsch apparatus STA 449 F3 Jupiter in the air at a heating rate of 10°C/min. Basic parameters of the pore structure were identified by MIP using the high-pressure porosimeter Quantachrome Poremaster 60 GT. The JEOL 7500F device was used to study microstructure by scanning electron microscopy. Chemical composition, with special emphasis on the SO<sub>3</sub> content bound in the cement matrix, was estimated by the analytical procedures given in STN EN 196–2 [19].

## **3. Results and discussion**

### **3.1 Basic properties of cements and mortars after basic curing**

Chemical composition of the cements (N – NONRIVAL, SR – sulfate-resistant, and PC – reference Portland) is listed in **Tables 1** and **2**. The content of chloride ions 0.09% wt. in N-cement, 0.07% wt. in SR cement, and 0.06% wt. in PC-cement, is almost the same. The mineral composition was calculated by the Bogue formulas (**Table 2**).

All types of cement meet the requirements for chemical properties, which are given as characteristic values in STN EN 197–1 [4] based on a loss on ignition (LOI), which is less than 5% by weight, an insoluble residue, which is less than 5% by weight, a sulfate content (expressed as SO<sub>3</sub>) of less than 4% by weight and a chloride content of less than 0.10% wt.

| Cement | LOI (% wt.) | Ins. res. (% wt.) | Content of the component (% wt.) |      |                                |                                |     |                 |                       |
|--------|-------------|-------------------|----------------------------------|------|--------------------------------|--------------------------------|-----|-----------------|-----------------------|
|        |             |                   | SiO <sub>2</sub>                 | CaO  | Al <sub>2</sub> O <sub>3</sub> | Fe <sub>2</sub> O <sub>3</sub> | MgO | SO <sub>3</sub> | Na <sub>2</sub> O eq. |
| N      | 1.9         | 4.06              | 19.9                             | 59.9 | 4.95                           | 3.06                           | 1.3 | 3.43            | 1.2                   |
| SR     | 3.5         | 2.22              | 21.3                             | 61.0 | 2.93                           | 4.59                           | 1.6 | 2.40            | 0.4                   |
| PC     | 1.6         | 2.33              | 17.9                             | 61.5 | 7.28                           | 2.96                           | 1.9 | 3.49            | 0.8                   |

**Table 1.**  
 Chemical composition of the cements.

| Cement | Mineral composition (% wt.) |                  |                  |                   |
|--------|-----------------------------|------------------|------------------|-------------------|
|        | C <sub>3</sub> S            | C <sub>2</sub> S | C <sub>3</sub> A | C <sub>4</sub> AF |
| N      | 44.64                       | 23.64            | 7.94             | 9.31              |
| SR     | 53.36                       | 20.81            | 0.00             | 13.97             |
| PC     | 50.63                       | 13.36            | 14.28            | 9.01              |

**Table 2.**  
 Mineral composition of the cements.

The content of SO<sub>3</sub> in SR cement is less than 3.5% by weight, which meets the additional requirements for sulfate-resistant cement for general use according to STN EN 197-1 [4]. The values of SO<sub>3</sub> content in N- and PC-cement are higher than in SR-cement. In the case of N-cement it is approaching and in the case of PC-cement it reaches the criterion for the maximum SO<sub>3</sub> content in sulfate-resistant cement up to 3.5% by weight. SR-cement is characterized by the highest proportion of calcium silicates (C<sub>3</sub>S and C<sub>2</sub>S) and tetra calcium aluminate ferrite (C<sub>4</sub>AF) compared to N- and PC-cement and C<sub>3</sub>A content of 0.00% by weight. Zero C<sub>3</sub>A content in SR-cement meets the additional requirement for C<sub>3</sub>A content for sulfate-resistant cement of type SR 0 according to STN EN 197-1 [4]. Many C<sub>3</sub>S and C<sub>2</sub>S phases in SR-cement are an opportunity for the formation of larger amounts of Ca(OH)<sub>2</sub> during hydration, which by its crystalline character markedly affects the formed pore structure and susceptibility to chemical degradation of a cement matrix. N- and PC-cements contain 7.94% wt. and 14.31% wt. C<sub>3</sub>A, respectively. Both exceed the requirement for a maximum C<sub>3</sub>A content of up to 5% by weight for the type of sulfate-resistant cement CEM I - SR 5 and therefore they cannot be marked as sulfate-resistant types of cement according to the criteria of STN EN 197-1 [4].

The comparison of basic cement properties is reported in **Table 3**. Rheological characteristics of the mortars are presented in **Table 4**. Early- and 28-day strength in basic water curing (BC) is introduced in **Table 5**. N-cement is characterized by the largest specific surface area, normal consistency, flexural and compressive strength values compared to SR- and PC-cement. It is assumed that due to the

| Cement | Specific surface area (m <sup>2</sup> /kg) | Normal consistency (% wt.) | Initial and final set (min) | Soundness (mm) |
|--------|--|----------------------------|-----------------------------|----------------|
| N      | 766.9                                      | 35.0                       | 205/270                     | 0.5            |
| SR     | 354.9                                      | 27.2                       | 185/225                     | 1.0            |
| PC     | 472.4                                      | 30.8                       | 265/315                     | 0.0            |

**Table 3.**  
 Specific surface area and the properties of fresh cement mixtures.

| Mortar | Consistency (mm) | Volume density (kg/m <sup>3</sup> ) | Air content (% vol.) |
|--------|------------------|-------------------------------------|----------------------|
| N      | 151              | 2236                                | 4.6                  |
| SR     | 186              | 2205                                | 6.3                  |
| PC     | 142              | 2239                                | 4.8                  |

**Table 4.**  
*Rheological properties of the fresh mortars.*

| Mortar | Strength (MPa) |        |          |        |
|--------|----------------|--------|----------|--------|
|        | compressive    |        | flexural |        |
|        | 2-day          | 28-day | 2-day    | 28-day |
| N      | 37.1           | 72.2   | 7.4      | 9.2    |
| SR     | 26.2           | 52.8   | 4.7      | 8.4    |
| PC     | 31.5           | 58.0   | 6.2      | 8.5    |

**Table 5.**  
*Flexural and compressive strength of the mortars.*

higher specific surface area of the N-cement, a denser and therefore less permeable microstructure of the mortar is formed during hydration, as a result of which its sulfate resistance can increase in an aggressive environment.

The normal consistency of the cements represents the water content per amount of cement in the cement paste required to achieve the standardized density [18], expressed in percentage. A higher value of the normal consistency of the N-cement means that a higher amount of water is required to achieve the same density of cement paste than with SR- and PC- cement. The cements meet the criterion for the initial setting according to the requirements of STN EN 197-1 [4] over 60 minutes (strength class 42.5 R) in the case of SR- and PC- cement and over 45 minutes (strength class 52.5 N) in the case of N-cement. The final setting time is not specified by the standard. All types of cement meet the criterion for soundness (volume stability) according to the requirements of STN EN 197-1 [4] that has to be below 10 mm.

The mortars are characterized by different consistency, bulk density, and air content. SR-mortar shows the highest consistency (plasticity 186 mm), lower the N- mortar (151 mm), and the densest was PC mortar (142 mm). In the other words SR- mortar needs less mixing water to achieve the same consistency as N- and PC- mortar. The most probable cause is that the missing tricalcium aluminate (C<sub>3</sub>A) phase in SR-cement enables lower binding water consumption to the hydrates of calcium aluminate origin (C-A-H hydrated phase). The rich calcium silicate phase alone is not able to absorb so much water at the beginning of hydration and therefore this cement system is more plastic. This experiment did not deal with adjusting the mortars to the same consistency. The mortars were made with the constant water-to-cement ratio 0.5, and therefore all results are from this viewpoint comparable.

The 28-day volume density, as well as dynamic modulus of elasticity of N-, SR- and PC-mortar, are 2250 kg/m<sup>3</sup>, 2290 kg/m<sup>3</sup>, and 2260 kg/m<sup>3</sup> as well as 45.3 GPa, 41.8 GPa and 43.1 GPa, respectively. The related strength parameters are reported in **Table 5**.

All cements meet the criteria for minimum compressive strength after 2 and 28 days (initial and standard strengths) according to the requirements of STN EN

197–1 [4]. The mortars with cements of strength class 42.5 R (PC- and SR-mortar) must meet the criteria for compressive strength after 2 days more than 20 MPa and after 28 days more than 42.5 MPa, as required by the STN EN 197–1 [4]. The N-mortar made of high-strength NONRIVAL CEM I 52.5 N meets the strength class of 52.5 N achieving compressive strength after 2 days above 20 MPa and after 28 days above 52.5 MPa. Chemical composition of the mortars after 28 days of basic curing (BC) in the water at  $(20 \pm 1)^\circ\text{C}$  is reported in **Table 6**.

The PC-mortar is characterized by the highest, N-mortar by lower, and SR-mortar by the lowest  $\text{SO}_3$  content. This finding is in good agreement with the  $\text{SO}_3$  content observed in the types of cement (**Table 1**). Changes in the  $\text{SO}_3$  contents are one of the important subjects of monitoring the effect of sulfate attack on the mortars over 5-year exposure time. Basic parameters of the pore structure of mortars after BC are listed in **Table 7**. The highest specific surface area of all open pores, the lowest median radius of all pores within the radii range 1.82 nm to 0.534 mm and micro-pores between 1.82 nm to 5.25  $\mu\text{m}$  points for the presence of the largest share of micro-pores in N-mortar compared to SR- and PC-mortar. This fact is reflected in the formation of a denser, less permeable pore structure of N-mortar also characterized by the lowest total pore volume, total porosity, and the lower permeability coefficient by one order of magnitude compared to SR- and PC-mortar.

The mineral composition of individual cement types together with their fineness generally influences the microstructure formation during hydration, from which depends the condition of the developed pore structure of mortars. The character of the pore structure subsequently determines the permeability of the mortar against the penetration of sulfate solution into the internal structure. The impermeable pore structure is one of the important properties of the cement matrix in terms of environmental resistance.

Explanatory notes to the **Table 7**: specific surface area of all measured pores - SSA, total pore volume - VTP in the measured range of porosimeter 1,82 nm - 0,534 mm, the median radius of micro-pores in the range of 1,82 nm - 5,25  $\mu\text{m}$ , that of macro-pores between 5,25  $\mu\text{m}$  - 0,534 mm and total pores within pore radii of

| Mortar | Ign. loss (% wt.) | Content of the component (% wt.) |       |                                |                                |      |                 |                 |                       |
|--------|-------------------|----------------------------------|-------|--------------------------------|--------------------------------|------|-----------------|-----------------|-----------------------|
|        |                   | SiO <sub>2</sub>                 | CaO   | Al <sub>2</sub> O <sub>3</sub> | Fe <sub>2</sub> O <sub>3</sub> | MgO  | SO <sub>3</sub> | Cl <sup>-</sup> | Na <sub>2</sub> O eq. |
| N      | 7,93              | 73.08                            | 15.28 | 0.95                           | 1.14                           | 0.38 | 0.82            | 0.03            | 0.15                  |
| SR     | 8,45              | 68.99                            | 18.43 | 0.91                           | 1.80                           | 0.55 | 0.69            | 0.02            | 0.07                  |
| PC     | 7,59              | 70.99                            | 16.69 | 1.23                           | 1.14                           | 1.04 | 0.92            | 0.02            | 0.13                  |

**Table 6.**  
 28-day chemical composition of the mortars.

| Mortar | SSA (m <sup>2</sup> /g) | VTP (cm <sup>3</sup> /g) | Pore median of   |                  |                  | TP (%) | CP (m/s)              |
|--------|-------------------------|--------------------------|------------------|------------------|------------------|--------|-----------------------|
|        |                         |                          | total pores (nm) | micro-pores (nm) | macro-pores (nm) |        |                       |
| N      | 6.93                    | 0.070                    | 40.10            | 30.80            | 9.30             | 13.70  | $7.0 \times 10^{-11}$ |
| SR     | 4.02                    | 0.077                    | 67.90            | 43.21            | 24.69            | 16.20  | $3.0 \times 10^{-10}$ |
| PC     | 4.85                    | 0.079                    | 59.99            | 42.24            | 17.75            | 14.92  | $2.0 \times 10^{-10}$ |

**Table 7.**  
 Pore structure parameters of the mortars after 28-day basic curing.

1,82 nm - 0,534 mm, total porosity TP estimated among pore radii between 1,82 nm - 0,534 mm and calculated coefficient of permeability CP for water valid within the scope of porosimetry measurements.

### 3.2 Partially accelerated sulfate resistance test

After 28-day BC in the water at  $(20 \pm 1) ^\circ\text{C}$  when the mortars reached naturally developed physical-mechanical properties, microstructure, and pore structure, one-half of the mortars were immersed in 5% sodium sulfate solution and the second half of the specimens was still left in the reference water. The partially accelerated test of sulfate resistance of cement mortar is based on long-term, usually two-year, but in this case, even five-year monitoring of a) changes of physical and mechanical properties by non-destructive and destructive testing and b) changes of microstructure and pore structure in 5% sodium sulfate. The obtained results from the sulfate exposure were compared to each other according to the type of cement as well as with those coming from the reference water.

#### 3.2.1 Changes in physical and mechanical properties

**Figure 1** shows the changes in dynamic modulus of elasticity (DME) of different mortars (N – NONRIVAL CEM I 52.5 N, SR - sulfate-resistant, and PC – Portland cement) during 5-year exposure in aggressive 5%  $\text{Na}_2\text{SO}_4$  solution and reference water after 28 days BC. **Figure 2** presents the percentage decrease in the DME of N-, SR- and PC-mortar in the sodium sulfate compared to the reference water.

The N-mortar and SR-mortar show comparable DME changes, while the PC-mortar is subject to the harmful effect of aggressive sulfate attack.

The length changes of mortars during the 28-day BC and 5-year exposure in 5%  $\text{Na}_2\text{SO}_4$  and water are illustrated in **Figure 3**. The PC-mortar expands significantly during 5 years of exposure in sulfate up to the level of 18.131 mm/m. This expansion gives evidence of the aggressive action of sodium sulfate. Visual observations of the

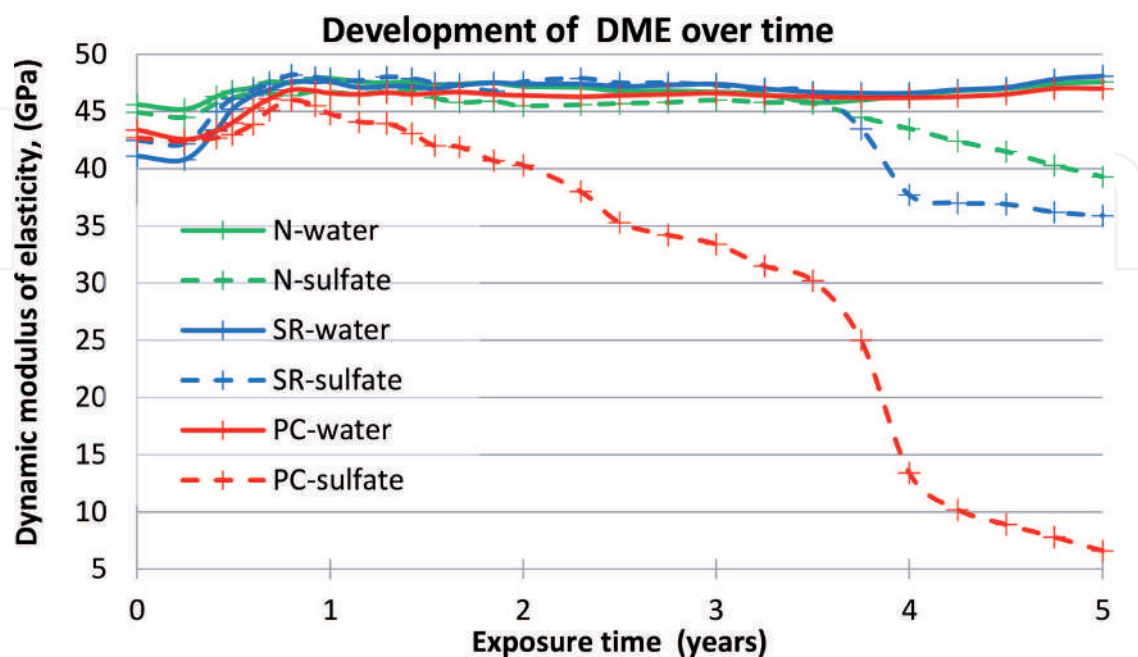


**Figure 1.** Changes in dynamic modulus of elasticity of the mortars over time.

### Comparison of the percentage losses in DME

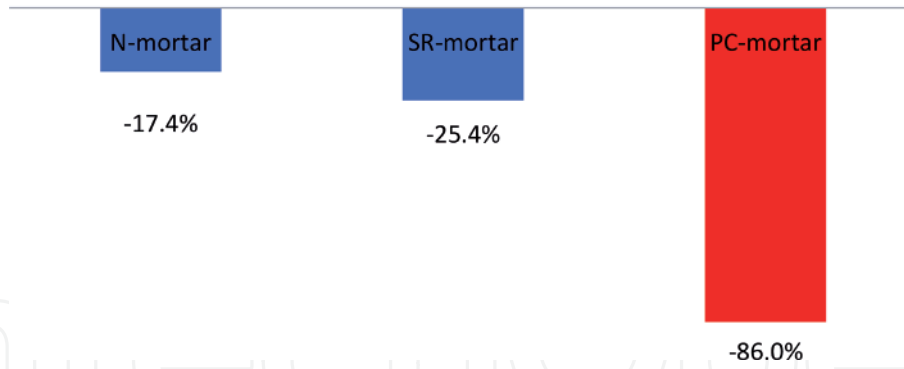


**Figure 2.** Percentage loss of dynamic modulus of elasticity of N-, SR- and PC-mortar after 5-year exposure in sodium sulfate compared to the reference water.

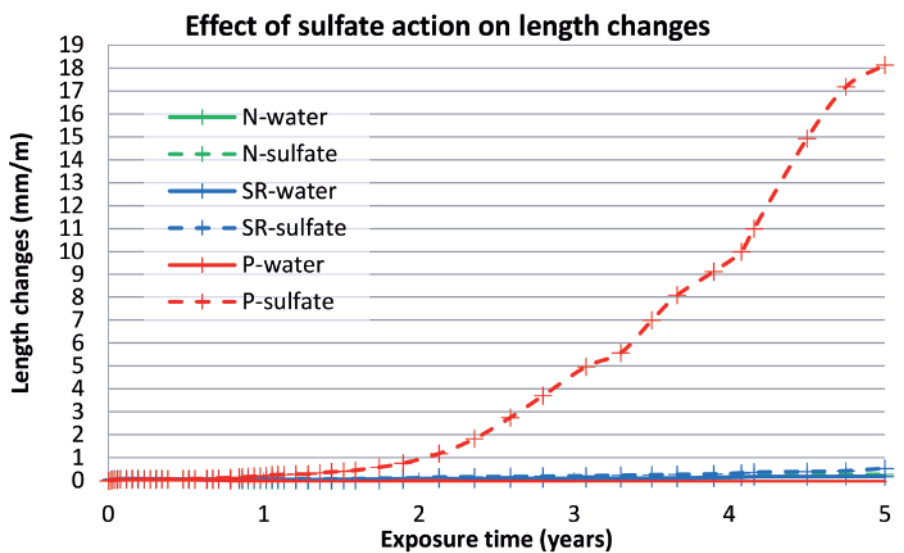


**Figure 3.** Length changes of the mortars over time.

PC-mortar show the cracks on the surface of the test prisms, which propagate into the mortar interior over the time. The cracks were mainly observed in the rounding of the prism corners by the loss of the peeled cement matrix. This fact is confirmed by the photo in **Figure 4**.

**Figure 5** shows the decrease in compressive strength of all mortars stored in sulfate for 5 years compared to reference water. The largest strength loss is recorded in PC-mortar.

The changes in flexural strength of SR- and N-mortar exposed for 5 years in sulfate are negligible (**Figure 6**). The PC-mortar immersed for the same time in aggressive solution significantly loses the flexural strength to a critical value of 2.8 MPa from 9.6 MPa in water storage. The related loss of flexural strength of PC-mortar is 70.8% wt. (**Figure 6**).

The evaluation of the strength characteristics results in the following partial findings: while N- and SR-mortar show similar sulfate resistance, the apparent strength losses of PC-mortar confirm the well-known evidence that Portland cement is unsuitable for use in a sulfate environment. N-mortar still reaches a sufficiently high strength after 5 years of sulfate attack.



**Figure 4.**  
*View on the disturbed surface of PC-mortar exposed for 5 years in 5% sodium sulfate solution.*

**Percentage loss in compressive strength between sulfate and water storage**

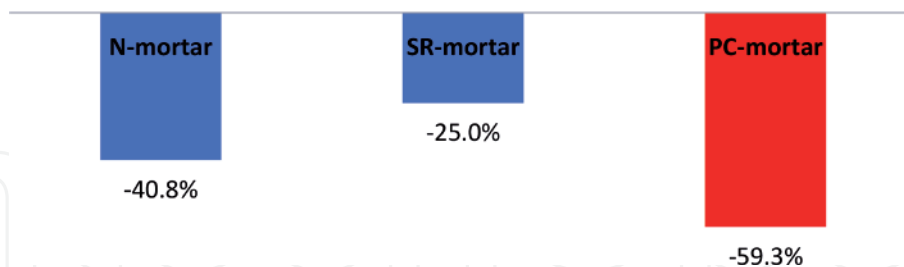


**Figure 5.**  
*Percentage loss in compressive strength of N-, SR- and PC-mortar after 5- year exposure in sodium sulfate compared to the reference water.*

### 3.2.2 Changes in microstructure and pore structure

Changes in the physical and mechanical properties of mortars during long-term water and sulfate exposure are a reflection of the formed microstructure and developed pore structure, which mainly depend on the composition and properties of the used types of cement. The mortar's microstructure was studied every year till the end of the experiment by a XRD, thermal and chemical analysis. After 5-year sulfate exposure, the pore structure was identified by MIP and the microstructure observed by the SEM technique. These results serve to elucidate the mechanism of sulfate resistance with special regard to revealing a nature of the sulfate resistance

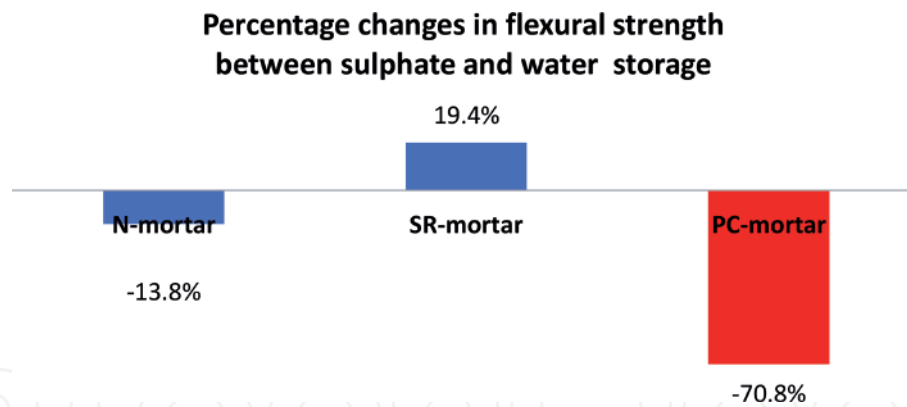


**Figure 6.**  
 Percentage changes in flexural strength of N-, SR- and PC mortar after 5-year exposure in sodium sulfate solution compared to the reference water.

of N-mortar. This section presents 5-year results that have made a decisive contribution to clarifying the mechanism of sulfate resistance of NONRIVAL CEM I 52.5 N that is explained in Section 4.

### 3.2.2.1 X-ray diffraction analysis

XRD analysis determines the qualitative portion of minerals, from which it is not possible to quantify their content, but a comparison of intensity and number of diffractions gives an approximate picture of the mineral content in the mortars. The presence of gypsum (G) and/or ettringite (E) is a decisive indicator of sulfate attack. A comparison of X-ray records of N-mortar after 5 years of exposure in water and 5%  $\text{Na}_2\text{SO}_4$  is illustrated in **Figure 7**.

Comparison of X-ray records of SR-mortar and PC-mortar after 5 years of exposure in water and 5%  $\text{Na}_2\text{SO}_4$  is given in **Figures 8** and **9**, respectively.

After 5 years of exposure to sodium sulfate, the PC-mortar shows a high proportion of the formed gypsum (G:  $\text{CaSO}_4 \cdot 2\text{H}_2\text{O}$ ) as well as also ettringite (E:  $3\text{CaO} \cdot \text{Al}_2\text{O}_3 \cdot 3\text{CaSO}_4 \cdot 32\text{H}_2\text{O}$ ) as reaction products of the sulfate attack.

**Figure 10** confirms that SR- and N- mortar are characterized by a negligible amount of G and E. Besides these products, every mortar contains portlandite [ $\text{CH}$ :  $\text{Ca}(\text{OH})_2$ ] and quartz coming from a standard sand Q:  $\text{SiO}_2$ .

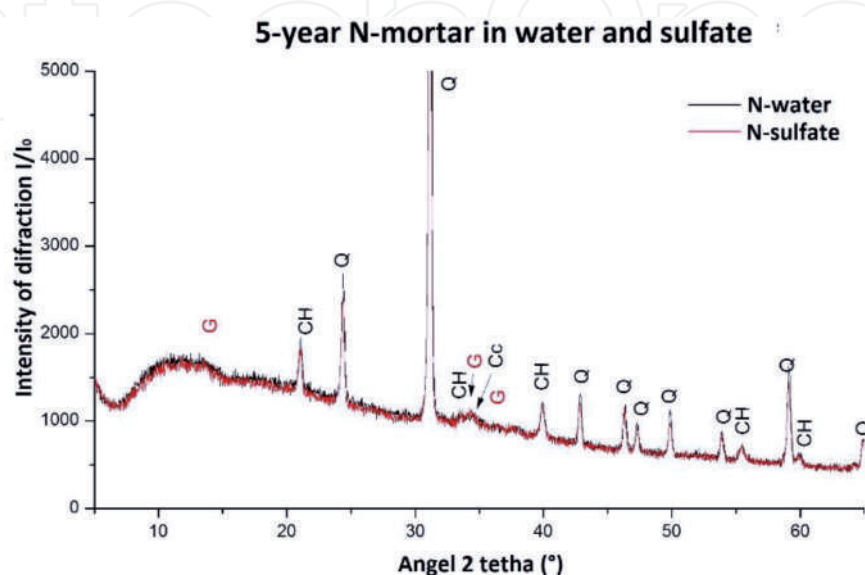


**Figure 7.**  
 Mineral composition of 5-year N-mortar in water and sulfate.

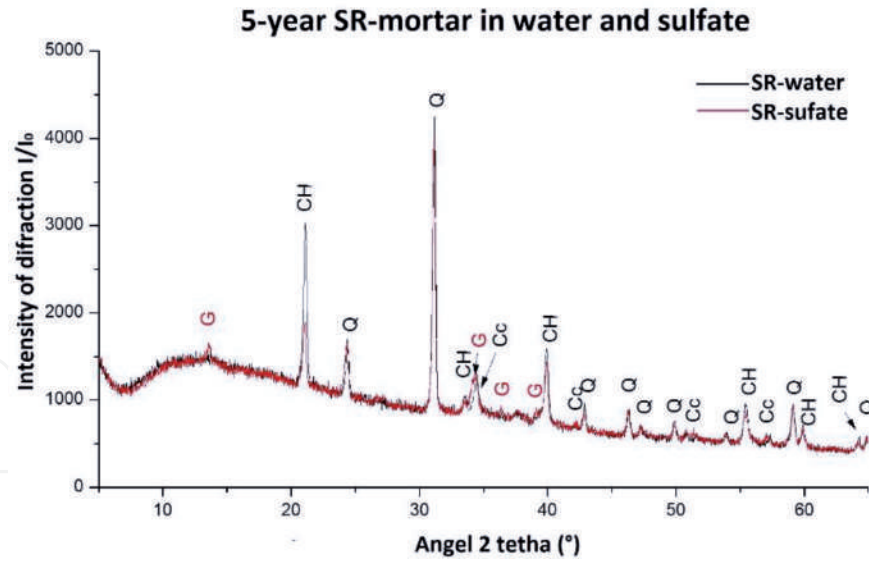


Figure 8. Mineral composition of 5-year SR-mortar in water and sulfate.

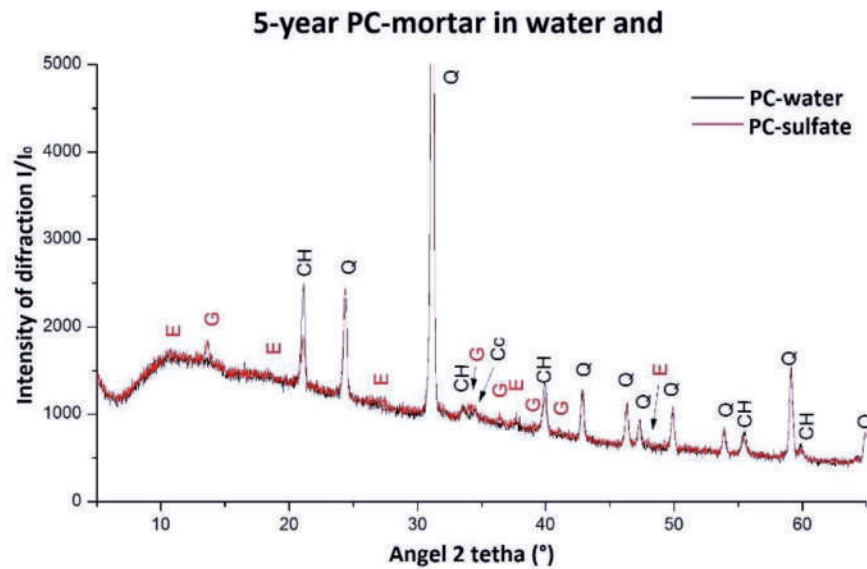


Figure 9. Mineral composition of 5-year PC-mortar in water and sulfate.

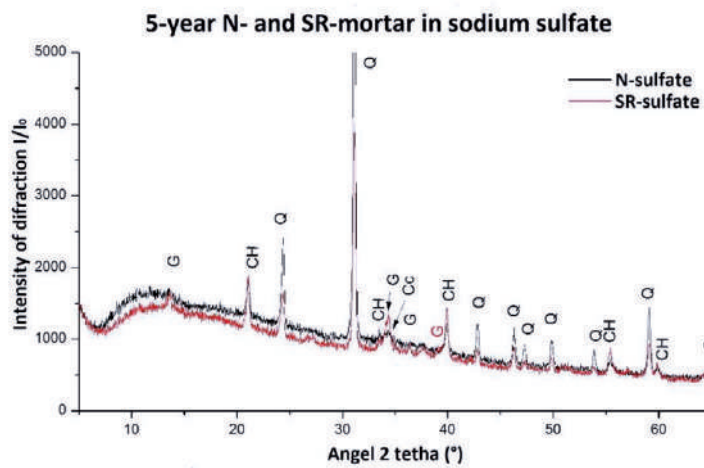
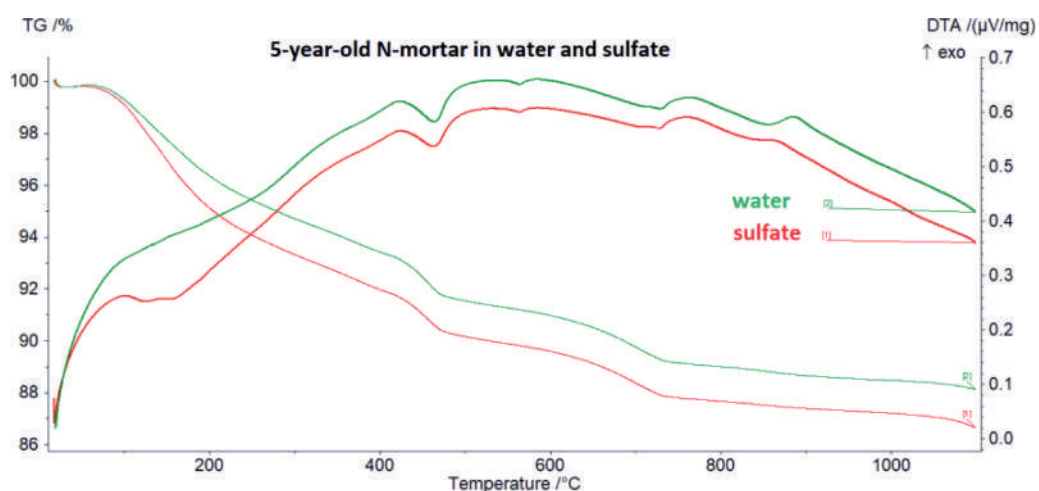


Figure 10. Comparison of X-diffraction patterns of 5-year N- and SR-mortar from sodium sulfate.

### 3.2.2.2 Thermal analysis

Thermal analysis (TG-DTA) qualitatively and quantitatively determines the proportion of cement hydration products and products of sulfate attack in the mortars based on the observed mass losses and the relevant endotherms in the respective temperature ranges. The dissociation energy provides information on the incorporation strength of individual releasable components identified by the XRD technique.

The results of the thermal analysis of the 5-year mortars are shown in **Figures 11–13**. The percentage values of present phases and related dissociation energies are reported in **Table 8**. According to **Table 8**, the N-mortar in water contains the lowest proportion of portlandite -  $\text{Ca}(\text{OH})_2$ . All mortars show a decrease in portlandite content after 5 years of exposure to sodium sulfate compared to water. The lowest 0.29% wt. loss is observed in the N-mortar. PC-mortar is characterized by portlandite decrease 3.25% wt. and SR-mortar 4.93% wt. The difference in energy required for the endothermic reaction in the temperature range of 100–200°C in sulfate solution and water can be taken as a measure of gypsum and ettringite incorporation in the mortar's microstructure. The energy value for N-mortar is 3.05 J/mg, for SR-mortar 13.92 J/mg and for PC-mortar 22.83 J/mg. The quantitative representation of G and E as the



**Figure 11.**  
*Comparison of TG-DTA plots of 5-year-old N-mortar in water and sulfate.*

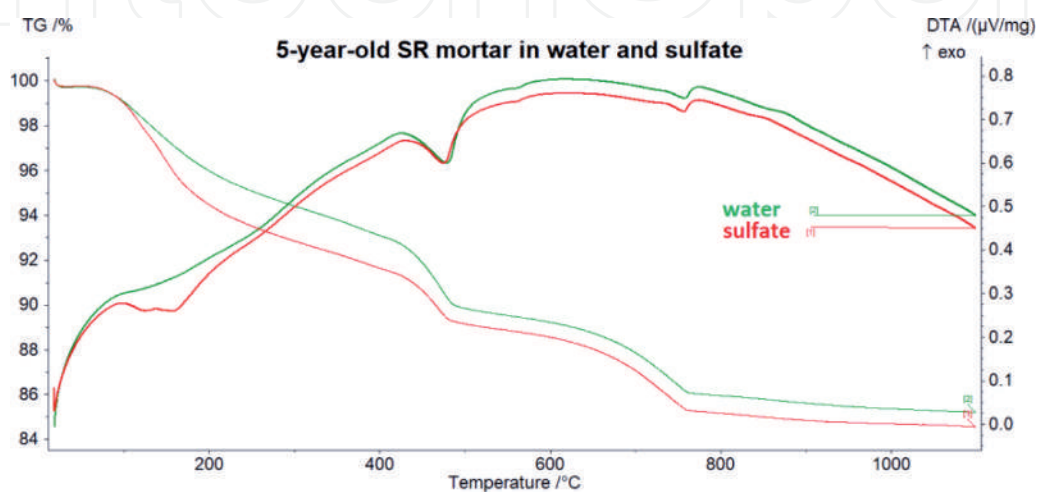


**Figure 12.**  
*Comparison of TG-DTA plots of 5-year-old SR-mortar in water and sulfate.*

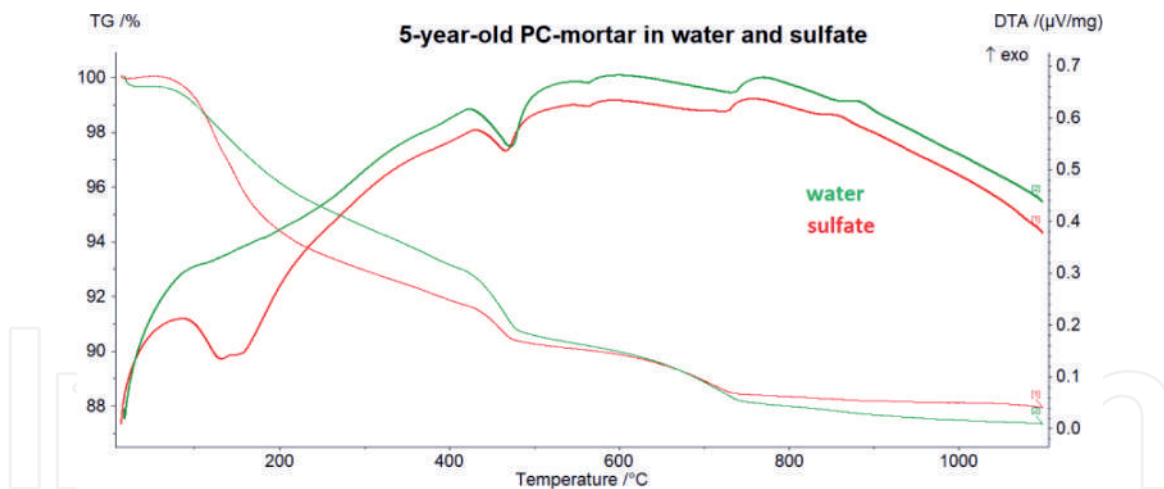


**Figure 13.**  
Comparison of TG-DTA plots of 5-year-old PC-mortar in water and sulfate.

| Mortar     | Total ignition loss between (20–1100) °C (% wt.) | Content of                  |                             | Loss in Ca(OH) <sub>2</sub> in sulfate (% wt.) | Dissociation energy between (100–200) °C (J/mg) | Energy difference between (100–200) °C (J/mg) |
|------------|--|-----------------------------|-----------------------------|--|---|---|
|            |  | Ca(OH) <sub>2</sub> (% wt.) | Ca(CO) <sub>3</sub> (% wt.) |  |   |   |
| N-water    | 11.86  | 10.03                       | 6.46                        | 0.29   | 0.00  | 3.05  |
| N-sulfate  | 13.35  | 9.74                        | 6.71                        |  | 3.05  |   |
| SR-water   | 14.85  | 15.91                       | 9.14                        | 3.25   | 0.00  | 13.92   |
| SR-sulfate | 15.44  | 12.66                       | 9.1                         |  | 13.92   |   |
| PC-water   | 12.64  | 13.07                       | 5.98                        | 4.93   | 0.00  | 22.83   |
| PC-sulfate | 12.06  | 8.14                        | 4.43                        |  | 22.83   |   |

**Table 8.**  
Phase composition of the mortars after 5 years of exposure in 5% sodium sulfate solution and reference water at (20 ± 1) °C.

products of sulfate attack is in N-mortar and SR-mortar equally marginal and even the same. On the contrary, PC-mortar shows at the same time the evident presence of gypsum and ettringite.

PC-mortar contains the most quantum of reaction products of the sulfate attack compared to SR- and N-mortar as previously approved by the X-ray analysis. TG-DTA data indicate the equally high sulfate resistance of the N- and SR-mortar.

### 3.2.2.3 Chemical analysis

The chemical analysis was used to compare the oxide content in mortars with a focus mainly on the SO<sub>3</sub> content. The analysis of the chemical composition does not unambiguously determine the proportion of sulfate attack reaction products but a comparison of the SO<sub>3</sub> content bound in these reaction products gives a picture of the intensity of the acting sulfate aggressiveness. The increase in SO<sub>3</sub> content in the mortar is due to the penetration of sulfate ions from the solution into the internal matrix and the transformation of calcium hydroxide and/or calcium silicate hydrate resp. calcium aluminate hydrate (C-S-H/C-A-H) to CaSO<sub>4</sub>·2H<sub>2</sub>O and 3CaO·Al<sub>2</sub>O<sub>3</sub>·3CaSO<sub>4</sub>·32H<sub>2</sub>O [1–3]. A typical symptom of sulfate attack of cement mortar is an increased SO<sub>3</sub> content, which announces the presence of gypsum and ettringite.

This fact is confirmed by the increase of  $\text{SO}_3$  in the mortars during 5 years of exposure to 5%  $\text{Na}_2\text{SO}_4$  (**Figure 14**). The content of  $\text{SO}_3$  is in the N-, SR- and PC-mortar after 28-day BC was 0.82%, 0.69% and 0.92% wt., respectively. The 5-year exposure records an increase in the bound  $\text{SO}_3$  content to the value of 3.60% wt. in N-mortar, 3.75% wt. in SR-mortar and 6.20% wt. in PC-mortar, while the content of  $\text{SO}_3$  in 5-year water storage is 1.54% wt. for N-mortar, 1.31% wt. for SR-mortar and 1.65% wt. for PC-mortar.

The chemical composition of the studied mortars with the attention focused on the typical symptom of sulfate attack - the  $\text{SO}_3$  content - shows that N- and SR- mortar after 5-year exposure in 5%  $\text{Na}_2\text{SO}_4$  are equally characterized by a slight increase in the bound  $\text{SO}_3$  content. In contrast, PC-mortar shows at the same time an evident increase of  $\text{SO}_3$ . Bearing in mind the previous findings of XRD and thermal analysis, chemical analysis points to the fact that the sulfate resistance of the N- and SR-mortar is very similar, even the same, and that both types of cement could be, from this point of view, fully comparable.

### 3.2.2.4 Pore structure

Basic pore structure parameters after 5 years of exposure to water and sulfate are listed in **Table 9**. The knowledge gained so far suggests that the reaction products (gypsum -G and ettringite -E) are formed during a sulfate attack, which first densifies the pore system. After depletion of the pore storage space by the voluminous G and E reaction products, a loss in the integrity of the formed microstructure starts to occur. In the advanced stage of the sulfate attack when there is observed a loss in mechanical properties and intense expansion, the mortar is characterized by the pore structure coarsening, in particular by the increased porosity. The increased porosity leads to the easier permeability of aggressive sulfate into the internal mortar body. The most evident indicators of these manifestations are the changes in the total pore median radius and total porosity. Changes in basic parameters of the pore structure have therefore a significant impact on the increased permeability.

N-mortar, regardless of the exposure either in water and or the aggressive sulfate, shows in the time horizon of the experiment only a slight pore structure coarsening

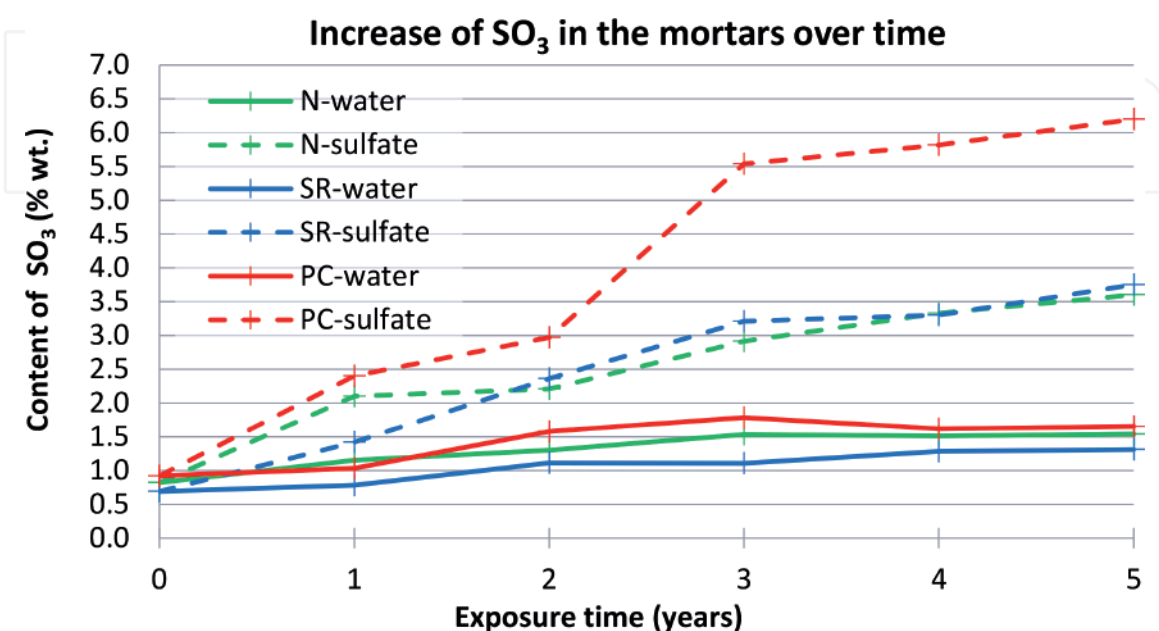


**Figure 14.** Changes in  $\text{SO}_3$  content in N-, SR- and PC-mortar immersed for 5 years in water and sodium sulfate after 28 days of basic curing in water.

| Mortar     | SPA<br>(m <sup>2</sup> /g) | TPV<br>(cm <sup>3</sup> /g) | Pore median radius     |                        | TP<br>(%) | CP (m/s)                |
|------------|----------------------------|-----------------------------|------------------------|------------------------|-----------|-------------------------|
|            |                            |                             | of total pores<br>(nm) | of micro-pores<br>(nm) |           |                         |
| N-water    | 7.10                       | 0.072                       | 33.52                  | 25.76                  | 15.41     | 2.0 × 10 <sup>-11</sup> |
| N-sulfate  | 5.41                       | 0.070                       | 38.84                  | 26.72                  | 14.32     | 1.2 × 10 <sup>-11</sup> |
| SR-water   | 6.02                       | 0.071                       | 64.95                  | 35.92                  | 14.95     | 8.0 × 10 <sup>-11</sup> |
| SR-sulfate | 5.90                       | 0.065                       | 65.40                  | 28.51                  | 13.49     | 7.0 × 10 <sup>-11</sup> |
| PC-water   | 6.86                       | 0.072                       | 37.84                  | 25.16                  | 15.25     | 3.0 × 10 <sup>-11</sup> |
| PC-sulfate | 5.71                       | 0.083                       | 292.0                  | 2.98                   | 17.03     | 1.6 × 10 <sup>-10</sup> |

*Explanatory notes – the same as for Table 7.*

**Table 9.**

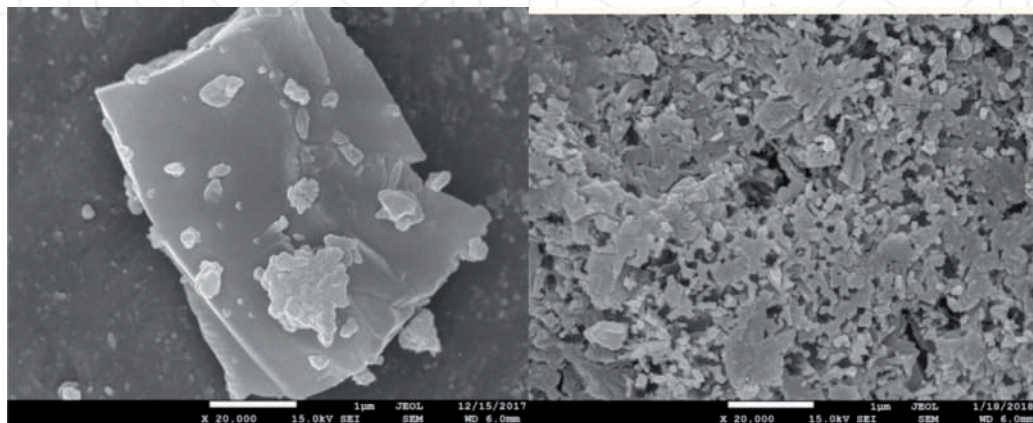
Comparison of basic parameters of the pore structure of 5-year mortars.

demonstrated by 1) slight decrease in the specific surface area of the measured pores, 2) slight decrease in the total pore volume, 3) a slight increase in the total pore and micro-pore median radii, 4) slight decrease in total porosity in the range of porosimeter measurements and 5) at unchanged permeability at the level of 10<sup>-11</sup>.

The permeability of the 5-year N-mortar kept in an aggressive sulfate solution is very close to the permeability of the mortar cured for the same time in the water. The reference SR-mortar shows very similar behavior as the N-mortar. The pore structure is not significantly influenced by the sulfate attack. By contrast with it, the PC-mortar is characterized by the typical consequences of sulfate attack proved mainly by an obvious increase in total pore median radius in the aggressive sulfate and the increase in permeability by one order of magnitude to 10<sup>-10</sup> m/s compared to reference water curing.

### 3.2.2.5 Scanning electron microscopy

The SEM visually identifies differences in the mortar microstructure between sulfate and water storage. Gypsum crystals have various shapes, most often acicular, prismatic or lenticular, while ettringite crystals are very thin and needle-like. The SEM images of N-mortar are shown in **Figure 15**, while those of PC-mortar in **Figure 16**. The SEM confirms the presence of crystalline Ca(OH)<sub>2</sub> in water as

**Figure 15.**

SEM image of N-mortar after 5-year exposure to water (left) and 5% solution of Na<sub>2</sub>SO<sub>4</sub> (right) (magnification 20,000 ×).

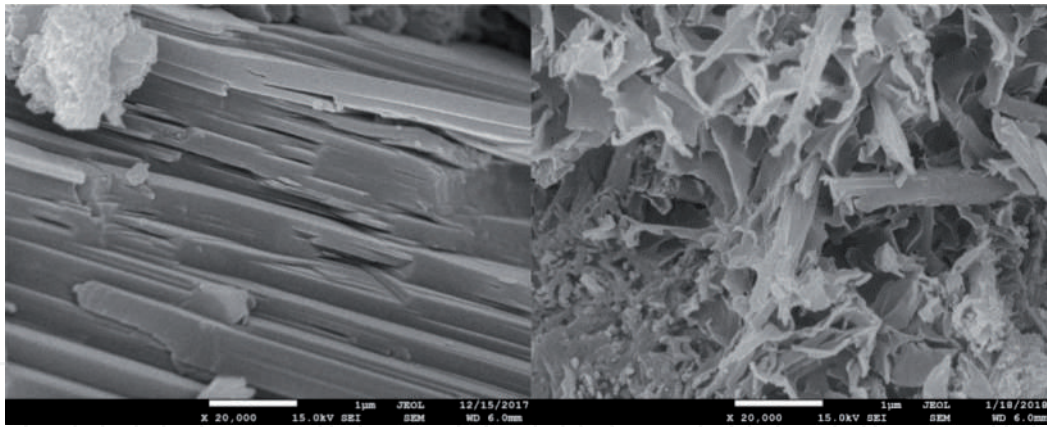


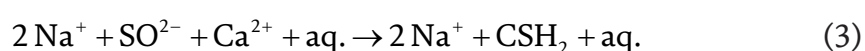
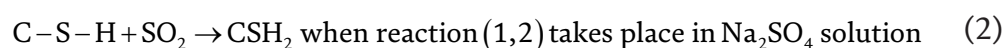
**Figure 16.** SEM image of PC-mortar after 5-year exposure to water (left) and 5% solution of  $\text{Na}_2\text{SO}_4$  (right) (magnification 20,000 ×).

well as the presence of gel hydration products of the C-S-H and C-A-H type with minimal occurrence of calcite, also taking into account differences depending on the type of cement. After 5 years of exposure to sodium sulfate, N-mortar records a negligible presence of rod-shaped crystallites (**Figure 15**), while the proportion of these reaction products, which most likely belong to gypsum and ettringite, is dominant in PC-mortar (**Figure 16**).

Summarization of the knowledge according to evaluation of the formed microstructure (XRD, TG-DTA, chemical analysis, SEM) and pore structure (MIP) of the mortars after 5 years of exposure is:

1. the N-mortar made with NONRIVAL CEM I 52.5 N is characterized by the same resistance to the aggressive sodium sulfate in terms of maintaining mechanical properties and structural integrity as the reference SR-mortar made with sulfate-resistant cement of none  $\text{C}_3\text{A}$  content;
  2. NONRIVAL CEM I 52.5 N, therefore, declares the same sulfate resistance as the sulfate-resistant CEM I 42.5 R – SR;
  3. PC-mortar shows disrupted structural integrity and confirms the well-known fact that ordinary Portland CEM I 42.5 R is not resistant to sulfate aggressiveness.
- 4. Explanation of the cause of sulfate resistance of NONRIVAL CEM I 52.5 N**

Degradation of the hydrated phase of the cement matrix by aggressive sulfate is characterized by the formation of gypsum  $\text{CaSO}_4 \times 2 \text{H}_2\text{O}$  ( $\text{CSH}_2$ ) together with ettringite  $3\text{CaO} \cdot \text{Al}_2\text{O}_3 \cdot 3\text{CaSO}_4 \cdot 32\text{H}_2\text{O}$  ( $\text{C}_6\text{AS}_3\text{H}_{32}$ ). Gypsum is formed by the reaction of sulfate ions with calcium hydroxide  $\text{Ca}(\text{OH})_2$  or with calcium silicate hydrate (C-S-H).



The formed gypsum binds with tricalcium aluminate ( $C_3A$ ) mainly to ettringite but monosulfate  $C_4ASH_{12}$  is also secondarily present.



Ettringite formation is accompanied by another minor reaction.



The damage mechanism is defined by gypsum and ettringite formation as the reaction products of aggressive sulfate action, being formed as high bulk, voluminous salts that cause destructive expansion of a cement stone. In the reaction 1 and 3, respectively active submicron-sized pozzolan present in NONRIVAL CEM I 52.5 N binds CaO from a supersaturated solution of  $Ca^{2+} OH^-$  by the pozzolanic reaction so that the formation of  $Ca(OH)_2$  and thus gypsum  $CSH_2$  is extensively eliminated.

Such limited  $Ca(OH)_2$  formation due to the pozzolanic reaction of submicron-sized addition subsequently prevents an excessive formation of generated gypsum, required for the ettringite development. The markedly reduced formation of  $Ca(OH)_2$  required for the reaction with sulfate ions (see Eq. 1) is the basic condition for suppressing the aggressive effect of sulfate solution on the NONRIVAL CEM I 52.5 N - containing mortar. This is regarded as a new effective reaction mechanism leading in the final effect to the increased sulfate resistance of NONRIVAL CEM I 52.5 N to the same level as that of a sulfate-resistant cement with none of  $C_3A$ .

Sulfate-resistant cement (SR) is characterized by blocking gypsum formation and subsequent ettringite due to the absence of  $C_3A$ , while NONRIVAL CEM 52.5 N blocks the formation of these reaction products by minimizing the  $Ca(OH)_2$  content by the presence of active submicron-based pozzolan. Both alternatives to preventing sulfate aggression mitigate the formation of  $CSH_2$  to a harmless content level but in a different way.

## 5. Conclusions

Five-year tests of the mortars in 5% sodium sulfate solution show the following key conclusions:

Sulfate resistance of cement NONRIVAL CEM I 52.5 N is the same as sulfate-resistant cement CEM I 42.5 R - SR. The cause lies in the thorough elimination of  $Ca(OH)_2$  formation by the active submicron-based pozzolanic addition. The formation of gypsum and ettringite is therefore extensively minimized to harmless content. Reference CEM I 42.5 R does not confirm the resistance to the sulfate solution. For the needs of construction practice, NONRIVAL CEM I 52.5 N represents an equivalent alternative to the use of sulfate-resistant cement in terms of resistance to sulfate aggression.

Other crucial findings coming from the 5-year experiment are:

NONRIVAL CEM I 52.5 N can be advantageously applied in technically demanding structural concrete, in which high strength but at the same time low permeability of the concrete foundation slab is required as a basic condition for ensuring its durability when exposed to aggressive sulfate for a long time. High strength and low penetration permeability are two equally important conditions for achieving a high durability.

Further research should focus on verifying a long-term performance of NONRIVAL CEM I 52.5 N in other aggressive environments.

The recommendation beyond domestic research is:

The development of the unified method, at the best standardized in EN or ASTM, even one common, for the evaluation of concrete's resistance to sulfate attack by an accelerated testing procedure, is required.

Equally urgent scientific task is the most accurate transformation of the accelerated test results to a realistic estimation of concrete service-life when subjected to natural aggressiveness e. g. related to the XA (1–3) exposure classes of STN EN 206 + A1.

## Acknowledgements

The financial support of this research project based on the contract related to the utility properties and durability of developed new cement kinds by the Považská cementárň. a. s. cement plant, Ladce (Slovakia), is greatly appreciated.

## Conflict of interest

The authors declare no conflict of interest.

## Author details

Michal Bačuvčík<sup>1\*</sup>, Pavel Martauz<sup>2</sup>, Ivan Janotka<sup>1</sup> and Branislav Cvopa<sup>2</sup>

<sup>1</sup> Building Testing and Research Institute, Bratislava, Slovakia

<sup>2</sup> Považská cementárň cement plant, Ladce, Slovakia

\*Address all correspondence to: [bacuvcik@tsus.sk](mailto:bacuvcik@tsus.sk)

## IntechOpen

© 2020 The Author(s). Licensee IntechOpen. This chapter is distributed under the terms of the Creative Commons Attribution License (<http://creativecommons.org/licenses/by/3.0>), which permits unrestricted use, distribution, and reproduction in any medium, provided the original work is properly cited. 

## References

- [1] Marchand J. Odler I. Skalmz J.P.: Sulfate attack on concrete. 1<sup>st</sup> ed. CRC Press: London; 2001. 213 p. ebook ISBN:9780429219337
- [2] Collepardi. M. The new concrete. 1<sup>st</sup> ed. ENCO s.r.l.: Mirano; 2006. 421 p. ISBN 88-901469-4-X
- [3] Tang S. Yao Y. Andrade C. Li Z: Recent durability studies on the concrete structure. Cement and Concrete Research. 2015. Vol. 78 (Part A). p. 143-154. URL [https://www.sciencedirect.com/public/Tang\\_et\\_al\\_2015b](https://www.sciencedirect.com/public/Tang_et_al_2015b)
- [4] STN EN 197-1: Cement. Part 1: Composition, specifications and conformity criteria for common cements. Bratislava: Slovak Office of Standards. Metrology and Testing; 2012
- [5] Bačuvčík. M. Long-term sulfate resistance of C3A - containing cement NONRIVAL of Ladce provenance. In: Proceedings of the Workshop of Norwegian grant NOVACEM Increasing environmental protection by innovative advanced technologies of cement production of the new generation. 5.-6. May. 2015; Chorvátsky Grob. Slovakia. p 12-13. ISBN 978-80-971912-2-1.
- [6] Shi C. Jiménez. F. Palomo A: New cement for the 21st century: The pursuit of an alternative to Portland cement. Cement and Concrete Research. Vol. 41. 2011. p. 750-763. <http://dx.doi.org/10.1016/j.cemconres.2011.03.016>
- [7] Gursel Petek A. Masanet E P. Horvath A. Stadel A: Life-cycle inventory analysis of concrete production: A critical review. Cement and Concrete Composites. 2014. Vol. 51. p. 38-48. DOI: 10.1016/j.cemconcomp.2014.03.005
- [8] Santhanan M. Cohen M D. Olek J: Effect of gypsum formation on the performance of the cement mortar during external sulfate attack. Cement and Concrete Research. 2003. Vol. 33. p. 325-332. DOI: 10.1016/S0008-8846(02)00955-9
- [9] Yu C.H. Sun. W. Scrivener K: Mechanism of expansion of mortars immersed in sodium sulfate solutions. Cement and Concrete Research. 2013. Vol. 43. p. 105-111. DOI: 10.1016/j.cemconres.2012.10.001
- [10] Müllauer W. Beddoe R E. Heinz. D.: Sulfate attack expansion mechanisms. Cement and Concrete Research. 2013. Vol. 52. p. 208-215. <https://doi.org/10.1016/j.cemconres.2013.07.005>
- [11] Tosun-Felekoglu K: The effect of C3A content on sulfate durability of Portland limestone cement mortars. Construction and Building Materials. 2012. Vol. 36. pp. 437-447. <https://doi.org/10.1016/j.conbuildmat.2012.04.091>
- [12] STN EN 206 + A1 Concrete. Specification, performance, production and conformity. Bratislava: Slovak Office of Standards. Metrology and Testing; 2017
- [13] STN EN 206/NA Concrete. Specification, performance, production and conformity. Bratislava: Slovak Office of Standards. Metrology and Testing; 2015
- [14] Janotka. I.. Martauz. P. Bačuvčík. M. Václavík. V.: Fundamental properties of industrial hybrid cement important for application in concrete. In Pavlo Krivenko editor. Intech Open: London. Open Access Compressive Strength of Concrete. Edt. by Pavlo Kryvenko. 2020. ISBN: 978-1-78985-568-5; p. 1-25.
- [15] Saleh H.M. Tawfik, M. A. Bayoumi T.A.: Chemical stability of seven years aged cement-PET composite waste form containing radioactive borate waste simulates.

Journal of Nuclear Materials. 2011.  
Vol. 411. 2011. p.185-92. DOI: 10.1016/j.jnucmat.2011.01.126

[16] Eskander B. Bayoumi T.A. Saleh H. M.: Performance of aged cement-polymer composite immobilizing borate waste simulates during flooding scenarios. Journal of Nuclear Materials. 2012. Vol. 420. p. 175-181. DOI: 10.1016/j.jnucmat.2011.09.029

[17] Zhutovsky, S. Hooton, R. D.: Accelerated testing of cementitious materials for resistance to physical sulfate attack. Construction and Building Materials. 2017. Vol. 145. p. 98-106. DOI:10.1016/j.conbuildmat.2017.03.239

[18] Gu, L. Visintin, P. Bennet, T.: Evaluation of accelerated degradation test methods for cementitious composites subject to sulfuric acid attack application to conventional and alkali/activated concretes. Cement and Concrete Composites. 2018. Vol. 87. p. 187-204. DOI: 10.1016/j.cemcon comp. 2017.12.015

[19] STN EN 196-2 Methods of testing cement. Part 2: Chemical analysis of cement. Bratislava: Slovak Office of Standards. Metrology and Testing; 2013

[20] STN EN 196-3 Methods of testing cement. Part 3: Determination of setting time and soundness. Bratislava: Slovak Office of Standards. Metrology and Testing; 2020

[21] STN EN 196-1 Methods of testing cement. Part 1: Determination of strength. Bratislava: Slovak Office of Standards. Metrology and Testing; 2019

[22] STN EN 1015-3 Methods of test for mortar for masonry. Part 3: Determination of consistence of fresh mortar (by flow table). Bratislava: Slovak Office of Standards. Metrology and Testing; 2000

[23] STN EN 1015-6 Methods of test for mortar for masonry. Part 6: Determination of bulk density of fresh mortar. Bratislava: Slovak Office of Standards. Metrology and Testing; 2000

[24] STN EN 1015-7 Methods of test for mortar for masonry. Part 7: Determination of air content of fresh mortar. Bratislava: Slovak Office of Standards. Metrology and Testing; 2000

[25] STN 72 2453 Testing of volume stability of mortar. Bratislava: Slovak Office of Standards. Metrology and Testing; 1968

[26] STN 73 1371 Method of ultrasonic pulse testing of concrete. Bratislava: Slovak Office of Standards. Metrology and Testing; 1981

# Impact of Nanosilica in Ordinary Portland Cement Over Its Durability and Properties

*Gude Reddy Babu, Pala Gireesh Kumar,  
Nelluru Venkata Ramana  
and Bhumireddy Madhusudana Reddy*

## Abstract

The present examination illustrates the impact on the hardened and fresh cement mortar and cement with the inclusion of nanosilica of size 40 nm in various environmental conditions (UltraTech, India). It is quite notified that an elevation in compressive strength as well as flexural strength along with an improvisation in the performance and life span of cement mortar. The samples of M5 grade blended with a ninety percentage of concrete and remaining with nanosilica was identified to have a finer working elevation in as well as in standards when collated with the conventional cement mortar. The corollary of hardened and fresh cement, strength parameters were looked upon with the aid of XRD (X-ray Diffraction). Also, the SEM (Scanning Electron Microscope) test holds a predominant role in analysis.

**Keywords:** OPC, Strength, HCl, MgSO<sub>4</sub>, XRD, nanosilica and SEM

## 1. Introduction

There is no other substitute for concrete that can be supplemented with an alternative because of its intrinsic qualities like get into any shape, quality and ability to consume locally available fine and coarse materials along with its strength, resistance to fire, with little support [1]. The use of concrete and its consumption is on par with wans and the activity of construction is set to have been emitting 8% of CO<sub>2</sub> [2]. Even though the substitute for concrete is not identified the area of development becomes the centre stage for identifying substitute materials. The contribution of nano technology has made big strides and effect on various aspects of science. Nano silica is preferably utilized in numerous approaches and is easily available as well.

The research and investigation in nano particles and their utilization in cement and mortar invariably becomes popular [3]. The properties of cement in both hardened as well as in fresh phase are majorly laid focus on. The density of concrete and cement can be improvised with the inclusion of nano as well as micro NS which have the tendency of acting as a material of filler, which results in up gradation of its quality [4–17]. Nano silica with separated molecule impact got an extraordinary pozzolonic property than other pozzolonic materials on comparison because of the nano size of particles and greater silica contents, accordingly both impacts are

important in making concrete [4, 6]. Expansion of Nano silica to solidify concrete and cement mortar then resulted in improvement of sharp and long haul considers and over utilisation of nano silica results in decrease in quality. Nano silica greatly improved qualities of cement and concrete in fresh and solidified stage and in durability in different environmental conditions [10–11, 18–19]. The nano particles are centered and a considerable research is carried out.

Therefore, the present research includes the impact and durability of 40 nm silica particles in cement mortar, durability existence under different environments both physical and chemical are taken up for examination [20–23]. For acquiring an accurate output, instruments of Scanning Electron Microscope (SEM) and X-ray diffraction (XRD) were resorted to. In this research, cement to sand proposition was 1: 3 and water to cement (concrete plus NS) proposition was set at 0.4.

## **2. Procedure**

In the set forth work area, the proportion of 1:3 is considered for cement-sand and 0.4 for water-cement. Also, nanosilica is incorporated along with cement starting from zero percentage and with every sample, an increase of 2% is followed until an overall 14% is achieved. Every sample is treated individually with starting with M0 and concluding with M7.

### **2.1 Blending of nano silica with cement**

Sticking to the particulars of Jo B W [24], the blending of NS with cement mortar is done for a minute maintaining 285 rpm. Prior to the blending process, the water is treated with NS and this was put into the rotational blender which runs at 140 rpm. This was done for 30 seconds so as to solidify the mixture and addition of a fine total was done. Adding to the process, a super plasticizer was annexed to the mix when the blender was running at a speed of 285 rpm. Now, a resting phase of 90 seconds is allocated to the blender and it resumes working for a minute with the same speed before rest. Finally, the mix was set out in a hardened figure.

### **2.2 Hardening or setting interval (setting time)**

IS of code 5513-1976 was used for detecting the time taken for setting.

### **2.3 Strength determination (compressive strength)**

The part 6 of 4031-1998 was considered to find the compressive quality of mortar.

### **2.4 Strength determination (flexural strength)**

Determining the flexural standards using the BS section 188 of 1881 of the year 1983 was done.

### **2.5 Durability aspect**

AR graded magnesium sulphate and hydrochloric acid, which are synthetic in nature, were used in the research. The ACI of 318-99 were followed and the compound grouping was done. An exemplar of the fixations projects over a span of 120 days for 1%, 240 days for 2%, 360 days for 3% and 480 days for 4%, provided the recharge of the fixations was for each 4-month tenure.

## 2.6 Temperature assessment

The blended samples of M0 as well as M5 were tested upon for the temperature check at 900 °C in a suppress heater. Also, the blended sample out-righting 28 days were dried for a span of 6 hours at normal temperature and then they were transferred to a muffle furnace. An altering is done with temperatures where each temperature has got three samples assessed for a period of two and half hours. The altering temperatures start from 100 °C and every alteration has an add-on of 100 °C up to 600 °C. Finally, the samples were put out to cool down at a temperature of 30 °C i.e., room temperature (Tables 1–5).

| Oxides                         | Percentage |
|--------------------------------|------------|
| Calcium oxide                  | 62.5       |
| Silicon dioxide                | 20.5       |
| Aluminium oxide                | 6.1        |
| Ferrous oxide                  | 3.1        |
| Magnesium oxide                | 1.6        |
| Sulphur trioxide               | 1.5        |
| Oxides of potassium and sodium | 1          |

**Table 1.**  
*Constitutes of cement.*

| Attributes                                 | Standard values (IS 12269-1987) | Obtained values |
|--|---------------------------------|-----------------|
| Compressive Strength (days)                | 27 MPa (Min)                    | 35.91 MPa       |
| 3  | 37 MPa (Min)                    | 46.72 MPa       |
| 7  | 53 MPa (Min)                    | 62.90 MPa       |
| 28   |                                 |                 |
| Relative Density                           | —                               | 3.10            |
| Setting Span                               | 30 min                          | 155 min         |
| Initial                                    | 600 min                         | 267 min         |
| Final                                      |                                 |                 |
| Soundness<br>(Le- Chatlier Expansion)      | 10 mm (Max)                     | 0.85 mm         |
| Specific Surface Area (m <sup>2</sup> /Kg) | 226                             | 314             |

**Table 2.**  
*Cement attributes.*

| Ennore sand grading                 | Value (%) |
|-------------------------------------|-----------|
| Passing through Sieve of 2 mm       | 100       |
| Retained over Sieve of 90 m         | 100       |
| 1 mm < Size of the particle         | 33.33     |
| 500 m < 1 mm > Size of the particle | 33.33     |
| 500 m > Size of the particle        | 33.33     |

**Table 3.**  
*Ennore sand attributes.*

| Attributes       | Obtained values |
|------------------|-----------------|
| Relative density | 1.33            |
| Surface area     | 50.5            |
| Particle size nm | 40              |
| SiO <sub>2</sub> | 99.7%           |
| Loss on Ignition | 0.3%            |

**Table 4.**  
*Attributes of nanosilica.*

| Attributes                       | Standard values<br>(IS: 456 – 2000) | Values of distilled<br>water | Values of drinkable<br>water |
|----------------------------------|-------------------------------------|------------------------------|------------------------------|
| power of hydrogen, ph            | 6.5- 8.5                            | 7.2                          | 7.5                          |
| Total Dissolved Solids<br>(mg/L) | 2000                                | 4.6                          | 11.0                         |
| Organic Solids (mg/L)            | 200                                 | 1.1                          | 6.0                          |
| Inorganic Solids (mg/L)          | 3000                                | 6.2                          | 17.0                         |
| Alkalinity (mg/L)                | 250                                 | 3.6                          | 11.0                         |
| Acidity (mg/L)                   | 50                                  | 0                            | 5.0                          |
| Sulphates (mg/L)                 | 400                                 | 3.2                          | 12.0                         |
| Chlorides                        | 500(RCC)                            | 1.5                          | 9.0                          |

**Table 5.**  
*Attributes of water.*

### 3. Deliberation of verdict

#### 3.1 Hardening or setting interval (setting time)

**Figure 1** reveals the corollary on setting time due to NS and uncovers the fact of lowering the hardening time with increment in NS quantity. The initial and final setting time for M0 was 155 min and 266 min, M1 was 153 min and 263 min, M2 was 148 min and 260 min, M3 was 143 min and 255 min, M4 was 137 min and 245 min, M5 was 131 min and 240 min, M6 was 126 min and 234 min, M7 was 123 min and 227 min. The cycle was advanced because of NS has a vast surface region; subsequently, hydration measure turns out to be quick.

#### 3.2 Analysis of strength (compression)

A rise in the strength upon inclusion of nanosilica up to 10% was portrayed in **Figure 2**. With further addition of NS, decrement in strength can be observed from the diagram. The finest of all samples is the M5 sample comprised of 90% cement and 10% NS. For 3 days, the increment strength observed was 17.8 MPa, 7 days resulted 21.58 MPa, 28 days directed a strength of 21.18 MPa, 90 days showcased 21.50 MPa, 180 days witnessed 21.32 MPa and finally, 365 days exhibited a strength of 20.66 MPa. From the analysis, it is truly clear that M6 blended with 88% of cement and the remaining with NS has seen a decrease in compressive strength whereas M5 figured the best strength notable.

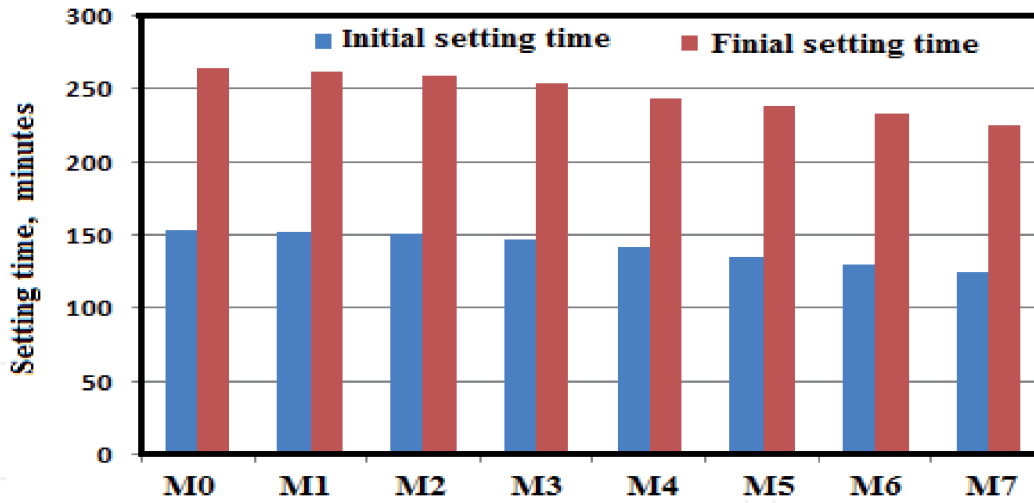


Figure 1.  
 Efficacy of nanosilica over setting span.

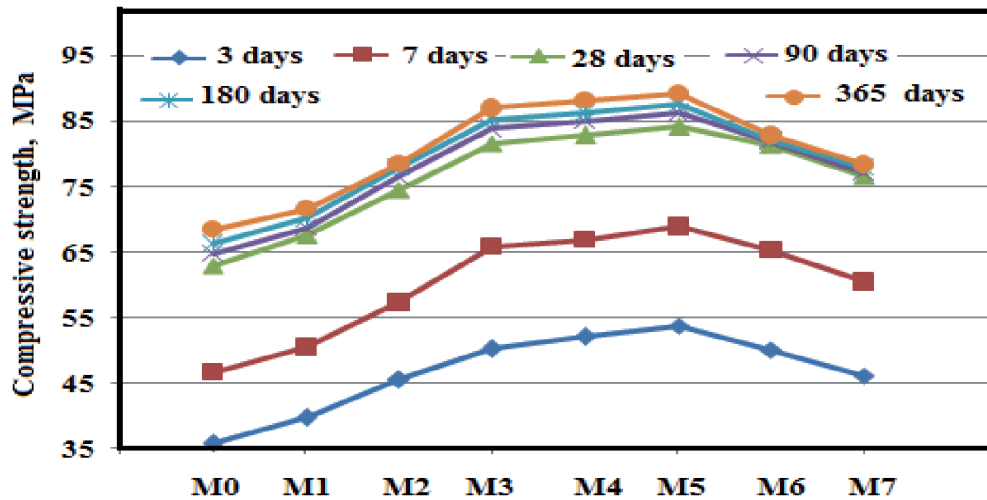


Figure 2.  
 Efficacy of nanosilica over strength attribute (compression).

### 3.2.1 Manoeuvre of XRD

The analysis was done for a couple of samples having 0% NS and 10% NS i.e., for M0 and M5 by X-ray diffraction, XRD. The samples were of OPC type and were hydrated for a span of 28 days. **Figure 3** shows that hydroxide of calcium showed up at  $18^\circ$  whereas the calcium silicate hydrate showed up at  $26^\circ$  individually for both the samples. Concentration and strength of hydroxide of calcium was predominantly high and that of silicate hydroxides of calcium was less when compared to OPC of 90% and nano silica of 10% test. The variation of strength for the sample of M0 and the sample of M5 was due to the reaction of oxides of silica with hydroxides of calcium (finished results of cement hydrate).

### 3.2.2 Manoeuvre of scanning electron microscope

**Figures 4** and **5** demonstrate the results for the sample M0 and also for the sample M5 which were hydrated for 28 days. The diagram of Scanning Electron Microscope (SEM) portrays the hydroxides of calcium's needle like structure along with the silicate hydroxide of calcium which was spread widely. The calcium hydroxide's long needle like structures in **Figure 4** can be collated with **Figure 5**.

Also, a high in silicate hydroxide of calcium's content can be seen in **Figure 5** when compared to **Figure 4**. The major difference in the structure of hydroxides of calcium and quantity of silicate hydroxide of calcium was due to the presence of oxides of silica in NS. These react with hydroxides of calcium in the cement hydrate and thereby, causing the differences.

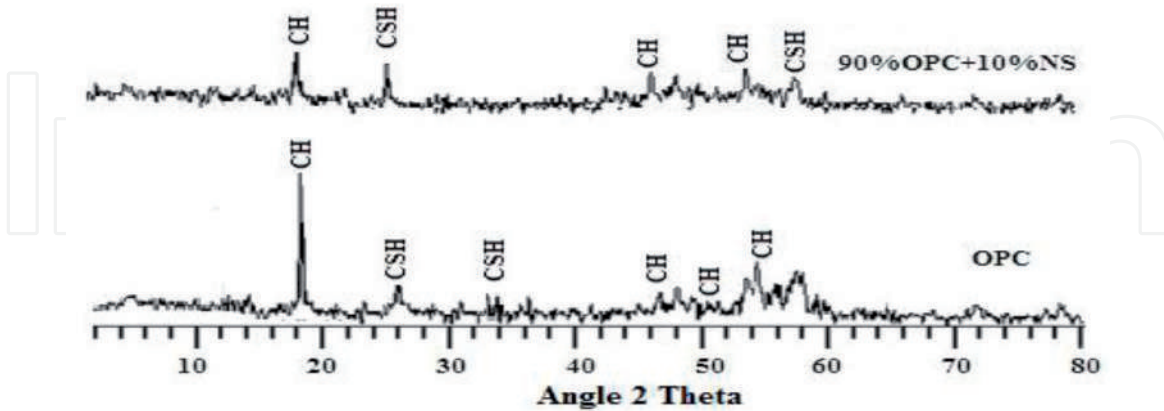


**Figure 3.**  
Depiction of Mo & M5 samples XRD (hydrated for 28 days).

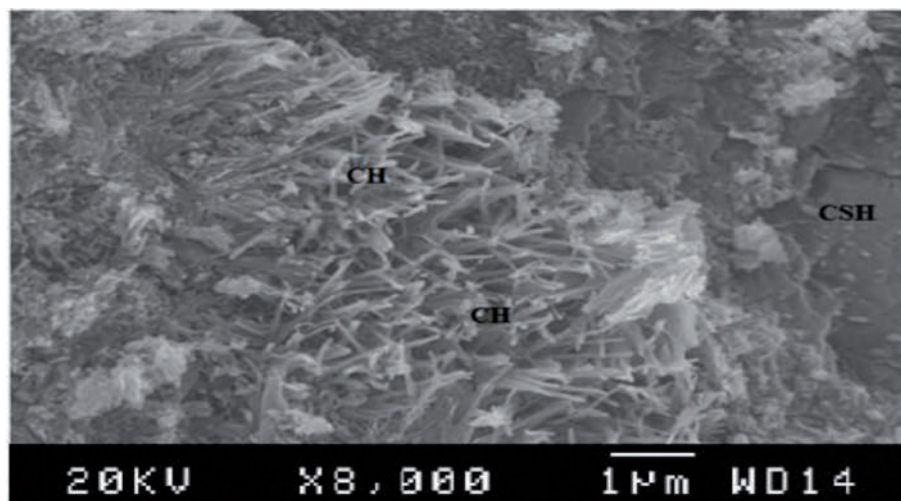


**Figure 4.**  
Depiction of Mo's SEM diagram (28 days of hydration).

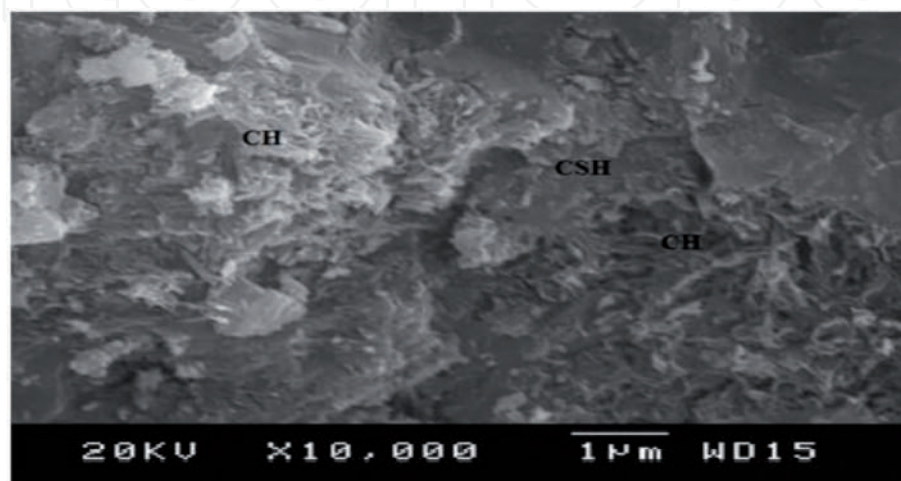


**Figure 5.**  
Depiction of M5's SEM diagram (28 days of hydration).

### 3.3 Analysis of flexural strength

The NS impact on flexural strength can be identified from the **Figure 6**. It was evident that cement with less than 10% NS exhibited expand in flexural strength by 10% whereas cement with NS in more than 10% showcased decline in the strength. The samples were identified upon M5 blend with a higher expansion rate with time. It was seen that 2 MPa was recorded for 3 days, 2.2 MPa for 7 days, 2.5 MPa for 28 days, 2.4 MPa for 90 days, 2.4 MPa for 180 days and finally 2.6 MPa for 365 days. From the analysis, we can notice that samples has shown a decrease in strength with NS percentage more than 10 but the value was higher when compared with the strength of sample with zero percentage of NS. The major concerns that led the expansion of the strength characteristics were the size of the particles and content of oxides of silica. An extra quantity of silicate hydroxide of calcium was witnessed due to the action of hydroxides of calcium and oxides of silica. Furthering this, the NS acts as a framework's filler material of cement mortar.

### 3.4 Probes on durability aspect

#### 3.4.1 Corollary of magnesium sulphate

**Figures 7 and 8** render the effect of Magnesium Sulphate ( $MgSO_4$ ) over compressive strength of the samples. If one observes in **Figure 7**, by and large, cement mortar strength quality increased irrespective of age, the equivalent can be observed in M0 examples of no  $MgSO_4$  fixation., Compressive strength qualities decreased as for time and focus with less than 4% fixation, and 4% centralization of  $MgSO_4$  has resulted in the greatest quality decrease.

M5 blend examples equivalents the above and were provided in **Figure 8**. Concerning the concentration and age of  $MgSO_4$ , M0 blend examples get altogether result in quality decrease compared to M5 blend examples Also the M0's compressive strength for 4% was noted to be 57.30 MPa for 120 days, 53.55 MPa for 240 days, 48.50 MPa for 260 days and finally 44.16 MPa for 480 days. In the similar context, the strength values of M5 were 78.26 MPa for 120 days, 74.1 MPa for 240 days, 67.0 MPa for 260 days and finally 64.0 MPa for 480 days. The contrast of strength characteristic between M0 and M5 was 21, 20.4, 20.3 and 19.7 MPa respectively.

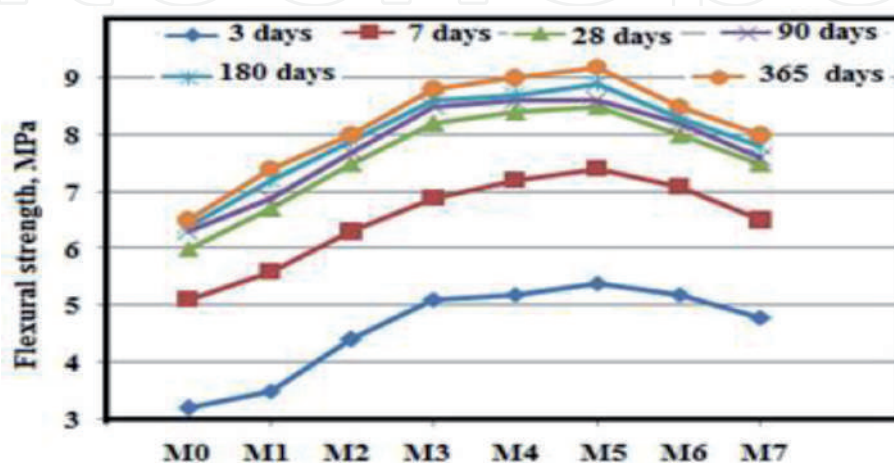


**Figure 6.**  
*Efficacy of nanosilica upon strength (Flexural).*

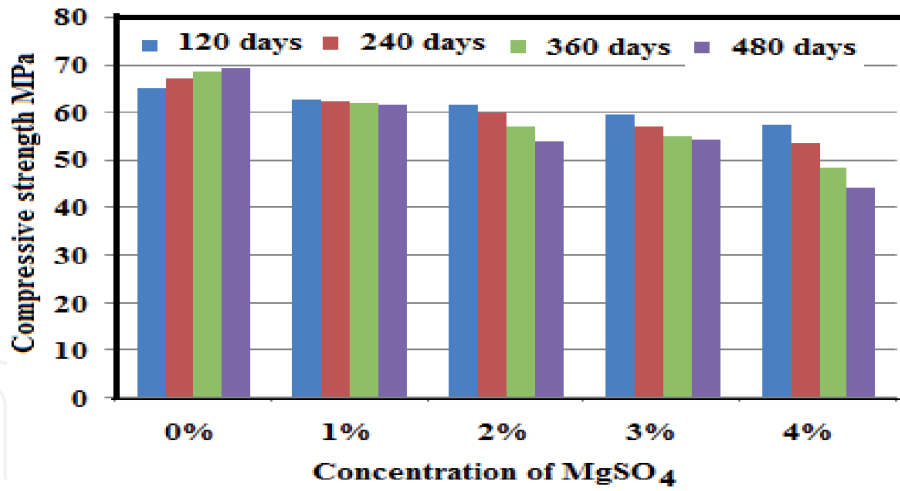


Figure 7.  
Corollary of MgSO<sub>4</sub> over Sample Mo.

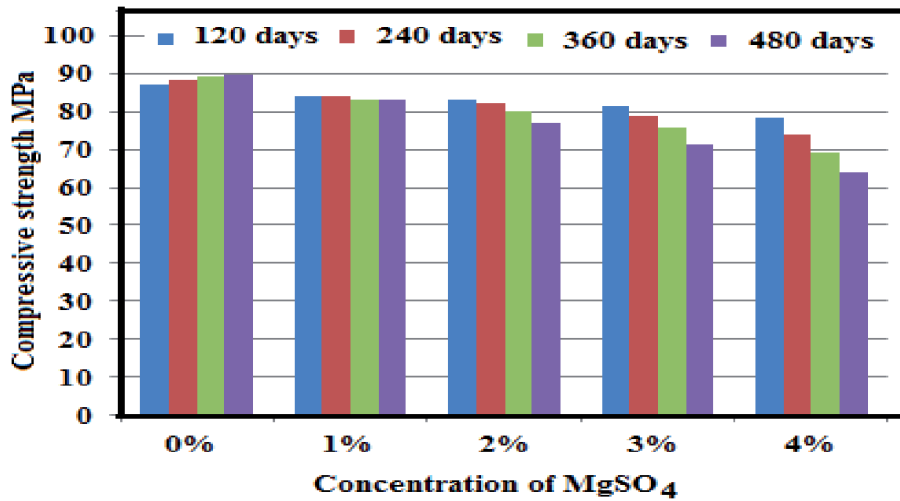


Figure 8.  
Corollary of MgSO<sub>4</sub> over Sample M5.

### 3.4.2 Manoeuvre of X-ray diffraction

The blended samples of OPC's M0 and M5 were hydrated for 28 days and the samples were kept in water with 4% of MgSO<sub>4</sub> for a span of 360 days. The results of the sample M0 and the sample M5 were represented as charts in the **Figure 9** where magnesium silicate hydrate was presented at 48°; at 18°, the hydroxide of calcium turned up and at 33°, magnesium's hydroxide was presented and finally the silica hydroxide of calcium was shown at 26°. It was noted that the hydroxide of calcium exhibited a high force of ascent and, additionally, the lower power ascent of silicate hydroxide of calcium of M0 diversified from M5. The contrast happened because of nanosilica quality. Also, hydroxide and silicate hydrate of magnesium were directed because of the reaction of MgSO<sub>4</sub> with hydroxide and silicate hydroxide of calcium. The quality of silicate hydrate of magnesium declined due to the non-binding nature, but M5 exhibits a finer standard when collated with M0 due to the inclusion of nanosilica.

### 3.4.3 Manoeuvre of scanning electron microscope

The blended samples of OPC's M0 and M5 were hydrated for 28 days and the samples were kept in water with 4% of MgSO<sub>4</sub> for a span of 360 days. The results

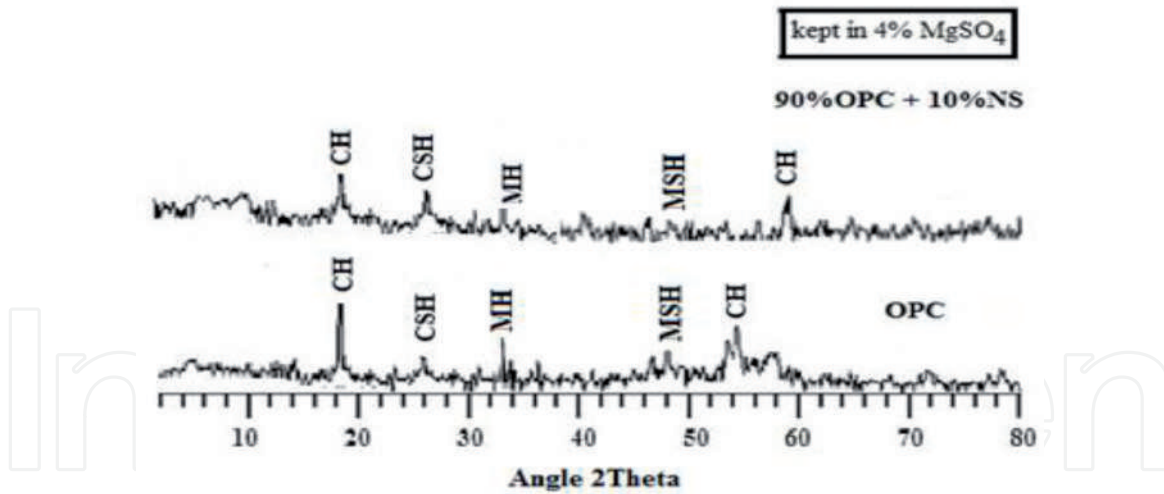


**Figure 9.**  
Depicting Mo & M5 samples XRD (Sample placed for 360 days in water with 4%  $MgSO_4$ ).

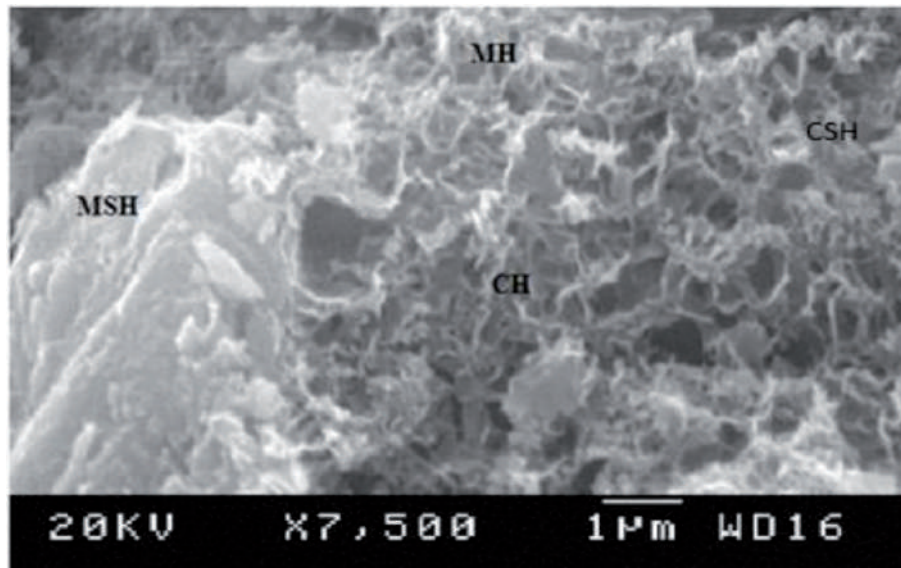


**Figure 10.**  
Depicting Mo's SEM diagram (Sample placed for 360 days in water with 4%  $MgSO_4$ ).

were represented as Scanning Electron Microscope diagrams in the **Figures 9** and **10** where hydroxide of calcium, silicate hydroxide of calcium, hydroxide of magnesium and silicate hydrate of magnesium were presented. Calcium hydroxide's needle structure was indicated in the **Figure 10** and further, it was made in contrast with the **Figure 11** whereas the content of calcium silicate hydroxide is high when compared to **Figure 10**. In further addition, magnesium's silicate hydrate and hydroxide witnessed a fine and more elegant outlook when collated with **Figure 11**. The inclusion of NS shows diversified nature of OPC. Also, placing the sample in water mixed with  $MgSO_4$  adds up to the work.

### 3.5 Corollary of hydrochloric acid

**Figures 12** and **13** render the effect of Hydrochloric Acid (HCl) over compressive strength of the samples. By and large, concrete mortar quality expanded irrespective of age, the equivalent can be seen at sample M0 which was placed in zero HCl fixations. It was also seen that a decline in compressive quality with concentration and time in **Figure 12** when M0 blend examples kept in less than 4% convergence of HCl and examples were given for HCl centralization with 4% has the greatest quality decrease.

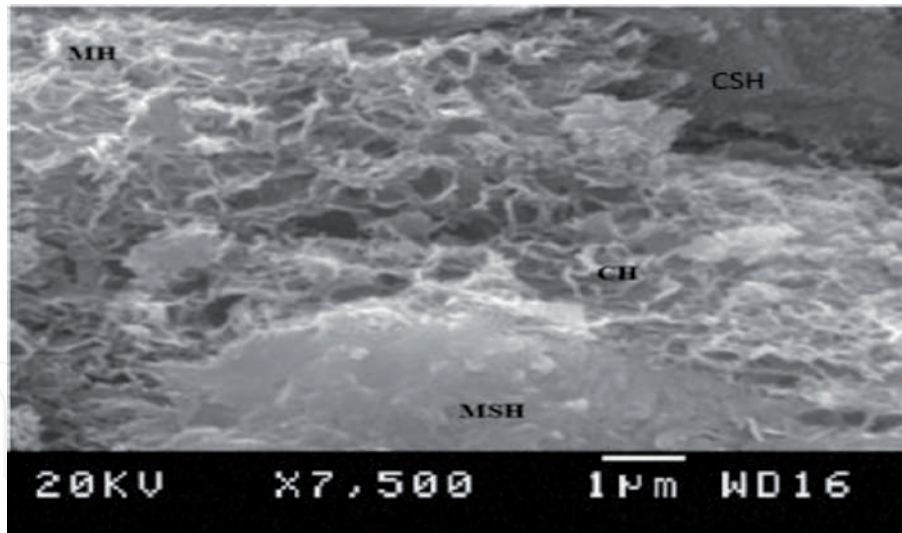


Figure 11. Depicting M5's SEM diagram (Sample placed for 360 days in water with 4%  $MgSO_4$ ).

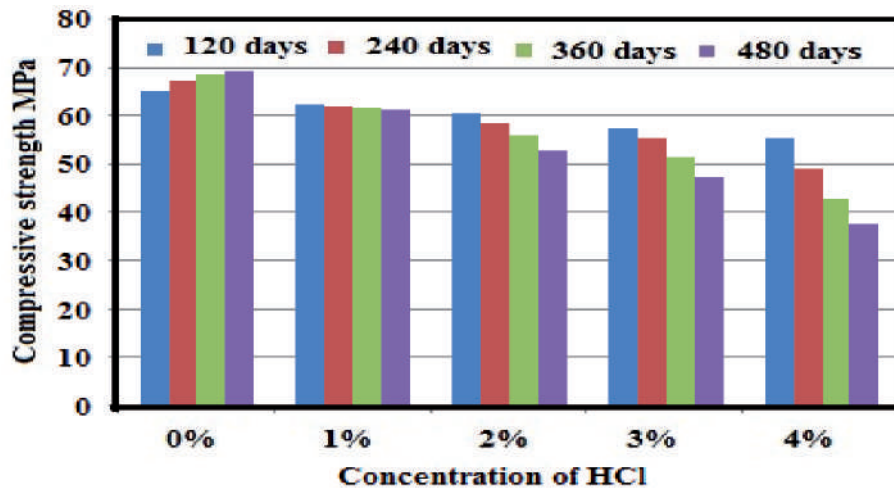


Figure 12. HCl Corollary over Sample Mo.

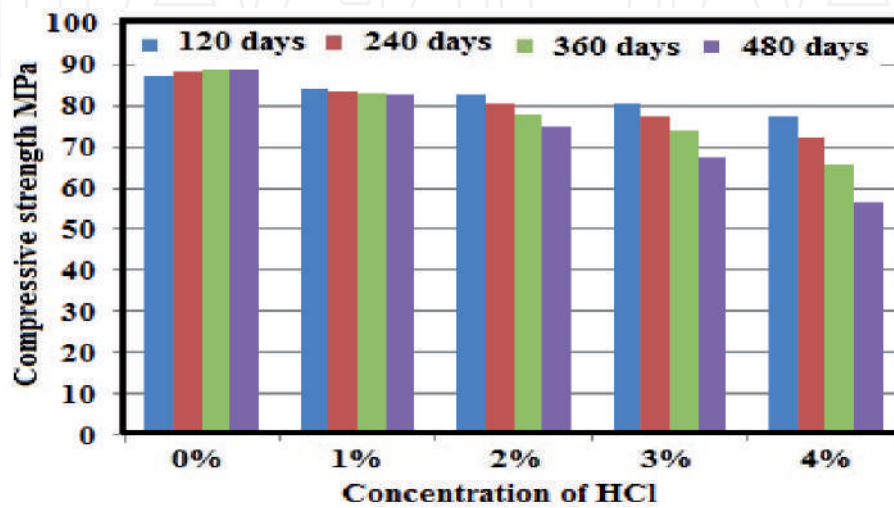


Figure 13. HCl Corollary over Sample M5.

The equivalent to above can likewise be seen in M5 blend examples which appear in **Figure 13**. Yet, M0 blend examples get noteworthy quality decrease contrasted with that of M5 blend examples. M0's and M5's compressive quality for a focus of 4% was is 55.35 MPa and 77.33 MPa for 120 days, 49.00 MPa and 72.30 MPa for 240 days, 42.60 MPa and 65.55 MPa for 260 days and 37.31 MPa and 56.30 MPa for 480 days. The differentiation in strength at 4% fixation for 120 days was 21.3 MPa, 240 days was 23.25 MPa, 260 days was 22.82 MPa and for 480 days was 18.96 MPa.

### 3.5.1 Manoeuvre of X-ray diffraction

The blended samples of OPC's M0 and M5 were hydrated for 28 days and the samples were kept in water with 4% of HCl for a span of 360 days. The results were represented in the **Figure 14** where hydroxide of calcium, silicate hydroxide of calcium, chlorides of calcium, Friedel's mixes of salt of M0 sample and M5 sample were presented individually at 18°, 26°, 33°, 37° and finally at 48.5°. It was notified that the ascent power of calcium hydroxide is high whereas the force ascent of silicate hydroxide of calcium is more for M5 than M0. The observed variation in ascent of M0 sample and M5 sample was majorly due to the expansion taking place in cement mortar due to the inclusion of NS. Adding to it, the reaction of hydroxides of calcium with HCl and chlorides of calcium with C<sub>3</sub>A frames the chlorides of calcium and Friedel's mixes of salt. Silicate hydroxide of calcium got destabilized due to its reaction with HCl resulting a decline in the quality of strength but the performance of M5 was way too good when collated to that of M0 because of essence of NS in cement mortar.

### 3.5.2 Manoeuvre of scanning electron microscope

The blended samples of OPC's M0 and M5 were hydrated for 28 days and the samples were kept in water with 4% of HCl for a span of 360 days. The results were represented as Scanning Electron Microscope diagrams in the **Figures 15** and **16** where hydroxides of calcium, silicate hydroxides of calcium, chlorides of calcium were shown. A significant improvement in case of above mentioned compounds can be noted in the **Figure 15** when contrasted with the **Figure 16**. The diagrams of Scanning Electron Microscope test uphold the investigation of X-ray Diffraction.

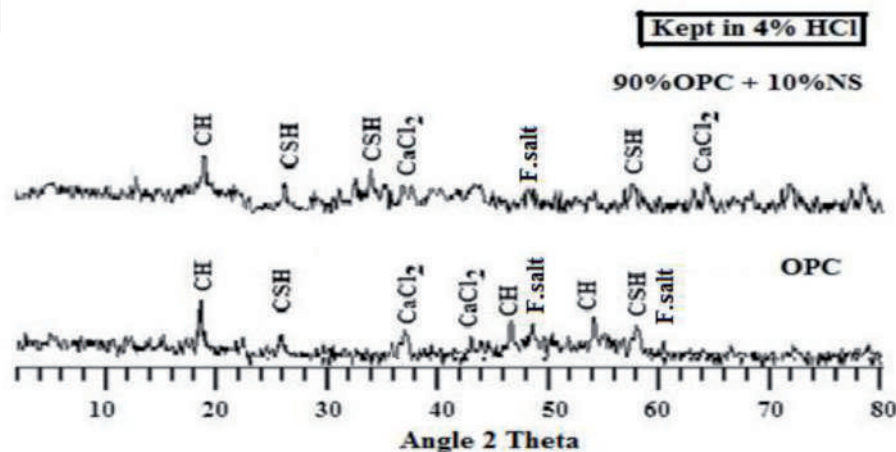


**Figure 14.** Depicting M0 & M5 samples XRD (Sample placed for 360 days in water with 4% HCl).

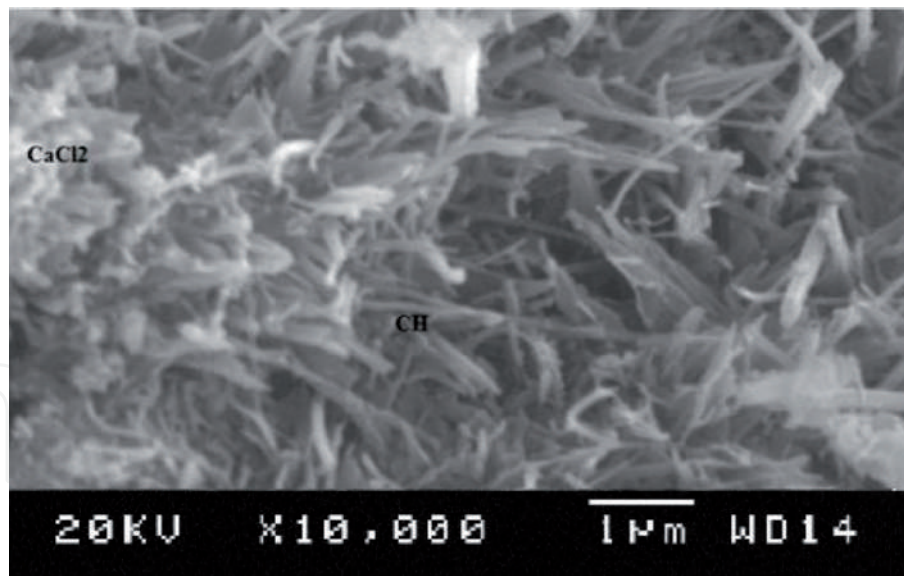


**Figure 15.**  
*Depicting M0's SEM diagram (Sample placed for 360 days in water with 4% HCl).*

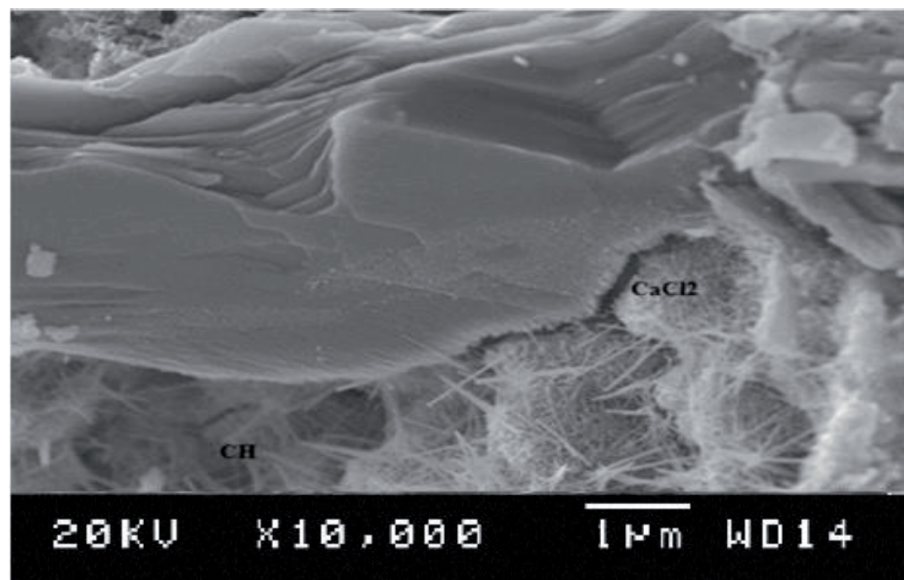


**Figure 16.**  
*Depicting M5's SEM diagram (Sample placed for 360 days in water with 4% HCl).*

### 3.6 Assessment of temperature corollary

Temperature's corollary on the blend samples of M0 and M5 were shown in the **Figure 17**. It was evidently clear that an increase in temperature of M0 and M5 samples results the compressive strength to lower. The strength values noted for M0 sample and M5 sample at various temperature conditions are 62.93 MPa and 84.12 MPa at 27 °C, 51.90 MPa and 73 MPa at 400 °C, 28.30 MPa and 48 MPa at 600 °C, 15.40 MPa and 28.41 MPa at 800 °C. The M0 sample and M5 sample exhibits decrease in compressive strength quality because of between layer water, losing free water and synthetically reinforced water. Furthermore warm extension of cement mortar and was unique. The quality decreases in case of compressive strength for sample of M0 and sample of M5 was critical over a temperature of 400 °C. But, more compressive quality was exhibited by M0 blend examples than M5 blend examples.

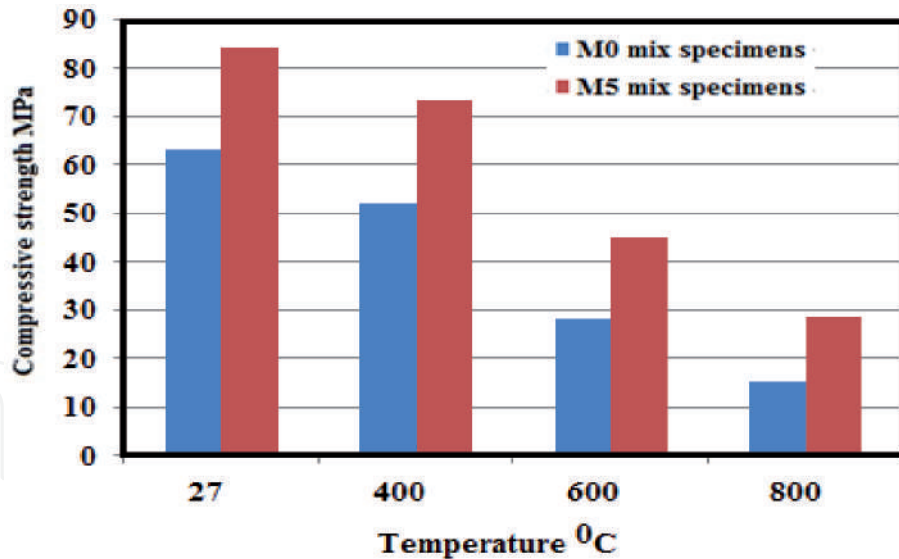


**Figure 17.**  
*Corollary of temperature.*

#### **4. Conclusion**

The strength qualities (compression and flexural) expanded by and large due to the NS of 40 nm in case of M5 blend. Cement's extraordinary pozzolonic property and its property as a good material for filling of NS instigated the rise in strength with cement and brilliant filling material.

NS has quickened setting measure because of its enormous surface area.

M5 mix examples have given much better execution in solidness in different environmental conditions than that of M0 blend examples.

IntechOpen

IntechOpen

### Author details

Gude Reddy Babu<sup>1\*</sup>, Pala Gireesh Kumar<sup>2</sup>, Nelluru Venkata Ramana<sup>3</sup>  
and Bhumireddy Madhusudana Reddy<sup>4</sup>

1 Department of Civil Engineering, Gudlavalleru Engineering College,  
Gudlavalleru, Andhra Pradesh, India

2 Department of Civil Engineering, Shri Vishnu Engineering College for  
Women (A), Bhimavaram, Andhra Pradesh, India

3 Construction Technology Department, V.T.U P.G. Centre, Kalaburagi, Karnataka,  
India

4 Department of Civil Engineering, Sri Venkateswara University College of  
Engineering, Tirupati, Andhra Pradesh, India

\*Address all correspondence to: greddybabu1966@gmail.com

### IntechOpen

© 2021 The Author(s). Licensee IntechOpen. This chapter is distributed under the terms of the Creative Commons Attribution License (<http://creativecommons.org/licenses/by/3.0>), which permits unrestricted use, distribution, and reproduction in any medium, provided the original work is properly cited. 

## References

- [1] P.K. Mehta, H. Meryman, Tools for reducing carbon emissions due to cement consumption, *Structure magazine*. (2009) pp. 11-15.
- [2] J. G. J. Olivier, J.-M. Greet, J. A. H. W. Peters, Trends in global CO<sub>2</sub> emissions 2012 report, PBL Netherlands Environmental Assessment Agency (2012) pp. 17.
- [3] I. Ali, New generation adsorbents for water treatment, *Chem. Rev.* 112 (2012) 5073-5091.
- [4] Y. Qing, Z. Zenan, K. Deyu, C. Rongshen, Influence of nano-SiO<sub>2</sub> addition on properties of hardened cement paste as compared with silica fume, *Constr. Build. Mater.* 21 (2007) 539-545.
- [5] A. Sadrmomtazi, A. Fasihi, F. Balalaei, A.K. Haghi, Investigation of mechanical and physical properties of mortars containing silica fume and nano-SiO<sub>2</sub>, in: *Third International Conference on Concrete and Development*, Tehran, Iran, 27-29 April, 2009, pp. 1153-1161.
- [6] H. Li, H. G. Xiao, J. Yuan, J. P. Ou, Microstructure of cement mortar with nanoparticles, *Compos. Part B* 35 (2004) 185-189.
- [7] H. Li, H. G. Xiao, J. Yuan, J. P. Ou, A study on mechanical and pressure-sensitive properties of cement mortar with nanophase materials, *Cem. Concr. Res* 34 (2004) 435-438.
- [8] H. Li, M. H. Zhang, J. P. Ou, Abrasion resistance of concrete containing nanoparticles for pavement, *Wear* 260 (2006) 1262-1266.
- [9] H. Li, M. H. Zhang, J. P. Ou, Flexural fatigue performance of concrete containing nano-particles for pavement, *Int. J. Fatigue* 29 (2007) 1292-1301.
- [10] L. Senff, J. A. Labrincha, V. M. Ferreira, D. Hotza, W. L. Repette, Effect of nanosilica on rheology and fresh properties of cement pastes and mortars, *Constr. Build. Mater.* 23 (2009) 2489-2491.
- [11] P. Mondal, S. P. Shah, L. Marks, A reliable technique to determine the local mechanical properties at the nanoscale for cementitious materials, *Cem. Concr. Res.* 37 (2007) 1440-1444.
- [12] B. W. Jo, C. H. Kim, G. H. Tae, J. B Park, Characteristics of cement mortar with nano-SiO<sub>2</sub> particles. *Constr. Build. Mater.* 21 (2007) 1351-1355.
- [13] R. S. Chen, Q. Ye, Research on the comparison of properties of hardened cement paste between nano-SiO<sub>2</sub> and silica fume adde., *Concrete* 1 (2002) 7-10.
- [14] M. Tang, H. Ba, Y. Li, Study on compound effect of silica fume and nano-SiO<sub>x</sub> for cement composite materials, *J. Chin. Ceram. Soc.* 31 (2003) 523-527.
- [15] D. F. Lin, M. C. Tsai, The effects of nanomaterials on microstructures of sludge ash cement paste, *J. Air Waste Manage. Assoc.* 56 (2006) 1146.
- [16] J. Y. Shih, T. P. Chang, T. C. Hsiao, Effect of nanosilica on characterization of Portland cement composite, *Mater. Sci. Eng. A* 424 (2006) 266-274.
- [17] T. Ji, Preliminary study on the water permeability and microstructure of concrete incorporating nano-SiO<sub>2</sub>. *Cem. Concr. Res.* 35 (2005) 1943-1947.
- [18] Jintao Liu, Qinghua Li, Xu. Shilang, Influence of nanoparticles on fluidity and mechanical properties of cement mortar, *Constr. Build. Mater.* 101 (2015) 892-901.

[19] Yamei Cai, Pengkun Hou, Xin Cheng, Peng Du, Zhengmao Ye, The effect of nanoSiO<sub>2</sub> on the properties of fresh and hardened cement based materials through its dispersion with silica fume, *Constr. Build. Mater.* 148 (2017) 770-780.

[20] R. Moradpour, E. Taheri-Nassaj, T. Parhizkar, M. Ghodsian, The effects of nanoscale expansive agents on the mechanical properties of non-shrink cement-based composites: the influence of nano-MgO addition, *Compos. B Eng.* 55 (2013) 193-202.

[21] Saloma, A. Nasution, I. Imran, M. Abdullah, Improvement of concrete durability by nanomaterials, *Proc. Eng.* 125 (2015) 608-612.

[22] E. Mohseni, F. Naseri, R. Amjadi, M.M. Khotbehsara, M.M. Ranjbar, Microstructure and durability properties of cement mortars containing nano-TiO<sub>2</sub> and rice husk ash, *Constr. Build. Mater.* 114 (2016) 656-664.

[23] Morteza Bastami, Mazyar Baghbadrani, Farhad Aslani, Performance of nano- Silica modified high strength concrete at elevated temperatures. *Constr. Build. Mater.* 68;2014: 656-664.

[24] Jo BW, Kim CH, Tae GH, Park JB. Characteristics of cement mortar with nano silica particles. *Constr. Build. Mater.* 21 (2007) 1351-1355.

# Simulation and Optimization of an Integrated Process Flow Sheet for Cement Production

*Oluwafemi M. Fadayini, Adekunle A. Obisanya,  
Gloria O. Ajiboye, Clement Madu, Tajudeen O. Ipaye,  
Taiwo O. Rabiou, Shola J. Ajayi and Joseph T. Akintola*

## Abstract

In this study the process flow diagram for the cement production was simulated using Aspen HYSYS 8.8 software to achieve high energy optimization and optimum cement flow rate by varying the flow rate of calcium oxide and silica in the clinker feed. Central composite Design (C.C.D) of Response Surface Methodology was used to design the ten experiments for the simulation using Design Expert 10.0.3. Energy efficiency optimization is also carried out using Aspen Energy Analyser. The optimum cement flow rate is found from the contour plot and 3D surface plot to be 47.239 tonnes/day at CaO flow rate of 152.346 tonnes/day and the SiO<sub>2</sub> flow rate of 56.8241 tonnes/day. The R<sup>2</sup> value of 0.9356 determined from the statistical analysis shows a good significance of the model. The overall utilities in terms of energy are found to be optimised by 81.4% from 6.511 x 10<sup>7</sup> kcal/h actual value of 1.211 x 10<sup>7</sup> kcal/h with 297.4 tonnes/day the carbon emission savings.

**Keywords:** central composite design, optimisation, response surface methodology, cement production, design expert

## 1. Introduction

Cement is a fine greyish or whitish inorganic, non-metallic powder commonly used as a binding agent in construction materials. It consists of pyroprocessed chemically combined hydraulic cement materials such as calcareous, siliceous, argillaceous and ferriferous [1]. Cement forms paste when mixed with water, which later becomes hard due to cement, mineral hydrate formation when solidified [2]. The various types of cement and their applications such as Portland, Siliceous fly ash, calcareous, slag and Fume silica cement differ by the amount of SiO<sub>2</sub>, Al<sub>2</sub>O<sub>3</sub>, Fe<sub>2</sub>O<sub>3</sub>, CaO, MgO, SO<sub>3</sub> and other materials such as Na<sub>2</sub>O and K<sub>2</sub>O composition [3]. Economic growth and urbanisation have made cement one of the most consumed commodity in world with global annual production increase from 3.3 Gt in 2010 to current 4.1 Gt which is still expected to grow moderately in the next decade due to expected infrastructure development in India and other developing Asian and African countries [4, 5]. Cement production consists of three sections: fuel and raw material processing, production of clinker via pyroprocessing and grinding and

blending of cement clinker nodules with additive materials such as gypsum and anhydrite for different types of cement types [6]. Natural occurring limestone is ground and mixed in required proportion with silicon and aluminium source such as clay and sand and iron-containing compounds to form a homogenous raw mix called raw meal. The raw meal is then pyroprocessed at a high temperature of about 1450 °C in rotary kiln system where it is dried, preheated, calcined and sintered into cement clinker. The pyroprocessing can be dry, wet, semi-dry or semi-wet and their selection depends on the moisture content of the raw meal, rotary kiln configuration and energy cost. The wet process is cheaper with a high-quality product but very high energy intensity because of the high moisture content of about 36% in raw meal. The dry process is usually more compact with low operational cost and energy consumption compared with the wet process but with lesser product homogeneity [2]. The clinker produced is further grinded with about 5% gypsum which prevents pre-set and controls the hydration rate of the cement. Other types of cement are produced by blending with hydraulic, pozzolanic or inert materials [7]. Cement production processes are energy-intensive and generate huge greenhouse emissions with the clinker energy intensity of about 3.4 GJ/t in 2018 [4] generating about 4% of the global CO<sub>2</sub> emission [8]. Strategies identified to reduce the emissions in cement production include improving heat recovery and energy efficiency [9–11], switching to low carbon source of energy [12], feedstock and material substitute [13–15], reducing the clinker-to-cement ratio [16] and advancing technology innovations such as carbon capture and storage [17, 18]. Cement and concrete technology modelling and simulation have also been used to improve energy efficiency and usage [19–22].

Optimization is a mathematical technique used to find the best solution to objective function (s) by maximising the desired variable and minimising the undesired variables under some set of constraints with the sole aim of improving performance and cost [23]. The optimisation technique in cement and concrete studies can be broadly classified as a meta-heuristic approach and statistical experimental design methods [24]. The meta-heuristic approach is an iterative method that intelligently exploits search space at learning strategies. It includes Genetic Algorithm (GAs), Particle swarm optimization (PSO), Harmony Search (HS), Ant Colony Optimization (ACO), Charged System Search (CSS), Big Bang-Big Crunch (BB-BC), Artificial Bee Colony algorithm (ABC), spherical interpolation of the objective function, Colliding bodies optimization (CBO), Vibrating Particles System (VPS), simulated annealing, krill herd (KH), Whale Optimization Algorithm (WOA), hybrid Harmony Search, force method and genetic algorithm, mine and improved mine blast algorithms [24–26] which are modelled from natural and social behaviours as well as physics laws.

Statistical experimental design methods are widely used to obtain desired optimise solution for a set of constraints [27]. Response Surface Methodology (RSM) is a statistical optimisation technique used to model and analyse a process to determine the effect of independent multivariable on the process response and to evaluate the relations between these variables [28]. RSM is based on understanding the topography of the response surface to determine the most appropriate response region [29]. RSM experimental design can be categorised into Box–Behnken Design (BBD), Central Composite Design (CCD), Dohlert design, Mixture response and three-level factorial design [30–32]. The BBD is created from 3 level factorial design [32] and gives quadratic response model with three minimum number of factors requiring three levels of factors (upper, centre, lower) for each factor and specific positioning of design points [33, 34]. The CCD is developed from the 2 factorial design and gives the quadratic response model with five levels for each factor. Hence it is more robust and insensitive to missing data or experimental runs [34].

In recent years, Response Surface Methodology has been applied to optimise several chemical processes such as extraction [29], adsorption [23], pharmaceutical wastewater treatment [28], leaching [35]. Studies on cement production optimisation have been carried out on clinker simulation using AspenTech [36], cement raw materials blending using a general nonlinear time-varying model [37], cement grinding using population balance model [6], clinker chemistry and kiln energy efficiency using metaheuristic optimization techniques [38], numerical and computational fluid dynamics study of cement calciner [16]. RSM has been efficient and accurate in studies on cement and concrete technology [39–43]. This study focused on the simulation of an integrated wet cement process flow sheet using Aspen HYSYS and optimisation of the cement production rate at minimum raw material feed using CCD of response surface methodology.

## 2. Methodology

### 2.1 Cement production simulation

Aspen HYSYS 8.8 was used for the steady-state simulation of the integrated process flow sheet for the cement production [44]. Within the simulation environment, topological optimization (proper arrangement of equipment) was done to enable very high energy savings or optimization. A pure component such as water,  $\text{CO}_2$  and air are added as conventional components, while non-conventional components are added as hypothetical components to the HYSYS environment based on their physical properties (molecular weight & density). **Figure 1** shows the block diagram of the production of cement while the HYSYS process flow diagram for the cement production simulation is shown in Figure A1 in the appendix. Limestone is decomposed in the first reactor to give off  $\text{CO}_2$  as gas, while the produced  $\text{CaO}$  is the feed to the Section A reactor to react with silicate to form Calcium disilicate. The produced Calcium disilicate reacts further with the unreacted  $\text{CaO}$  in reactor B to produce Calcium trisilicate. Calcium oxide ( $\text{CaO}$ ) further reacts with Aluminium oxide to produce tricalcium aluminate, another constituent of cement, while the final product component is produced in section C, where  $\text{CaO}$  reacts with Aluminate and Ferric oxide to produce tetracalciumaluminoferrite. These separate

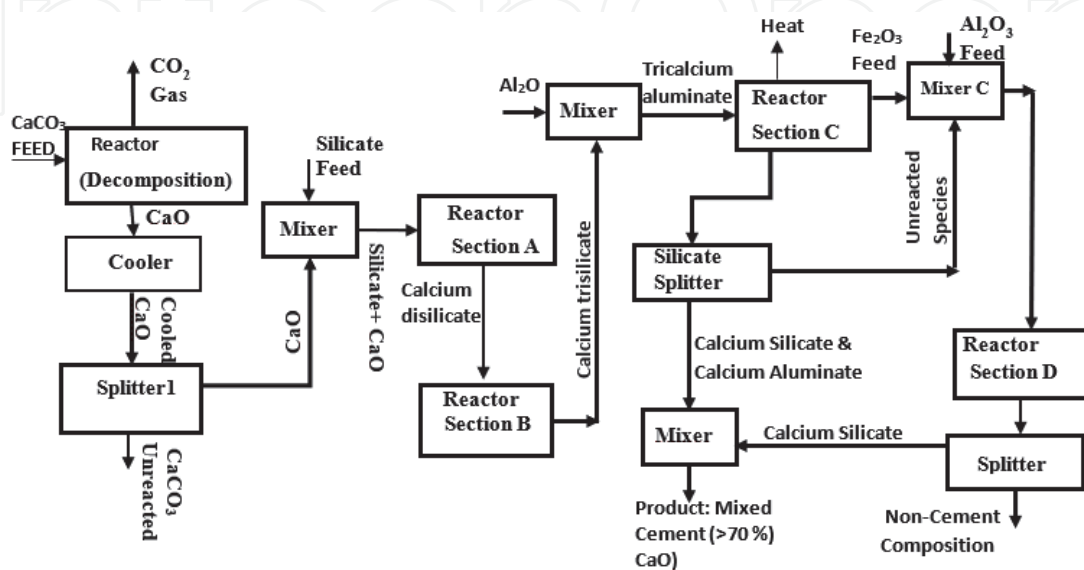
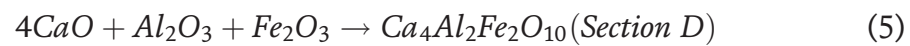
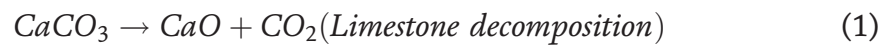


**Figure 1.**  
 Process flow diagram for the production of cement.

components produced at a different section of the simulated Kiln are mixed to achieve a matrix compound of the cement product, having over 70% of CaO.

## 2.2 Aspen Hysys simulation

Aspen Hysys was used for the steady-state simulation of the integrated process flow sheet for the cement production. Within the simulation environment, topological optimization (proper arrangement of equipment) was done to enable very high energy savings or optimization. A pure component such as water, CO<sub>2</sub> and air are added as conventional components, while non-conventional components are added as hypothetical components to the HYSYS environment based on their physical properties (molecular weight and density). Based on the process description, the different reactions taking place in each simulated reactor, as presented in the flowchart are:



The various products in the various sections of the process reactors are; Tricalcium silicate (Ca<sub>2</sub>SiO<sub>4</sub>) which is responsible for early strength and the initial set of the cement; Dicalcium silicate (Ca<sub>3</sub>SiO<sub>5</sub>) which increases the strength as it age; Tricalcium aluminate (Ca<sub>3</sub>Al<sub>2</sub>O<sub>6</sub>) which contributes to the concrete strength development in the first few days but least desirable due to its reactivity with sulphate containing soils and water; Tetracalciumaluminoferrite (Ca<sub>4</sub>Al<sub>2</sub>Fe<sub>2</sub>O<sub>10</sub>) which reduces clinkering temperature. The equipment design parameters employed in this work are provided in **Table 1**.

The flow rate of the major raw materials for the production of cement in the clinkering reactor as depicted by Eqns. (6–12) are carefully chosen based on the standard provided by Winter N. B. [45]. The Chemical parameters based on the oxide composition are very useful in describing clinker characteristics. The following parameters are widely used.

- a. *Lime Saturation Factor (LSF)*: is the measure of the ratio of alite to belite in the clinker. It is estimated by the ratio of CaO to the sum of other three main oxides SiO<sub>2</sub>, Fe<sub>2</sub>O<sub>3</sub> and Al<sub>2</sub>O<sub>3</sub>. The equation is given by:

$$LSF = \frac{CaO}{2.8SiO_2 + 1.2Al_2O_3 + 0.65Fe_2O_3} \quad (6)$$

$$LSF = \frac{190}{2.8(60) + 1.2(15) + 0.65(10)} = 0.98 \quad (7)$$

LSF values in clinkers range between 0.92–0.98. The LSF value of 0.98 falls within an acceptable range.

- b. *Silica Ratio (SR)*: This is also known as Silica Modulus. The expression of SR is given as:

$$SR = \frac{SiO_2}{Al_2O_3 + Fe_2O_3} \quad (8)$$

| Simple separator                 | Delta P        | Stream fractions                |                         |                                 |                          |
|----------------------------------|----------------|---------------------------------|-------------------------|---------------------------------|--------------------------|
|                                  | 0.000          | Solids in vapour                | 0.0100                  |                                 |                          |
|                                  |                | Solids in liquid                | 0.0100                  |                                 |                          |
|                                  |                | Liquid in bottoms               | 0.0100                  |                                 |                          |
| Exchanger                        | Delta P (bar)  | Delta T (°C)                    | Duty (kcal/h)           |                                 |                          |
| Cooler                           | 0.000          | 655                             | 2.691 x 10 <sup>7</sup> |                                 |                          |
| Component Splitter               | Top Temp. (°C) | Bottom Temp. (°C)               | Top Pressure (bar)      | Bottom Pressure (bar)           | Duty                     |
| Splitter 1                       | 30             | 30                              | 1                       | 1                               | 2.054 x 10 <sup>5</sup>  |
| Splitter 2                       | 1252           | 1252                            | 1                       | 1                               | 1.825 x 10 <sup>4</sup>  |
| Splitter 3                       | 1252           | 1252                            | 1                       | 1                               | 1.923 x 10 <sup>4</sup>  |
| Reactors                         | Delta P        | Vessel volume (m <sup>3</sup> ) | Liquid level (%)        | Liquid volume (m <sup>3</sup> ) | Duty (kcal/h)            |
| CaCO <sub>3</sub> decomp reactor | 0.0000         | 0.0000                          | 50.00                   | 25.00                           | 2.6764 x 10 <sup>7</sup> |
| Section A reactor                | 0.0000         | 50.00                           | 50.00                   | 25.00                           | 7.6209 x 10 <sup>6</sup> |
| Section B reactor                | 0.0000         | 50.00                           | 50.00                   | 25.00                           | 2.6131 x 10 <sup>6</sup> |
| Section C reactor                | 0.0000         | 50.00                           | 50.00                   | 25.00                           | 4.5634 x 10 <sup>5</sup> |
| Section D reactor                | 0.0000         | 50.00                           | 50.00                   | 25.00                           | 7.4721 x 10 <sup>5</sup> |

**Table 1.**  
*Equipment design parameter.*

Based on the experimental design for the simulated cement production process. The flow rate of Al<sub>2</sub>O<sub>3</sub> and Fe<sub>2</sub>O<sub>3</sub> are 15 tonnes/day and 10 tonnes/day respectively. The low level and high levels of SiO<sub>2</sub> are found to be 50 tonnes/day and 60 tonnes/day respectively. Hence, the SR values are the high and low value of the SiO<sub>2</sub> flow rate are calculated as follows:

$$SR = \frac{50}{15 + 10} = 2.0 \quad (9)$$

$$SR = \frac{60}{15 + 10} = 2.4 \quad (10)$$

A high silicate ratio means that more calcium silicates are present in the clinker and less aluminate and ferrite. SR is typical, between 2.0 and 3.0. The SR values of 2.0 and 2.4 fall within an acceptable range of 2.0 and 3.0.

c. *Aluminate Ratio (AR)*: This is the ratio of aluminate and ferrite phases in the clinker. AR value ranges between 1–4 in Portland clinkers. The flow rate of Al<sub>2</sub>O<sub>3</sub> and Fe<sub>2</sub>O<sub>3</sub> used in the process simulation are 15 tonnes/day and 10 tonnes/day respectively. The equation governing the AR of the oxide is given by

$$AR = \frac{Al_2O_3}{Fe_2O_3} \quad (11)$$

$$AR = \frac{15}{10} = 1.5 \quad (12)$$

The mass flow and corresponding clinker quality parameters are presented in **Table 2**.

### 2.3 Multivariate design of experiment

The central composite design of response surface methodology was used to analyse the effect of CaO and SiO<sub>2</sub> on cement production rate. The total number of experimental runs (N) required for  $n$  independent variables and  $n_c$  number of replica centre points is given by Eq. 13

$$N = 2^n + 2n + n_c \quad (13)$$

Design Expert 10.0.3 software was used to generate the experimental design from the ten experimental runs to study the combined effect of two variables on the response. For two variables factor in the experiments; four factorial points ( $2^n$ ), four axial points ( $2n$ ) and two replicates at the central points ( $n_c$ ) at distance  $\alpha = 1.414$  from the centre were used for the CCD design. A polynomial empirical model was developed from the ten experimental runs to correlate the response with the independent variables. The mathematical expression can be expressed as:

$$Y = \beta_0 + \sum_{i=1}^n \beta_i X_i + \sum_{i=1}^n \beta_{ii} X_i^2 + \sum_{1 \leq i < j}^n \beta_{ij} X_i X_j + \varepsilon \quad (14)$$

Where  $Y$  = Predicted response,  $\beta_0$  = constant coefficient,  $\beta_i$  = Linear coefficient,  $\beta_{ii}$  = Quadratic,  $\beta_{ij}$  = Interaction coefficients and  $\varepsilon$  = model random error,  $n$  the number of variable factors,  $X_i$  and  $X_j$  are the coded values of the variable parameters [35].

The response generated function distance from the centre  $\alpha = 2^{n/4}$ . The codes are calculated as a function of the range the factors as shown in **Table 3**.

The central composite experimental design for the synthesis of cement via simulation is depicted in **Table 4**. The mass flow rate of CaO and SiO<sub>2</sub> measured in tonnes/day are the independent variables or predictors which are studied for their effect on the response variable (cement flow rate) at a constant Al<sub>2</sub>O<sub>3</sub> and Fe<sub>2</sub>O<sub>3</sub> flow rates.

### 2.4 Model fitting and statistical analysis

The interaction between the variables and the response data as well as the statistical parameters were analysed graphically by analysis of variance (ANOVA) in the Design-Expert software. Regression analysis, significance, F-test, surface and contour plots of the response were also generated from the software. A probability

|            | Mass flow (tonnes/day) |                  |                                |                                | Clinker quality parameter |     |     |
|------------|------------------------|------------------|--------------------------------|--------------------------------|---------------------------|-----|-----|
|            | CaO                    | SiO <sub>2</sub> | Al <sub>2</sub> O <sub>3</sub> | Fe <sub>2</sub> O <sub>3</sub> | LSF                       | SR  | AR  |
| High level | 190                    | 60               | 15                             | 10                             | 0.98                      | 2.4 | 1.5 |
| Low level  | 135                    | 50               | 15                             | 10                             | 0.82                      | 2.0 | 1.5 |

**Table 2.**  
Raw material mass flow and clinker quality parameter.

|                   | Code      | Mathematical relationship                                 |
|-------------------|-----------|---|
| Lower axial point | $-\alpha$ | $X_{min}$   |
| Lower level       | - 1       | $[(X_{max} + X_{min})/2] - [\alpha(X_{max} - X_{min})/2]$ |
| Centre point      | 0         | $(X_{max} + X_{min})/2$                                   |
| Upper level       | 1         | $[(X_{max} + X_{min})/2] + [\alpha(X_{max} - X_{min})/2]$ |
| Upper axial point | $\alpha$  | $X_{max}$   |

**Table 3.**  
 Relationship between the variable values and their assigned codes.

| Factor | Name                          | Units      | Low | High | $-\alpha$ | $+\alpha$ |
|--------|-------------------------------|------------|-----|------|-----------|-----------|
| A      | Flow rate of CaO              | tonnes/day | 135 | 190  | 123.609   | 201.391   |
| B      | Flow rate of SiO <sub>2</sub> | tonnes/day | 50  | 60   | 47.9289   | 62.0711   |

**Table 4.**  
 Design of Experiment using central composite (C.C.D) Design of Response Surface Methodology (R.S.M).

value of 95% confidence level was used to evaluate the significance of the model terms and coefficients.

### 3. Results and discussion

#### 3.1 Simulation and optimisation of cement flow

All simulations were done in duplicate and the experimental design were generated by the Central Composite Design (C.C.D) of the Design-Expert Software, which resulted in a total of 10 experimental (simulation) runs and the results of the experiments (simulations) are shown in **Table 5**.

| Run No. | Factors      |        |               |         | Response                |             |
|---------|--------------|--------|---------------|---------|-------------------------|-------------|
|         | Coded levels |        | Actual values |         | The flow rate of cement |             |
|         | A            | B      | A             | B       | HYSYS Simulation        | C.C.D Model |
| 1       | 1.000        | 1.000  | 190           | 60      | 46.6                    | 45.6674     |
| 2       | -1.000       | -1.000 | 135           | 50      | 30.74                   | 31.9851     |
| 3       | 0.000        | 0.000  | 162.5         | 55      | 46.04                   | 46.04       |
| 4       | 0.000        | -1.414 | 162.5         | 47.9289 | 30.57                   | 31.271      |
| 5       | 1.000        | -1.000 | 190           | 50      | 44.3                    | 42.1551     |
| 6       | -1.414       | 0.000  | 123.609       | 55      | 46.04                   | 43.4867     |
| 7       | 0.000        | 0.000  | 162.5         | 55      | 46.04                   | 46.04       |
| 8       | -1.000       | 1.000  | 135           | 60      | 46.6                    | 49.0574     |
| 9       | 1.414        | 0.000  | 201.391       | 55      | 46.04                   | 48.2808     |
| 10      | 0.000        | 1.414  | 162.5         | 62.0711 | 46.84                   | 45.8265     |

**Table 5.**  
 Simulation and predicted results from central composite design (C.C.D).

The change in mean response in cement flow per unit increase in variable occurs when other predictors area kept constant and is estimated by the coefficient of estimation and is presented **Table 6**.

The empirical quadratic equation for the optimal cement product rate as a function of CaO and SiO<sub>2</sub> mass flow in coded form as derived from **Table 7** was obtained according to the CCD and is given in Eq. 15

$$C = 46.04 + 1.70A + 5.15B - 3.39AB - 0.078A^2 - 3.75B^2 \quad (15)$$

The test of the significance and the adequacy of the model and its coefficients lack fitness which was based on F-value or P-value at 95% confidence level was tested from analysis of variance (ANOVA) and the result is presented in **Table 7**. The result shows that the model at an F value of 20.35 and a very low P-value of 0.0005 indicates that the statistical regression model was significant. The result also shows that A, B, AB and B<sup>2</sup> are significant terms.

The regression statistical analysis is summarised in **Table 8**. The R squared value of 0.9356 is in good agreement with the adjusted R-square value of 0.8896, showing a good fit of the model, as the closer the R squared value to 1.00, the more significant the model. The adequate precision of 13.55 indicates the low noise level and a

| Factor                | Coefficient |    | Standard | 95% CI |       | VIF  |
|-----------------------|-------------|----|----------|--------|-------|------|
|                       | Estimate    | df | Error    | Low    | High  |      |
| Intercept             | 46.04       | 1  | 0.86     | 44.00  | 48.08 |      |
| A-Flowrate of CaO     | 1.70        | 1  | 0.68     | 0.080  | 3.31  | 1.00 |
| B-Flow rate of Silica | 5.15        | 1  | 0.68     | 3.53   | 6.76  | 1.00 |
| AB                    | -3.39       | 1  | 0.97     | -5.67  | -1.11 | 1.00 |
| A <sup>2</sup>        | -0.078      | 1  | 0.73     | -1.81  | 1.65  | 1.02 |
| B <sup>2</sup>        | -3.75       | 1  | 0.73     | -5.48  | -2.01 | 1.02 |

**Table 6.**  
Coefficient estimation for cement flow rate in terms of coded factors.

| Source         | Sum of squares | df | Mean   | F value | p-value (Prob > F) |
|----------------|----------------|----|--------|---------|--------------------|
| Model          | 379.61         | 5  | 75.92  | 20.35   | 0.0005             |
| A              | 22.98          | 1  | 22.98  | 6.16    | 0.0421             |
| B              | 211.86         | 1  | 211.86 | 56.78   | 0.0001             |
| AB             | 45.97          | 1  | 45.97  | 12.32   | 0.0099             |
| A <sup>2</sup> | 0.042          | 1  | 0.042  | 0.011   | 0.9180             |
| B <sup>2</sup> | 97.60          | 1  | 97.60  | 26.16   | 0.0014             |
| Residual       | 26.12          | 7  | 3.73   |         |                    |
| Lack of Fit    | 26.12          | 3  | 8.71   |         |                    |
| Pure Error     | 0.000          | 4  | 0.000  |         |                    |
| Cor. Total     | 405.73         | 12 |        |         |                    |

**Table 7.**  
ANOVA results for the statistical model for cement flow rate.

| Parameter      | Values |
|----------------|--------|
| R-Squared      | 0.9356 |
| Adj R-Squared  | 0.8896 |
| Pred R-Squared | 0.5422 |
| Mean           | 43.69  |
| Std. Dev.      | 1.93   |
| C.V. %         | 4.42   |
| Adeq Precision | 13.554 |

**Table 8.**  
 Statistical information for the statistical model for cement flow rate.

strong signal for optimisation. Hence, this indicates the two predictors (flow rate of CaO and flow rate of SiO<sub>2</sub>) could predict the flow rate of cement, thus the model equation, contour plot and 3D surface plot could be used to predict the response (flow rate of the cement).

### 3.2 Surface plots

The contour plot which shows the possible relationship between the CaO, SiO<sub>2</sub> and cement product mass flow is presented in **Figure 2**. The darker red regions indicate higher C (response) values. Here, the optimum flow rate of cement is found from the isolines to be 47.748 tonnes/day at a flow rate of 152.346 tonnes/day of CaO and 56.8241 tonnes/day SiO<sub>2</sub>.

The three-dimensional (3D) response surface plots obtained from the model equation using Design Expert 10.03 is depicted in **Figure 3**. This depicts the effect

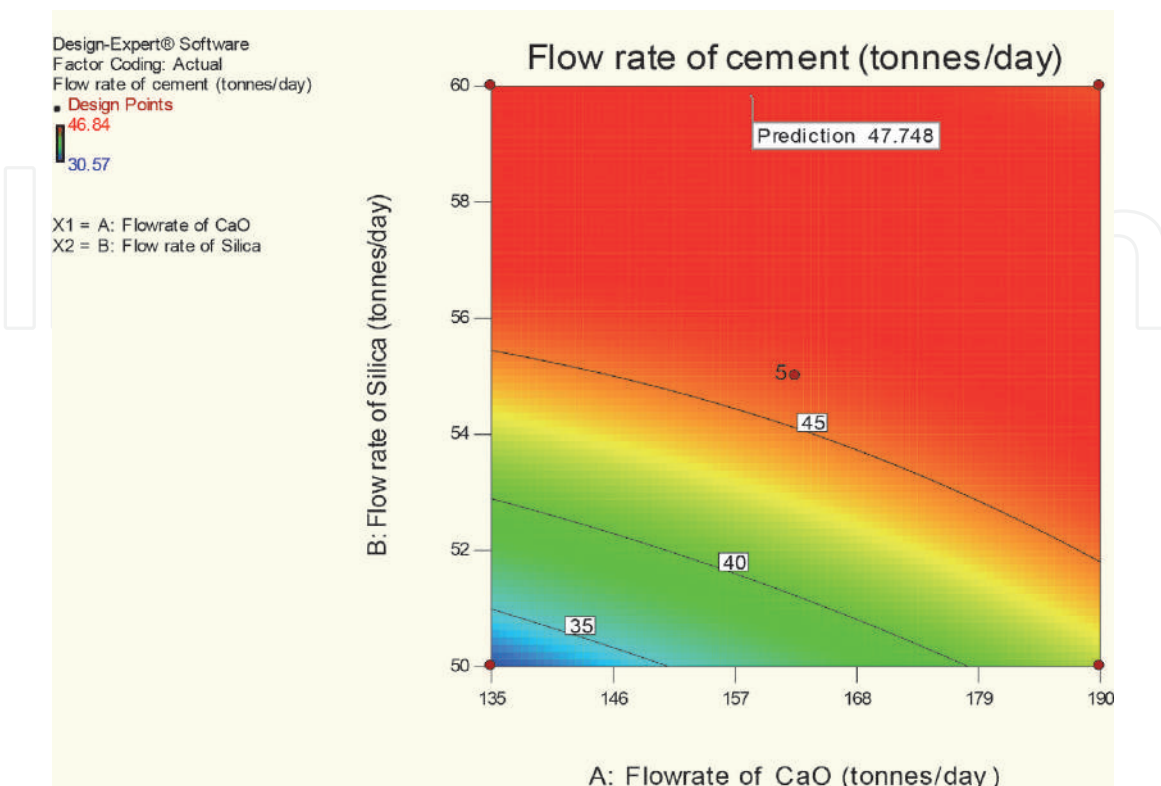


**Figure 2.**  
 Contour surface plot showing the effects of the flow rate of CaO and flow rate of SiO<sub>2</sub> on the flow rate of cement.

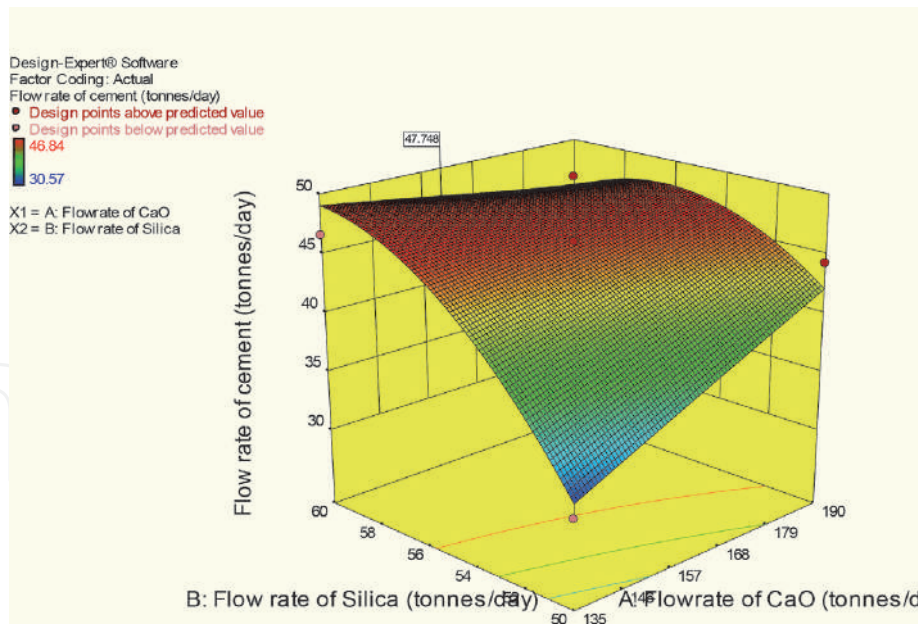


**Figure 3.**  
 Response surface plot of the effects of CaO and SiO<sub>2</sub> mass flow on cement production.

of the flow rate of CaO, the flow rate of SiO<sub>2</sub> on the flow rate of cement. The flow rate of cement was observed to increase with an increase in the flow rate of CaO. Conversely, increasing the flow rate of SiO<sub>2</sub> did not increase the flow rate of cement. Hence, the major predictor in cement production in the clinkering section is the flow rate of CaO.

The optimization plot of the cement output is shown in **Figure 4**. The optimum cement flow rate of 47.239 tonnes/day is found to be at CaO flow rate of 152.346 tonnes/day and SiO<sub>2</sub> flow rate of 56.8241 tonnes/day.

### 3.3 Energy optimization

Aspen Energy Analyser was used to determine the percentage of energy savings based on converged steady-state simulation of the process flow sheet in **Figure 1**. The total energy savings as a function of process utilities and carbon emissions are present in **Figure 5**.

The overall utilities in terms of energy are found to be optimised from the actual value of  $6.511 \times 10^7$  kcal/h to  $1.211 \times 10^7$  kcal/h and indicating available energy savings of  $5.3 \times 10^7$  kcal/h, with overall energy savings of 81.40% which also correspond to 297.4 tonnes/day carbon emission reduction.

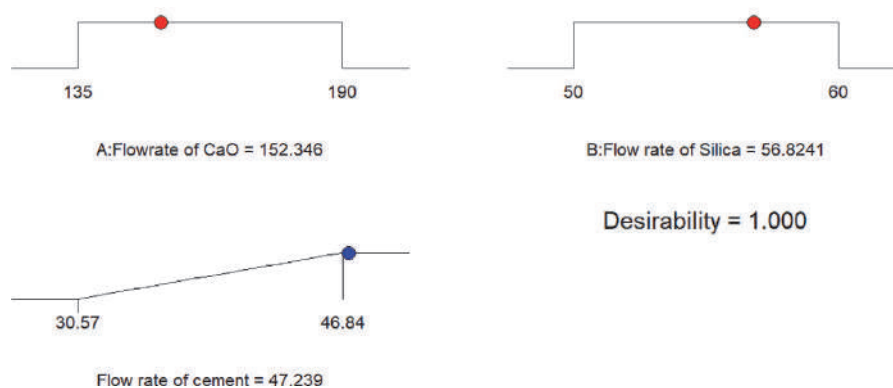


**Figure 4.**  
 Optimization plot showing the effects of the flow rate of CaO and flow rate of SiO<sub>2</sub> on the flow rate of cement.

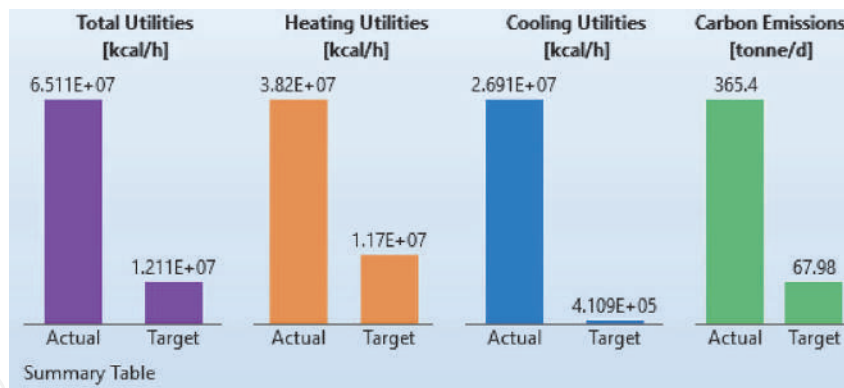


**Figure 5.** Energy savings at optimum feed ( $\text{CaO}$  and  $\text{SiO}_2$ ) rate and product (cement) flow rate.

## 4. Conclusion

Process flow diagram for the cement production was simulated to achieve high energy optimization and optimum cement flow rate by minimising the flow rate of the feed ( $\text{CaO}$  and  $\text{SiO}_2$ ). Central composite Design (C.C.D) of Response Surface Methodology used to design the experiment for the simulation using Design Expert 10.0.3. The optimum cement flow rate is found from surface and contour plots to be 47.239 tonnes/day at  $\text{CaO}$  flow rate of 152.346 tonnes/day and  $\text{SiO}_2$  flow rate of 56.8241 tonnes/day. The R squared value of 0.9356 determined from the statistical analysis shows a very high significance of the model. Energy efficiency optimization is also carried out using Aspen Energy Analyser. The overall utilities in terms of energy are found to be optimised by 81.4 % from  $6.511 \times 10^7$  kcal/h actual value to  $1.211 \times 10^7$  kcal/h with 297.4 tonnes/day the carbon emission savings.

Further work could be performed on fault identification and diagnosis of the process plant. Incorporated with an automated plant to guarantee the safety of workers, reduce environmental problems and increase yield to sustain production improvement.

## 5. Recommendations

This research work sought to recommend the following concerns in which cement production could be improved:

1. Research and development (R&D) in the cement production, processing and utilisation should be encouraged. This will play a vital role in the construction industry, operation and maintenance of efficient road network and effective transportation system.
2. Automation of cement and kiln sections of the cement production is recommended
3. Optimization of the cement production can be tailored into the fabrication of high tech cement equipment and parts.
4. Optimization of the limestone crusher to quantify the amount of crushed limestone is needed.
5. Looking into future the results obtained in this research will open up several important possibilities in the cement production at optimum conditions. This will have a multiplier effect on infrastructural amenities development.

## Conflict of interest

There is no conflict of interest associated with this work.

## Appendix

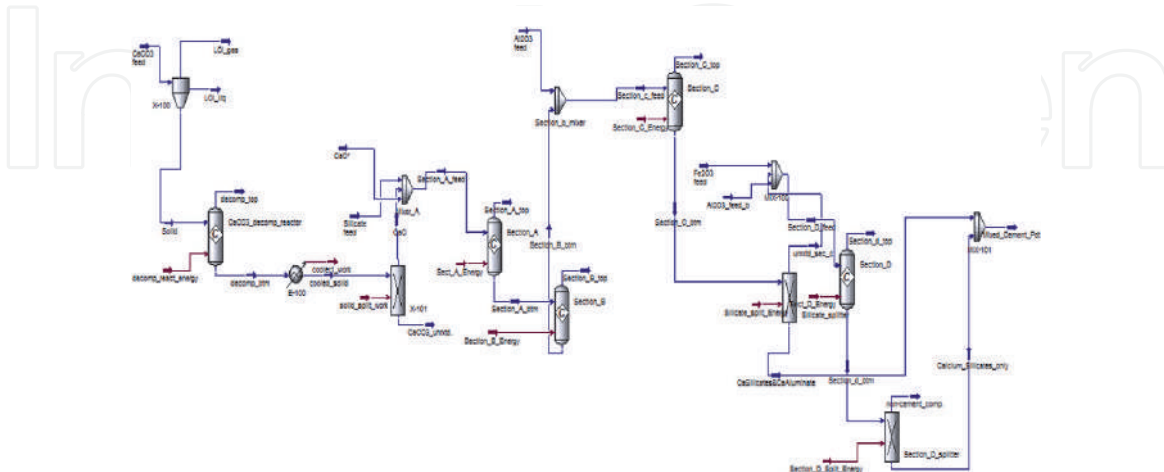


**Figure A1.**  
*HYSYS process flow simulation diagram for the production of cement.*

## Author details

Oluwafemi M. Fadayini<sup>1\*</sup>, Adekunle A. Obisanya<sup>2</sup>, Gloria O. Ajiboye<sup>2</sup>,  
Clement Madu<sup>1</sup>, Tajudeen O. Ipaye<sup>3</sup>, Taiwo O. Rabi<sup>4</sup>, Shola J. Ajayi<sup>1</sup>  
and Joseph T. Akintola<sup>1</sup>

1 Department of Chemical Engineering, Lagos State Polytechnic, Ikorodu, Lagos, Nigeria

2 Department of Chemical Engineering, Yaba College of Technology, Yaba, Lagos, Nigeria

3 Department of Civil Engineering, Lagos State Polytechnic, Ikorodu, Lagos, Nigeria

4 Department of Mechanical Engineering, Lagos State Polytechnic, Ikorodu, Lagos, Nigeria

\*Address all correspondence to: olufeday@gmail.com;  
fadayini.o@mylaspotech.edu.ng

## IntechOpen

© 2021 The Author(s). Licensee IntechOpen. This chapter is distributed under the terms of the Creative Commons Attribution License (<http://creativecommons.org/licenses/by/3.0>), which permits unrestricted use, distribution, and reproduction in any medium, provided the original work is properly cited. 

## References

- [1] EPA, "Mineral Products Industry," in *Compilation of air pollutant emission factors. Volume I: stationary point and area sources*, AP-42 5th., Research Triangle Park, NC: U.S. Environmental protection agency, 1995.
- [2] N. Martin, E. Worrell, and L. Price, "Energy Efficiency and Carbon Dioxide Emissions Reduction Opportunities in the U.S. Cement Industry," Berkeley, 1999. doi: 10.2172/751775.
- [3] S. P. Dunuweera and R. M. G. Rajapakse, "Cement Types, Composition, Uses and Advantages of Nanocement, Environmental Impact on Cement Production, and Possible Solutions," *Adv. Mater. Sci. Eng.*, vol. 2018, 2018, doi: 10.1155/2018/4158682.
- [4] IEA, "Cement," Paris, 2020. [Online]. Available: <https://www.iea.org/reports/cement>.
- [5] TERI, "CEMENT INDUSTRY; Trends Report," New Delhi, 2017. [Online]. Available: <http://www.teriin.org/library/files/Cement-Industry-Trends-Report2017.pdf>.
- [6] A. Jankovic, W. Valery, and E. Davis, "Cement grinding optimisation," *Miner. Eng.*, vol. 17, no. 11–12, pp. 1075–1081, 2004, doi: 10.1016/j.mineng.2004.06.031.
- [7] D. Olsen, S. Goli, D. Faulkner, and A. Mckane, "Opportunities for Energy Efficiency and Demand Response in the California Cement Industry," no. December. Lawrence Berkeley National Laboratory, 2010.
- [8] J. G. J. Olivier and J. A. H. W. Peters, "Trends in Global CO<sub>2</sub> and Total Greenhouse Gas Emissions: Report 2019," The Hague, 2020. [Online]. Available: [www.pbl.nl/en](http://www.pbl.nl/en).
- [9] H. Mikulčić, M. Vujanović, N. Markovska, R. V. Filkoski, M. Ban, and N. Duić, "CO<sub>2</sub> emission reduction in the cement industry," *Chem. Eng. Trans.*, vol. 35, pp. 703–708, 2013, doi: 10.3303/CET1335117.
- [10] S. Zhang, H. Ren, W. Zhou, Y. Yu, and C. Chen, "Assessing air pollution abatement co-benefits of energy efficiency improvement in cement industry: A city-level analysis," *J. Clean. Prod.*, vol. 185, pp. 761–771, 2018, doi: 10.1016/j.jclepro.2018.02.293.
- [11] M. J. S. Zuberi and M. K. Patel, "Bottom-up analysis of energy efficiency improvement and CO<sub>2</sub> emission reduction potentials in the Swiss cement industry," *J. Clean. Prod.*, vol. 142, pp. 4294–4309, 2017, doi: 10.1016/j.jclepro.2016.11.178.
- [12] N. Chatziaras, C. S. Psomopoulos, and N. J. Themelis, "Use of waste-derived fuels in cement industry: a review," *Manag. Environ. Qual. An Int. J.*, vol. 27, no. 2, pp. 178–193, 2016, doi: 10.1108/MEQ-01-2015-0012.
- [13] E. Marchetti, "Use of Agricultural Wastes as Supplementary Cementitious Materials," KTH ROYAL INSTITUTE OF TECHNOLOGY, 2020.
- [14] A. Naqi and J. G. Jang, "Recent progress in green cement technology utilizing low-carbon emission fuels and raw materials: A review," *Sustain.*, vol. 11, no. 2, 2019, doi: 10.3390/su11020537.
- [15] R. Maddalena, J. J. Roberts, and A. Hamilton, "Can Portland cement be replaced by low-carbon alternative materials? A study on the thermal properties and carbon emissions of innovative cement," *J. Clean. Prod.*, vol. 186, no. April, pp. 933–942, 2018, doi: 10.1016/j.jclepro.2018.02.138.
- [16] H. Mikulcic, M. Vujanovic, and N. Duic, "Improving the Sustainability of Cement Production by Using Numerical

Simulation of Limestone Thermal Degradation and Pulverized Coal Combustion in a Cement Calciner,” *J. Clean. Prod.*, vol. 88, pp. 262–271, 2015.

[17] P. Markewitz *et al.*, “Carbon capture for CO<sub>2</sub> emission reduction in the cement industry in Germany,” *Energies*, vol. 12, no. 12, pp. 1–27, 2019, doi: 10.3390/en12122432.

[18] WSP Parson Brinkerhoff and DNV GL, “Industrial Decarbonisation & Energy Efficiency Roadmaps to 2050: Cement,” 2015.

[19] C. Cseryei and A. G. Straatman, “Numerical modelling of a rotary cement kiln with improvements to shell cooling,” *Int. J. Heat Mass Transf.*, vol. 102, pp. 610–621, 2016, doi: 10.1016/j.ijheatmasstransfer.2016.06.058.

[20] H. R. Goshayeshi and F. K. Poor, “Modeling of Rotary Cement Kiln (In Persian),” *Energy Power Eng.*, vol. 8, pp. 23–33, 2016.

[21] S. Sadighi, M. Shirvani, and A. Ahmad, “Rotary cement kiln coating estimator: Integrated modelling of the kiln with shell temperature measurement,” *Can. J. Chem. Eng.*, vol. 89, no. 1, pp. 116–125, Feb. 2011, doi: 10.1002/cjce.20365.

[22] K. V. Sabarish, M. Akish Remo, and P. Paul, “Optimizing the Concrete Materials by Taguchi Optimization Method,” *IOP Conf. Ser. Mater. Sci. Eng.*, vol. 574, no. 1, 2019, doi: 10.1088/1757-899X/574/1/012002.

[23] S. Saini, J. Chawla, R. Kumar, and I. Kaur, “Response surface methodology (RSM) for optimization of cadmium ions adsorption using - C 16–6 - 16 incorporated mesoporous MCM - 41,” *SN Appl. Sci.*, vol. 1, no. 8, pp. 1–10, 2019, doi: 10.1007/s42452-019-0922-5.

[24] C. TAO, “Optimization of Cement Production and Hydration for

Improved,” UNIVERSITY OF FLORIDA, 2017.

[25] F. Omidinasab and V. Goodarzimehr, “A hybrid particle swarm optimization and genetic algorithm for truss structures with discrete variables,” *J. Appl. Comput. Mech.*, vol. 6, no. 3, pp. 593–604, 2020, doi: 10.22055/JACM.2019.28992.1531.

[26] L. J. Li, Z. B. Huang, and F. Liu, “A heuristic particle swarm optimization method for truss structures with discrete variables,” *Comput. Struct.*, vol. 87, no. 7–8, pp. 435–443, Apr. 2009, doi: 10.1016/j.compstruc.2009.01.004.

[27] M. J. Simon, “Concrete Mixture Optimization Using Statistical Methods: Final Report,” 2003. [Online]. Available: <http://www.fhwa.dot.gov/publications/research/infrastructure/pavements/03060/03060.pdf>.

[28] S. Barisci and O. Turkey, “Optimization and modelling using the response surface methodology (RSM) for ciprofloxacin removal by electrocoagulation,” *Water Sci. Technol.*, vol. 73, no. 7, pp. 1673–1679, 2016, doi: 10.2166/wst.2015.649.

[29] A. Y. Aydar, “Utilization of Response Surface Methodology in Optimization of Extraction of Plant Materials,” in *Statistical Approaches With Emphasis on Design of Experiments Applied to Chemical Processes*, V. Silva, Ed. InTech, 2018, pp. 157–168.

[30] S. A. Adeyeye, “Banana Drying Kinetics,” in *Banana Nutrition - Function and Processing Kinetics*, IntechOpen, 2020, pp. 0–20.

[31] M. N. Chollom, S. Rathilal, F. M. Swalaha, B. F. Bakare, and E. K. Tetteh, “Comparison of response surface methods for the optimization of an up-flow anaerobic sludge blanket for the treatment of slaughterhouse wastewater,” *Environ. Eng. Res.*, vol. 25,

no. 1, pp. 114–122, 2020, doi: 10.4491/eer.2018.366.

[32] A. I. Khuri, “Response Surface Methodology and Its Applications In Agricultural and Food Sciences,” *Biometrics Biostat. Int. J.*, vol. 5, no. 5, pp. 155–163, 2017, doi: 10.15406/bbij.2017.05.00141.

[33] B. Olawoye, *A comprehensive handout on central composite design (CCD)*, no. July. 2016.

[34] Shari, “Choosing the Best Design for Process Optimization,” 2017. <https://www.statease.com/blog/choosing-best-design-process-optimization/> (accessed Nov. 27, 2020).

[35] S. Kumar, H. Meena, S. Chakraborty, and B. C. Meikap, “International Journal of Mining Science and Technology Application of response surface methodology ( RSM ) for optimization of leaching parameters for ash reduction from low-grade coal,” *Int. J. Min. Sci. Technol.*, vol. 28, no. 4, pp. 621–629, 2018, doi: 10.1016/j.ijmst.2018.04.014.

[36] B. Hokfors, M. Eriksson, and E. Vigg, “Modelling the cement process and cement clinker quality,” *Adv. Cem. Res.*, vol. 26, no. 6, pp. 311–318, 2014, doi: 10.1680/adcr.13.00050.

[37] X. Li, H. Yu, and M. Yuan, “Modeling and Optimization of Cement Raw Materials Blending Process,” *Math. Probl. Eng.*, vol. 2012, 2012, doi: 10.1155/2012/392197.

[38] C. Tao, “Optimization of cement production and hydration for improved performance, energy conservation, and cost,” UNIVERSITY OF FLORIDA, 2017.

[39] G. Cibilakshmi and J. Jegan, “A DOE approach to optimize the strength properties of concrete incorporated with different ratios of PVA fibre and nano-

Fe<sub>2</sub>O<sub>3</sub>,” *Adv. Compos. Lett.*, vol. 29, p. 2633366X2091388, 2020, doi: 10.1177/2633366x20913882.

[40] T. F. Awolusi, O. L. Oke, O. O. Akinkulore, and O. D. Atoyebi, “Comparison of response surface methodology and hybrid-training approach of artificial neural network in modelling the properties of concrete containing steel fibre extracted from waste tyres,” *Cogent Eng.*, vol. 6, no. 1, 2019, doi: 10.1080/23311916.2019.1649852.

[41] M. Sonebi and M. T. Bassuoni, “Investigating the effect of mixture design parameters on pervious concrete by statistical modelling,” *Constr. Build. Mater.*, vol. 38, pp. 147–154, Jan. 2013, doi: 10.1016/j.conbuildmat.2012.07.044.

[42] K. E. Alyamac, E. Ghafari, and R. Ince, “Development of eco-efficient self-compacting concrete with waste marble powder using the response surface method,” *J. Clean. Prod.*, vol. 144, pp. 192–202, Feb. 2017, doi: 10.1016/j.jclepro.2016.12.156.

[43] L. Soto-Pérez, V. López, and S. S. Hwang, “Response Surface Methodology to optimize the cement paste mix design: Time-dependent contribution of fly ash and nano-iron oxide as admixtures,” *Mater. Des.*, vol. 86, pp. 22–29, Dec. 2015, doi: 10.1016/j.matdes.2015.07.049.

[44] R. C. Carpio, L. D. S. Coelho, R. J. Silva, and A. B. Jorge, “Case Study in Cement Kilns Alternative Secondary Fuels Mixing Using Sequential Quadratic Programming, Genetic Algorithms, and Differential Evolution,” 2005, doi: 10.1590/S1678-58782008000400010.

[45] N. Winter, “Understanding Cement,” 2005. <https://www.understanding-cement.com/clinker.html> (accessed Nov. 02, 2020).

# Peculiarities of Portland Cement Clinker Synthesis in the Presence of a Significant Amount of $\text{SO}_3$ in a Raw Mix

*Oleg Sheshukov and Michael Mikheenkov*

## Abstract

Due to the depletion of the raw material base and a technogenic materials addition into a raw mix for the Portland cement clinker synthesis, sulfur and its oxides amount in a raw mix increases. According to literature the Portland cement clinker synthesis in the presence of a sulfur oxides significant amount is difficult. As the content of  $\text{SO}_3$  in the raw mix increases the amount of  $\text{C}_2\text{S}$  increases while  $\text{C}_3\text{S}$  and  $\text{C}_3\text{A}$  amount decrease. With an equal total content of  $\text{C}_2\text{S}$  and  $\text{C}_3\text{S}$  in the clinker their ratio  $\text{C}_3\text{S}/\text{C}_2\text{S}$  decreases with an increased content of  $\text{SO}_3$ . These factors lead to a deterioration in the Portland cement clinker quality. The clinker formation reactions thermodynamic analysis and some experimental studies allow determining reasons for the Portland cement clinker quality deterioration. It was found that the presence significant amount of a  $\text{SO}_3$  in the raw mix the synthesis in solid phase of low-basic  $\text{C}_4\text{A}_3\bar{\text{S}}$  (ye'elinite) is the thermodynamically preferred rather than high-basic  $\text{C}_3\text{A}$  and  $\text{C}_4\text{AF}$ . As a result, excess and crystallized free lime inhibits the  $\text{C}_3\text{S}$  synthesis through the liquid phase. The experimental studies result helped to develop a methodology for calculating the composition of a raw mix from materials with significant amount of  $\text{SO}_3$ . It allows to reduce the  $\text{SO}_3$  negative effect on the Portland cement clinker synthesis and to obtain high-quality Portland cement.

**Keywords:** high-sulfate raw material, Portland cement clinker, alite, belite, brownmillerite, ye'elinite, calculation procedure

## 1. Introduction

Sulfur and its oxides in the form of sulfate and sulfide minerals appear in the raw mixture of Portland cement clinker with the main raw materials for the preparation of clinker, namely clay and carbonate rock as well as additives and fuel. The technogenic origin additives of the metallurgical and heat-power industry, namely slags, fly ashes and oil cokes have especially high concentration of sulfur compounds [1–3]. According to [4] sulfur with calcium oxide forms calcium sulfate  $\text{CaSO}_4$  under conditions of oxidative burning. Depending on the burning temperature the latter with the alkaline components of the raw mix forms alkaline metal sulfates or with clinker minerals forms sulfo spurrit  $2(\text{C}_2\text{S})\text{C}\bar{\text{S}}$  and ye'elinite  $\text{C}_4\text{A}_3\bar{\text{S}}$  and participates in the alkali-sulfate cycle of the furnace.

When the  $\text{SO}_3$  content in the clinker is less than 2.0% it has a positive effect on the synthesis of Portland cement clinker since the alkali metal sulfates formed in its presence are effective melts that reduce the temperature of appearance of the liquid phase and its viscosity providing accelerated synthesis of clinker minerals [5, 6].

The positive role of  $\text{SO}_3$  in clinker is also evident when using a raw mixture with a significant content of alkalis. When the molar ratio of  $\text{SO}_3/(\text{Na}_2\text{O} + \text{K}_2\text{O})$  is close to 1, the excess alkali is removed from the raw material mixture due to the removal of alkali metal sulfates during heating [4, 6].

If the  $\text{SO}_3$  content in the clinker exceeds 2.0%, there are negative phenomena associated with both the quality of Portland cement clinker and its production technology.

According to [7, 8] when the content of  $\text{SO}_3$  in the raw mixture increases the amount of  $\text{C}_2\text{S}$  increases,  $\text{C}_3\text{S}$  decreases and when the total content of these phases in the clinker is equal, their  $\text{C}_3\text{S}/\text{C}_2\text{S}$  ratio decreases.

Since alite ( $\text{C}_3\text{S}$ ) is the most active and refractory component of Portland cement clinker the alite reduction leads to a decrease of the clinker refractoriness and activity. A decrease of the clinker refractoriness appears in the formation of rings in the furnace and incrustation in the calcinators cyclones and a decrease in activity shows in the drop in the strength of Portland cement.

It was found [9, 10] that not only the  $\text{C}_3\text{S}$  content but also  $\text{C}_3\text{A}$  content decrease in high-sulfate clinker. The reason for the decrease in the  $\text{C}_3\text{A}$  content in high-sulfate clinker is the isomorphic substitution of silicon for aluminum in silicate phases.

The reasons for the decrease of alite ( $\text{C}_3\text{S}$ ) content in Portland cement clinker with an increase of  $\text{SO}_3$  content in it are not found in the literature.

The main purpose of this study is to determine the reasons for the  $\text{SO}_3$  negative impact on the Portland cement clinker synthesis and to develop a method to prevent it.

To achieve this goal, it is needed to:

- analyze literary sources;
- perform thermodynamic calculations;
- conduct experimental research;
- determine the reasons for the  $\text{SO}_3$  negative influence on the Portland cement clinker synthesis;
- develop methods to prevent that negative impact.

## 2. Materials and experiment methods

Raw mixtures were burnt to produce Portland cement clinker with following modular characteristics:  $\text{LSF} = 0.92$ ,  $n = 2.3$  and  $p = 1.69$ . For the preparation of Portland cement clinker a raw mix based on limestone, clay, quartz sand and natural gypsum was used. When preparing the raw mix the composition was modeled by the introduction of gypsum into the raw mix with raw components in the ratio: raw mix/gypsum = 95/5%, to achieve  $\text{SO}_3$  in the raw mix of more than 2.0%. The raw mix was homogenized in a laboratory mill by joint grinding of raw components and gypsum for 30 minutes. The homogeneous mixture was moistened and pressed at a pressure of 50 MPa.

| Material                       | CaO   | SiO <sub>2</sub> | Al <sub>2</sub> O <sub>3</sub> | Fe <sub>2</sub> O <sub>3</sub> | SO <sub>3</sub> | MgO  | LOI   | Total |
|--------------------------------|-------|------------------|--------------------------------|--------------------------------|-----------------|------|-------|-------|
| Limestone (CaCO <sub>3</sub> ) | 56.35 | 0.04             | 0.06                           | 0.04                           | 0.03            | 0.37 | 42.8  | 99.69 |
| Clay                           | 1.21  | 50.70            | 19.90                          | 11.80                          | 0               | 1.40 | 14.81 | 99.90 |
| Quartz sand                    | 0.03  | 98.80            | 0.45                           | 0.03                           | 0               | 0    | 0.13  | 99.40 |
| Natural gypsum                 | 32.02 | 0.80             | 0.45                           | 0.23                           | 44.50           | 0    | 22.0  | 100.0 |
| Clinker without gypsum         | 67.17 | 22.19            | 6.08                           | 3.59                           | 0.035           | 0.85 | 0     | 99.99 |
| Clinker with gypsum            | 65.25 | 21.12            | 5.80                           | 3.42                           | 2.26            | 0.80 | 1.1   | 99.99 |

**Table 1.**  
The chemical composition of raw materials and clinker, mass %.

The samples were burnt at temperatures from 1100 to 1300 °C. The synthesized clinker was crushed to a residue on the sieve No. 008 no more than 5.0% and the sugar-glycerate method was used to determine the content of CaO<sub>free</sub> in it. The phase composition of fully synthesized clinkers was determined by chemical and x-ray methods. Qualitative x-ray phase analysis was performed using an XRD-7000 diffractometer (Shimadzu). Quantitative x-ray phase analysis was performed using a STADI-P diffractometer (STOE, Germany). The shooting was made under CuK $\alpha$ -radiation (40 kV, 30 mA), with graphite monochromator, in the range of scattering angles  $2\Theta = 10\text{--}70$  deg., with a step of 0.02 deg. and an excerpt of 2 s. The results were analyzed using the PDF-2 database (Release 2008 RDB 2.0804). Thermal analysis (TA) of hydration products was performed using the DSC method (differential scanning calorimetry) on the STA 449 F3 Jupiter thermal analyzer (Netzsch-Geratebau GmbH). The temperature varied from room temperature (approximately 20°C) to 800°C at a heating rate of 10°C/min. The samples of the hydration products prepared by a grinding of synthesized clinker and on their basis cement paste prepared. The size of cement pastes were 20 x 20 x 20 mm, which were prepared under the condition of water: cement ratio of 0.4. After preparation, all samples were placed in box with water at temperature of 20°C. In a box samples were maintained 28 day before full hydration. Chemical analysis of cement was performed in accordance with the requirements of Russian Standard 5382–91. For reception of micro-photos the optical microscope Olympus GX-51 (Japan) was used. Samples of clinker was polished and their surface was etching by Nital [11]. After this procedure alite was painted in green-violet color, and belite in light brown color.

The chemical composition of raw materials and clinker is shown in **Table 1**.

### 3. Experimental results and discussion

The results of qualitative phase analysis of clinker based on a raw mix with the addition of 5% gypsum are shown in **Figure 1**.

**Figure 2** shows a micrograph of clinker.

The content of free lime in a clinker based on a raw mix with the addition of 5% gypsum is shown in **Table 2**.

Analysis of the data presented in **Figures 1** and **2** and **Table 2** shows that the introduction of 5% gypsum into the raw mix suppresses the alite formation and contributes to the formation of a significant amount of free lime in the clinker. The diffraction peaks which are typical for free lime are present in a clinker based on a raw mix with the addition of 5% gypsum burnt at a temperature of 1300°C and the diffraction peaks which are typical for alite are not fixed at this temperature.

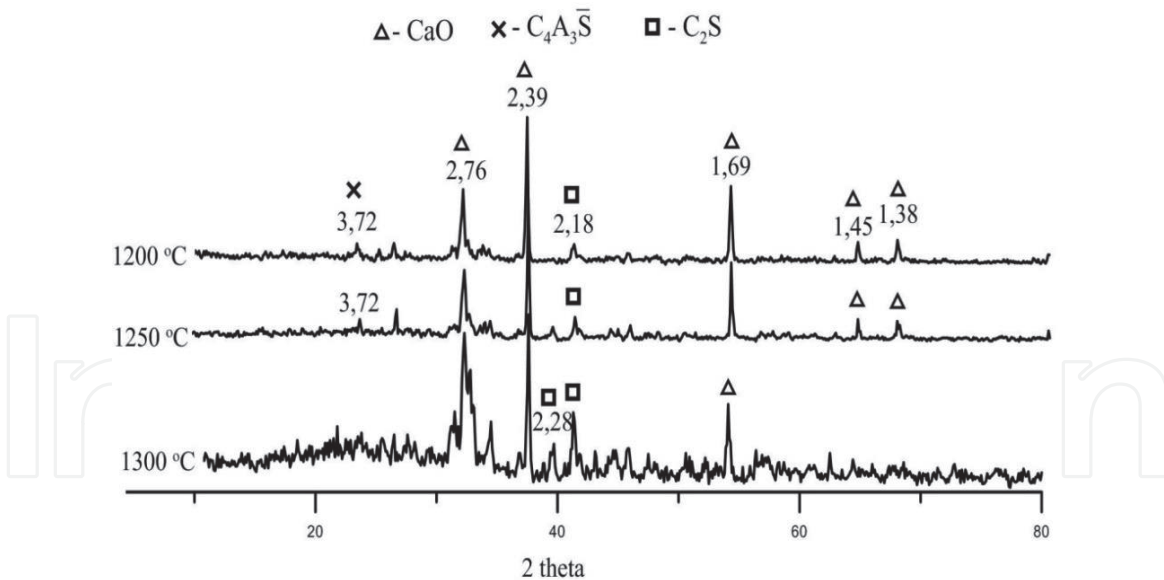


**Figure 1.**  
The results of qualitative phase analysis of clinker based on a raw mix with the addition of 5% gypsum.

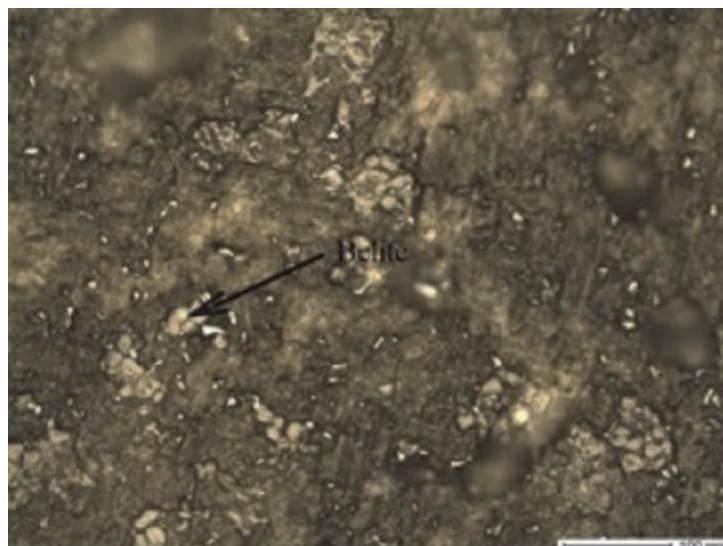


**Figure 2.**  
A micrograph of clinker based on a raw mix with the addition of 5% gypsum.

| Material  | The content of free lime in a clinker, mass %, at the burning temperature, °C |       |      |
|---|---|-------|------|
|   | 1100  | 1200  | 1300 |
| Clinker based on a raw mix with the addition of 5% gypsum | 14.0  | 13.84 | 11.6 |

**Table 2.**  
The content of free lime in a clinker.

Clinker completely melts when it is heated to a temperature of 1350°C. Analysis of the melt heated to a temperature of 1600°C indicates that alite is formed during this overheating but there is 6.2% free lime in the clinker.

The reason for suppressing the alite formation in a high-sulfate clinker is likely the formation of a well-crystallized  $\text{CaO}_{\text{free}}$  which is not soluble in the liquid phase, does not interact with  $\text{C}_2\text{S}$  and does not form  $\text{C}_3\text{S}$ . The absence of alite in the clinker

reduces its refractoriness and contributes to the appearance of a melt at temperatures below the temperatures of Portland cement clinker synthesis.

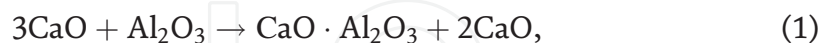
The formation of a significant amount of free lime in the clinker during the decomposition of gypsum is unlikely because with the stoichiometric ratio of CaO and SO<sub>3</sub> in gypsum anhydrite, respectively 41.19% and 58.81%, 2.06% of CaO<sub>free</sub> can be formed from the decomposition of 5.0% of gypsum and according to the data presented in **Table 2**, more than 11% of CaO<sub>free</sub> is formed at a temperature of 1300°C.

To determine the reasons for the appearance of a significant amount of free lime in a high-sulfate clinker a thermodynamic analysis of the reactions of C<sub>3</sub>A and C<sub>4</sub>AF formation was performed according to the data of [12] as well the reactions of C<sub>4</sub>A<sub>3</sub> $\bar{S}$  formation presented in [13]. The analysis results are presented in **Table 3**.

According to the data presented in **Table 4**, the synthesis of C<sub>3</sub>A and C<sub>4</sub>AF in a low-sulfate clinker is thermodynamically possible from the simple minerals, namely CaO, Al<sub>2</sub>O<sub>3</sub> and Fe<sub>2</sub>O<sub>3</sub> (reactions No. 1–2). In a high-sulfate clinker, reaction of the formation of ye’elimite C<sub>4</sub>A<sub>3</sub> $\bar{S}$  (reaction No. 3) is thermodynamically preferable since the free Gibbs energy of it is more negative than that of reactions No. 1 and 2.

There are different opinions about the formation mechanism of ye’elimite C<sub>4</sub>A<sub>3</sub> $\bar{S}$  in clinker during heating. According to [13] the synthesis of ye’elimite due to an excess of lime at the time of its formation begins with the formation of mayenite according to the scheme C<sub>12</sub>A<sub>7</sub> → CA → C<sub>3</sub>A<sub>3</sub>C $\bar{S}$ . According to our data [14] in the pressed raw mix due to its higher reaction ability the synthesis of ye’elimite proceeds according to the scheme CA<sub>2</sub> → CA → C<sub>2</sub>A<sub>2</sub> → C<sub>3</sub>A<sub>3</sub> → C<sub>3</sub>A<sub>3</sub>C $\bar{S}$  with the formation of calcium monoaluminate (CA) at temperatures about 700°C and its presence throughout the burning temperature range up to 1300°C. In the presence of calcium monoaluminate the formation of C<sub>3</sub>A and C<sub>4</sub>AF is thermodynamically impossible (reactions No. 4–6). Based on these studies the authors of [12] concluded that in the presence of calcium monoaluminate C<sub>3</sub>A and C<sub>4</sub>AF are formed not in solid-phase synthesis but from a melt.

Therefore if the calculation of the raw mix is carried out according to the usual scheme for the formation of C<sub>3</sub>A and C<sub>4</sub>AF minerals in a high-sulfate clinker, and in fact in a high-sulfate clinker low-base aluminates and calcium ferrites are formed before the melt appears, then due to the difference in the lime content in these minerals, free lime can be formed in the clinker by reactions:



| No. | Reactions  | The value of ΔG <sub>o</sub> , kJ/mol at temperature, K |        |        |        |        |
|-----|--|---|--------|--------|--------|--------|
|     |  | 298   | 1023   | 1200   | 1400   | 1500   |
| 1   | 3CaO + Al <sub>2</sub> O <sub>3</sub> = 3CaO·Al <sub>2</sub> O <sub>3</sub>  | -17.0   | -41.8  | -47.0  | -52.9  | -55.7  |
| 2   | 4CaO + Al <sub>2</sub> O <sub>3</sub> + Fe <sub>2</sub> O <sub>3</sub> = 4CaO·Al <sub>2</sub> O <sub>3</sub> ·Fe <sub>2</sub> O <sub>3</sub>         | -49.3   | -64.9  | -64.1  | -60.83 | -58.1  |
| 3   | 3CaO + 3Al <sub>2</sub> O <sub>3</sub> + CaSO <sub>4</sub> = 3CaO·3Al <sub>2</sub> O <sub>3</sub> ·CaSO <sub>4</sub>                                 | -99.1   | -445.1 | -583.6 | -758.9 | -853.5 |
| 4   | CaO·Al <sub>2</sub> O <sub>3</sub> + 2CaO = 3CaO·Al <sub>2</sub> O <sub>3</sub>  | +33.7   | +32.3  | +31.7  | +33.26 | +34.4  |
| 5   | CaO·Al <sub>2</sub> O <sub>3</sub> + CaO + 2CaO·Fe <sub>2</sub> O <sub>3</sub> = 4CaO·Al <sub>2</sub> O <sub>3</sub> ·Fe <sub>2</sub> O <sub>3</sub> | +10.4   | +39.7  | +49.0  | +60.3  | +66.2  |
| 6   | CaO·Al <sub>2</sub> O <sub>3</sub> + 2CaO + CaO·Fe <sub>2</sub> O <sub>3</sub> = 4CaO·Al <sub>2</sub> O <sub>3</sub> ·Fe <sub>2</sub> O <sub>3</sub> | +42.4   | +72.1  | +79.77 | +79.8  | +83.7  |

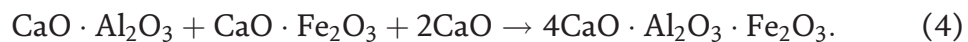
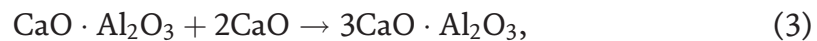
**Table 3.** Thermodynamic analysis of formation reactions C<sub>3</sub>A and C<sub>4</sub>AF according to data of [12] and formation reaction C<sub>4</sub>A<sub>3</sub> $\bar{S}$  according to data of [13].

Free lime begins to accumulate in the clinker from the decomposition beginning temperature of calcium carbonate to the appearance of the liquid phase due to the difference in the lime content in the tricalcium aluminate  $C_3A$  accepted in calculation and actually formed calcium monoaluminate CA. Totally because of gypsum decomposition and the difference between the limes content in the calcium aluminates, well-crystallized free lime in an amount of about 5% can be formed in the clinker from the decomposition beginning temperature of calcium carbonate until the appearance of the liquid phase, and this amount is sufficient to suppress the alite formation when the liquid phase appears.

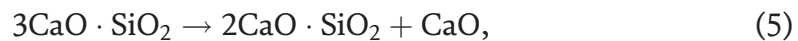
Since the alite formation in clinker is suppressed and only belite is formed, so due to the difference in the lime content in these minerals the total content of free lime at the synthesis completion temperatures is already about 11%. When the melt temperature rises up to 1600 °C a small amount of alite is formed but the  $CaO_{free}$  however does not dissolve and is remained in an amount of about 6%.

To prevent the formation of  $CaO_{free}$  in high-sulfate clinker it is proposed to calculate the raw mix of Portland cement clinker in accordance with our patent [15] in two stages. At the first stage the calculation of calcium monoaluminate  $CaO \cdot Al_2O_3$  synthesis in a high-sulphate clinker is made, meanwhile during burning intermediate metastable phase – ye'elinite  $C_4A_3\bar{S}$  will form in a high-sulphate clinker. It decays when the liquid phase appears.

Since the formation of high-base phases is thermodynamically more likely when a liquid phase occurs, and  $C_3A$  and  $C_4AF$  can only be formed from low-base phases if free lime is present by reactions:



At a burning temperature of about 1300°C in the absence of  $CaO_{free}$  its source can only be the reaction of converting alite to belite and the decomposition of calcium sulfate by reactions:



Since it is possible to convert alite to belite in a high-sulphate clinker by reaction 5, the calculation of the raw mix at the first stage is made for the formation of the maximum amount of alite in it which is possible at  $SC = 1$ . The calculation of the saturation coefficient of the raw mix by lime at the first stage is made using the well-known formula of Kinda V.A. [16] with  $SC = 1$  for the formation of CA in the clinker (the coefficient for  $Al_2O_3$  is 0.55):

$$SC = \frac{CaO - 0,55Al_2O_3 - 0,35Fe_2O_3 - 0,7SO_3}{2,8SiO_2}. \quad (7)$$

At a conclusion of this formula are used molar parities  $CaO$ ,  $Al_2O_3$ ,  $Fe_2O_3$  and  $SiO_2$  at formation in clinker the basic clinker minerals  $C_3S$ ,  $C_2S$ ,  $C_3A$  and  $C_4AF$ .

English analogue of the formula given is the formula for calculation LSF [17]:

$$LSF = \frac{CaO}{2,8SiO_2 + 1,2Al_2O_3 + 0,65Fe_2O_3}. \quad (8)$$

Factors in the given formula are taken from phase diagram CaO-Al<sub>2</sub>O<sub>3</sub>-SiO<sub>2</sub> and CaO-Al<sub>2</sub>O<sub>3</sub>-SiO<sub>2</sub>-Fe<sub>2</sub>O<sub>3</sub> at optimum relationship oxides providing absence free lime in clinker. If to use Kinda V.A's design procedure [16], that the formula (8) becomes full analogue of the formula (7):

$$LSF = \frac{CaO}{2,8SiO_2 + 1,65Al_2O_3 + 0,35Fe_2O_3 + 0,7SO_3} \quad (9)$$

For calculation degree of saturation (DS) of clinker metastable minerals by sulphate in the presence of gypsum Atakuziev T.A.'s formula [18] is used considering that sulfatization C<sub>2</sub>S, CA in clinker is possible. Taking into account the given updating the formula DS calculation looks as follows:

$$DS = \frac{SO_3 - 0,261Al_2O_3}{0,667SiO_2} \quad (10)$$

At DS = 0 C<sub>3</sub>A<sub>3</sub>C $\bar{S}$  will be formed in the raw mix and at DS = 1 sulfosporite 2(C<sub>2</sub>S)C $\bar{S}$  will also be formed.

At the second stage the calculation of the synthesis of alite Portland cement with the required modular characteristics is made. It is assumed that when the liquid phase appears the gypsum is completely decomposed by the reaction 6 and the chemical composition of the clinker formed after gypsum decomposition is considered to be the chemical composition of one of the raw mix components. Other components of the raw mix are limestone and a corrective additive – quartz sand. At the second stage the saturation coefficient (LSF) is calculated using the formula (9) but only for the synthesis of tricalcium aluminate 3CaO·Al<sub>2</sub>O<sub>3</sub> in the clinker (the coefficient for Al<sub>2</sub>O<sub>3</sub> is 1.65).

#### 4. Example of calculation of high-sulphate raw material mixture No. 1

At the first stage on the basis of raw components the chemical composition of which is shown in **Table 1** the raw mix of high-sulphate clinker is calculated for the synthesis of calcium monoaluminate in it according to the formulas (9) and (10) with the modular characteristics LSF = 1 and DS = 0. At DS = 0 calcium sulfoaluminate C<sub>3</sub>A<sub>3</sub>C $\bar{S}$  can be formed in the raw mix based on calcium monoaluminate.

**Table 4** shows the calculated composition of the raw mix and the chemical composition of clinkers before and after the gypsum decomposition.

At the second stage a typical Portland cement clinker with modular characteristics LSF = 0.92, n = 2.3, p = 1.7 is calculated on the basis of clinker after decomposition of gypsum as one of the components of the raw mix and corrective additives: limestone and quartz sand.

The calculated composition of the raw mix for obtaining Portland cement clinker and its chemical composition is shown in **Table 5**.

Finally the composition of the raw mix is calculated by multiplying the quantity of raw components of the clinker shown in **Table 4** by the quantity of clinker shown in **Table 5**, and is summed up with the quantity of raw components shown in **Table 5**:

$$CaCO_3 = (71.31 \times 0.633) + 30.7 = 75.8\% \quad (11)$$

$$Clay = 25.71 \times 0.633 = 16.3\% \quad (12)$$

| Clinker                                  | Raw mix composition |       |         | Chemical composition of clinker, mass % |                  |                                |                                |                 |       |
|--|---------------------|-------|---------|---|------------------|--------------------------------|--------------------------------|-----------------|-------|
|  | Lime-stone          | Clay  | Gyp-sum | CaO                                     | SiO <sub>2</sub> | Al <sub>2</sub> O <sub>3</sub> | Fe <sub>2</sub> O <sub>3</sub> | SO <sub>3</sub> | Total |
| Clinkers before the gypsum decomposition | 71.31               | 25.71 | 2.98    | 64.66                                   | 20.39            | 8.06                           | 4.79                           | 2.1             | 100   |
| Clinkers after the gypsum decomposition  | 71.31               | 25.71 | 2.98    | 66.05                                   | 20.83            | 8.23                           | 4.89                           | 0               | 100   |

**Table 4.** The calculated composition of the raw mix and the chemical composition of clinkers before and after the gypsum decomposition.

| Clinker                 | Raw mix composition |                         |                  | Chemical composition of clinker, mass % |                  |                                |                                |                 |       |
|-------------------------|---------------------|-------------------------|------------------|---|------------------|--------------------------------|--------------------------------|-----------------|-------|
|                         | Lime-stone          | The first stage clinker | SiO <sub>2</sub> | CaO                                     | SiO <sub>2</sub> | Al <sub>2</sub> O <sub>3</sub> | Fe <sub>2</sub> O <sub>3</sub> | SO <sub>3</sub> | Total |
| Portland cement clinker | 30.7                | 63.3                    | 6.0              | 68.2                                    | 22.1             | 6.1                            | 3.6                            | 0               | 100   |

**Table 5.** The calculated composition of the raw mix for obtaining alite Portland cement clinker and its chemical composition.

$$\text{SiO}_2 = 6.0\%; \quad (13)$$

$$\text{Gypsum} = 2,98 \times 0,633 = 1,97\%. \quad (14)$$

The actual gypsum content after the introduction of corrective additives will decrease by:

$$\text{Gypsum} = 2.98 - 1,97 = 1.01\%. \quad (15)$$

Then the quantity of corrective additives is calculated. The quantity of corrective additives is equal to the difference between the quantity of raw components calculated using the formulas (11)–(14) and the quantity of raw components calculated at the first stage and shown in **Table 4**.

The quantity of corrective additives is equal to:

$$\text{CaCO}_3 = 75.8 - 71.31 = 4.49\%; \quad (16)$$

$$\text{Clay} = 16.3 - 25.71 = -9.4\%; \quad (17)$$

$$\text{SiO}_2 = 6.0 - 0 = 6.0\%. \quad (18)$$

A negative value for the clay amount means that it should be reduced.

**Figure 3** shows the data of qualitative phase analysis of clinker prepared in accordance with correction calculation No. 1 and burnt at temperatures of 1150, 1200, 1250 and 1300°C.

X-ray analysis indicates the absence of CaO<sub>free</sub> in a clinker prepared in accordance with corrective calculations No. 1, at a burning temperature of 1200°C or higher. Stable alite in such clinker is formed already at the burning temperature of 1250°C as evidenced by the appearance of diffraction maxima with  $d = 1.76 \text{ \AA}$  and  $d = 3.04 \text{ \AA}$  which are typical for alite at this temperature. The change in the intensity of the diffraction maxima of the main phases of the clinker prepared in accordance with the correction calculation No. 1 and burnt at temperatures of 1150, 1200, 1250 and 1300°C is shown in **Figure 4**.

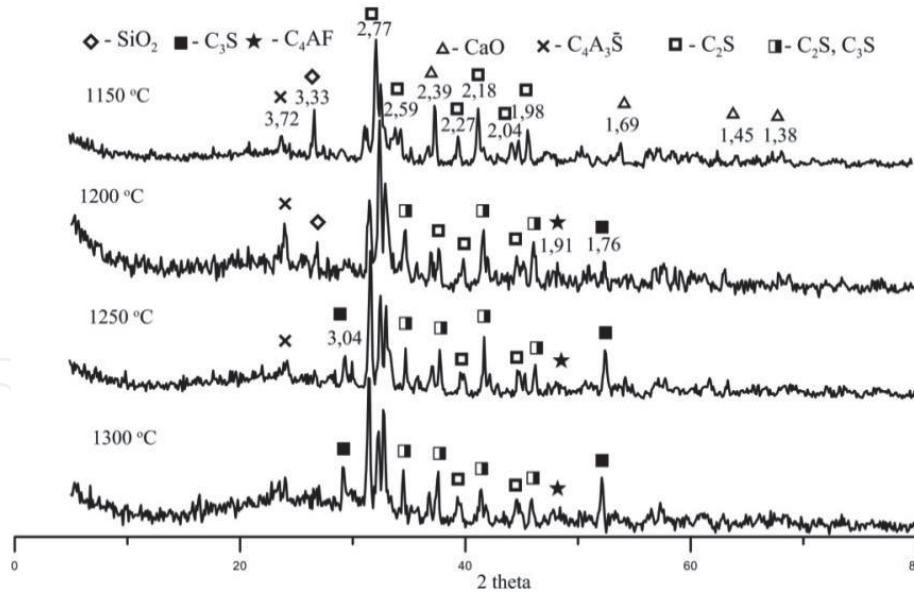


**Figure 3.**  
 The data of qualitative phase analysis of clinker prepared in accordance with correction calculation No. 1 and burnt at temperatures of 1150, 1200, 1250 and 1300 °C.

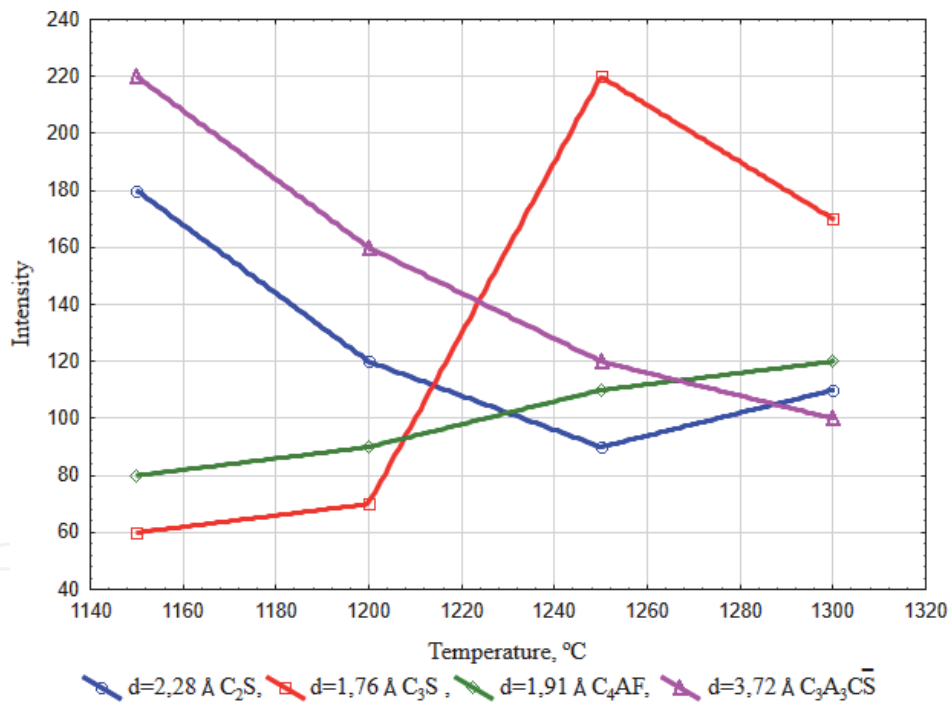


**Figure 4.**  
 The change in the intensity of the diffraction maxima of the main phases of the clinker prepared in accordance with the correction calculation No. 1 and burnt at temperatures of 1150, 1200, 1250 and 1300 °C.

Diffraction peak with  $d = 1.76 \text{ \AA}$  which is typical for  $C_3S$ , increases up to a temperature of 1250 °C and decreases starting from a temperature of 1250 °C. The diffraction peak with  $d = 2.28 \text{ \AA}$  which is typical for  $C_2S$  on the contrary decreases to a temperature of 1250 °C and increases at temperatures above of 1250 °C which indicates the transformation of alite part into belite according to Eq. (5). The intensity of the diffraction maximum with  $d = 3.72 \text{ \AA}$  which is typical for  $C_3A_3\bar{C}\bar{S}$ , decreases above the temperature of 1150 °C, which indicates the decomposition of  $CaSO_4$  in accordance with the reaction (6) and decay as a result.

To determine the actual phase composition of the clinker prepared in accordance with the correction calculation No. 1 and synthesized at a temperature of 1300°C a quantitative x-ray phase analysis was performed and it is shown in **Figure 5**.

**Table 6** shows the phase composition of clinker synthesized in accordance with correction calculation No. 1 based on quantitative phase analysis.

On the basis of clinker prepared in accordance with corrective calculation No. 1 and synthesized at a temperature of 1300°C Portland cement was prepared by joint grinding of clinker with gypsum dihydrate (**Figure 6**). The cement activity was

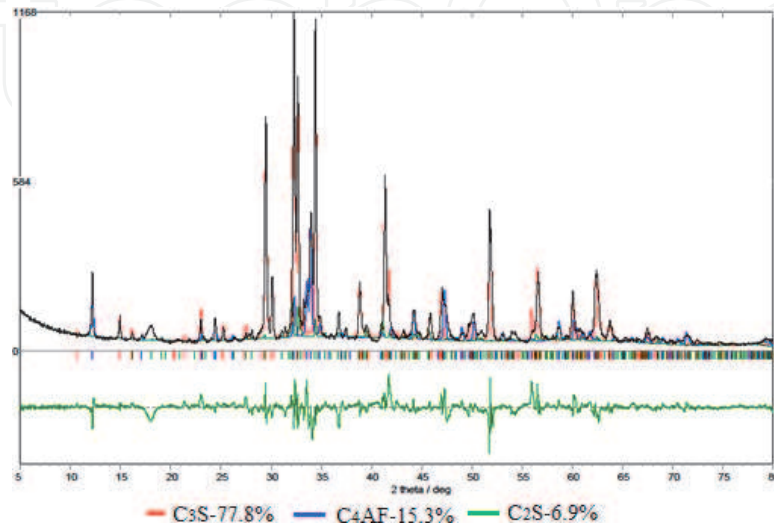


**Figure 5.**

*The phase analysis data of clinker synthesized on the basis of raw mix in accordance with correction calculation No. 1.*

| Name of mineral phase                           | Quantity in clinker, mas. % |
|---|-----------------------------|
| Three calcium silicate (alite) C <sub>3</sub> S | 77.8                        |
| Two calcium silicate (belit) C <sub>2</sub> S   | 6.9                         |
| Brownmillerit C <sub>4</sub> AF                 | 15.3                        |

**Table 6.**

*The phase composition of clinker synthesized in accordance with correction calculation No. 1.*

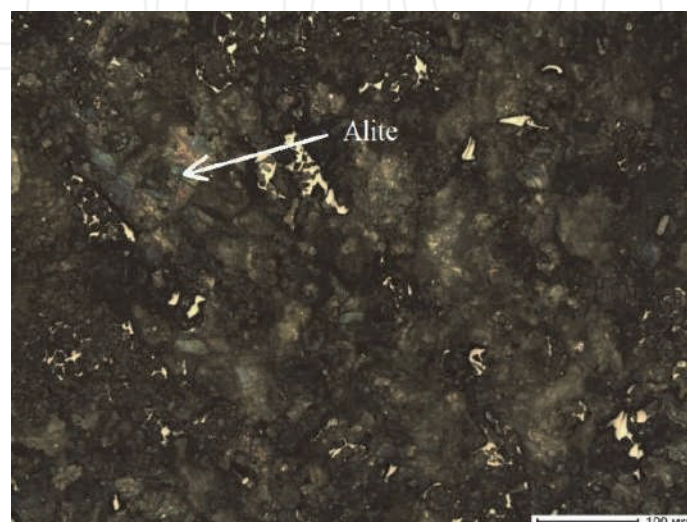


**Figure 6.**

*A micrograph of clinker synthesized in accordance with correction calculation No. 1.*

| Clinker type  | Composition, % |        | SO <sub>3</sub> , % | S*, m <sup>2</sup> /kg | R008, % | ND, % | Setting time, hour-minute |       |
|---------------|----------------|--------|---------------------|------------------------|---------|-------|---------------------------|-------|
|               | Clinker        | Gypsum |                     |                        |         |       | Initial                   | Final |
| Clinker No. 1 | 96             | 4      | 3.96                | 348                    | 12.7    | 25.2  | 2-50                      | 4-15  |

\*S – Blaine’s specific surface; R008 – residue on the sieve No. 008; ND – normal density.

**Table 7.**  
*The physical and mechanical properties of Portland cement.*

| Clinker type  | Compressive strength, MPa, after, days |      |      |      |
|---------------|--|------|------|------|
|               | 2                                      | 7    | 14   | 28   |
| Clinker No. 1 | 21.8                                   | 31.1 | 42.5 | 67.3 |

**Table 8.**  
*Portland cement compressive strength.*

determined on cubes with a size of 2x2x2 cm prepared from cement paste of normal density. The physical and mechanical properties of cement are shown in **Tables 7 and 8**.

## 5. Example of calculation of high-sulphate raw material mixture No. 2

At the first stage on the basis of raw components the chemical composition of which is shown in **Table 2** the raw mix of high-sulphate clinker is calculated for the synthesis of calcium monoaluminate in it according to the formulas (9) and (10) with the modular characteristics LSF = 1 and DS = 1. At DS = 1 calcium sulfoaluminate C<sub>3</sub>A<sub>3</sub>C $\bar{S}$  can be formed in the raw mix based on calcium monoaluminate and sulfoaluminat 2(C<sub>2</sub>S)C $\bar{S}$  can be formed in the raw mix based on belite.

**Table 9** shows the calculated composition of the raw mix and the chemical composition of clinkers before and after the gypsum decomposition.

At the second stage a alite Portland cement clinker with modular characteristics LSF = 0.92, n = 2.3, p = 1.7 is calculated on the basis of clinker after decomposition of gypsum as one of the components of the raw mix and corrective additives: limestone and quartz sand.

The calculated composition of the raw mix for obtaining alite Portland cement clinker and its chemical composition is shown in **Table 10**.

Finally the composition of the raw mix is calculated by multiplying the quantity of raw components of the clinker shown in **Table 9** by the quantity of clinker

| Clinker                                  | Raw mix composition |      |        | Chemical composition of clinker, mass % |                  |                                |                                |                 |       |
|--|---------------------|------|--------|---|------------------|--------------------------------|--------------------------------|-----------------|-------|
|  | Lime-stone          | Clay | Gypsum | CaO                                     | SiO <sub>2</sub> | Al <sub>2</sub> O <sub>3</sub> | Fe <sub>2</sub> O <sub>3</sub> | SO <sub>3</sub> | Total |
| Clinkers before the gypsum decomposition | 59.8                | 21.3 | 18.9   | 60.3                                    | 16.5             | 6.6                            | 3.9                            | 12.7            | 100   |
| Clinkers after the gypsum decomposition  | 59.8                | 21.3 | 18.0   | 69.1                                    | 18.9             | 7.5                            | 4.5                            | 0               | 100   |

**Table 9.**  
*The calculated composition of the raw mix and the chemical composition of clinkers before and after the gypsum decomposition.*

| Clinker                 | Raw mix composition |                         | Chemical composition of clinker, mass % |      |                  |                                |                                |                 |     |
|-------------------------|---------------------|-------------------------|---|------|------------------|--------------------------------|--------------------------------|-----------------|-----|
|                         | Lime-stone          | The first stage clinker | SiO <sub>2</sub>                        | CaO  | SiO <sub>2</sub> | Al <sub>2</sub> O <sub>3</sub> | Fe <sub>2</sub> O <sub>3</sub> | SO <sub>3</sub> | Σ   |
| Portland cement clinker | 20.8                | 72.9                    | 6.4                                     | 68.3 | 22.1             | 6.0                            | 3.6                            | 0               | 100 |

**Table 10.**

The calculated composition of the raw mix for obtaining alite Portland cement clinker and its chemical composition.

shown in **Table 10**, and is summed up with the quantity of raw components shown in **Table 10**:

$$\text{CaCO}_3 = (59,8 \times 0,729) + 20,8 = 64,3\%; \quad (19)$$

$$\text{Clay} = 21,3 \times 0,729 = 15,5\%; \quad (20)$$

$$\text{SiO}_2 = 6,4\%; \quad (21)$$

$$\text{Gypsum} = (18,9 \times 0,729) = 13,8\%. \quad (22)$$

Then the quantity of corrective additives is calculated. The quantity of corrective additives is equal to the difference between the quantity of raw components calculated using the formulas (19) and (20) and the quantity of raw components calculated at the first stage and shown in **Table 9**.

The quantity of corrective additives is equal to:

$$\text{CaCO}_3 = 64,3 - 59,8 = 4,4\%; \quad (23)$$

$$\text{Clay} = 15,5 - 21,3 = -5,8\%; \quad (24)$$

$$\text{SiO}_2 = 6,4 - 0 = 6,4\%; \quad (25)$$

A negative value for the clay amount means that it should be reduced the same as in the calculation example No. 1.

The actual gypsum content after the introduction of corrective additives will decrease by:

$$\text{CaSO}_4 = 18,9 - 13,8 = 5,1. \quad (26)$$

**Figure 7** shows the data of qualitative x-ray phase analysis of clinker prepared in accordance with calculation mentioned above and burnt at temperatures of 1100, 1200, 1300 and 1350°C.

X-ray analysis indicates the absence of CaO<sub>free</sub> in a clinker prepared in accordance with corrective calculations No. 2 at a burning temperature above 1300°C. Stable alite C<sub>3</sub>S is formed at the burning temperature of 1350°C as evidenced by the appearance of diffraction maxima with d = 1.76 Å and d = 3.04 Å which are typical for alite at this temperature.

The intensity of the diffraction maximum with d = 3.72 Å which is typical for C<sub>3</sub>A<sub>3</sub>C $\bar{5}$  increases to a temperature of 1300°C but above this temperature it is not fixed which indicates the decomposition of CaSO<sub>4</sub> in accordance with the reaction (No. 6) and decay as a result.

According to the qualitative phase analysis data a significant amount of gypsum is released up to the burning temperature of 1300°C which is fixed by the diffraction maximum with d = 3.47 Å. Gypsum remains are fixed even at a temperature of 1350°C.

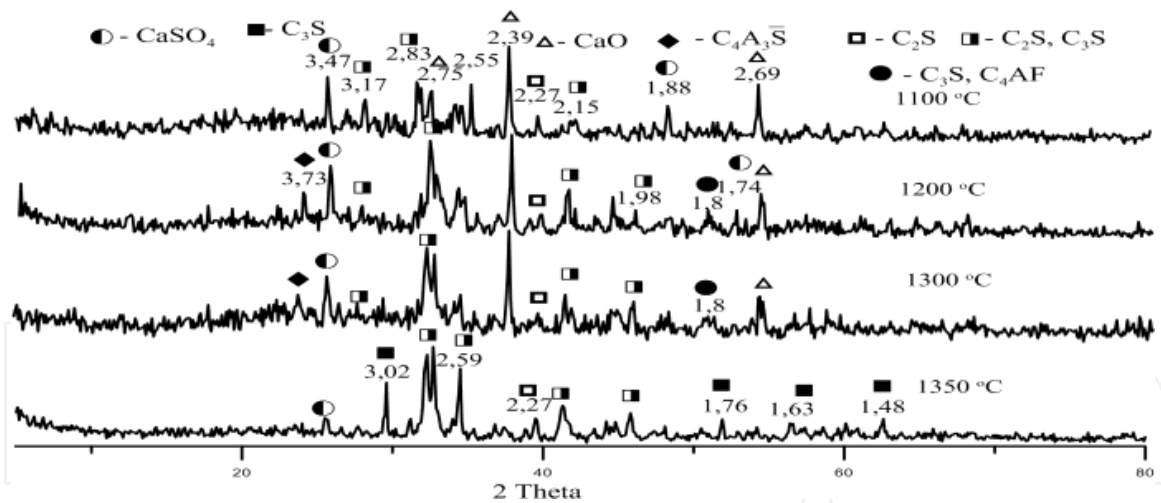


**Figure 7.**  
 The data of qualitative phase analysis of clinker prepared in accordance with calculation No. 2 and burnt at temperatures of 1100, 1200, 1300 and 1350°C.

To determine the actual phase composition of the clinker prepared in accordance with the correction calculation No. 2 and synthesized at a temperature of 1350°C a quantitative x-ray phase analysis was performed. Its results shown in **Figure 8**.

**Table 11** summarizes the results of quantitative x-ray phase analysis of synthesized clinker.

The test results show that in accordance with corrective calculation No. 2 a significant amount of  $C_3S$  is retained when preparing clinker based on a high-sulphate raw mix that initially contains 12.7%  $SO_3$  (**Figure 9**).

On the basis of clinker prepared at temperature of 1350°C Portland cement was prepared by joint grinding of clinker with natural gypsum. The cement activity was determined on cubes with a size of 2x2x2 cm prepared from cement paste of normal density.

The physical and mechanical properties of cement are shown in **Tables 12** and **13**.

Examples data of corrective calculations show that using the proposed calculation method it is possible to save a significant amount of  $C_3S$  in a clinker synthesized on the basis of a high-sulphate raw mix.

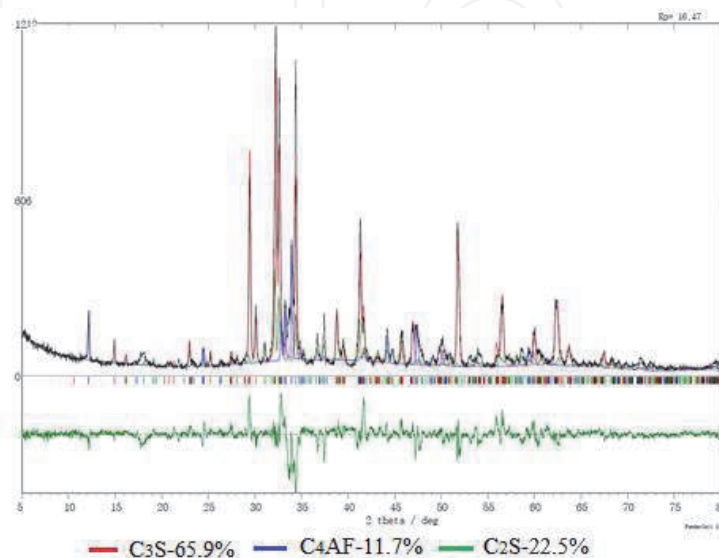


**Figure 8.**  
 The phase analysis data of clinker synthesized on the basis of raw mix in accordance with correction calculation No. 2.

| Name of mineral phase                           | Quantity in clinker, mas. % |
|---|-----------------------------|
| Three calcium silicate (alite) C <sub>3</sub> S | 65.9                        |
| Two calcium silicate (belit) C <sub>2</sub> S   | 22.5                        |
| Brownmillerit C <sub>4</sub> AF                 | 11.7                        |

**Table 11.**

The phase composition of clinker synthesized in accordance with correction calculation No. 2.

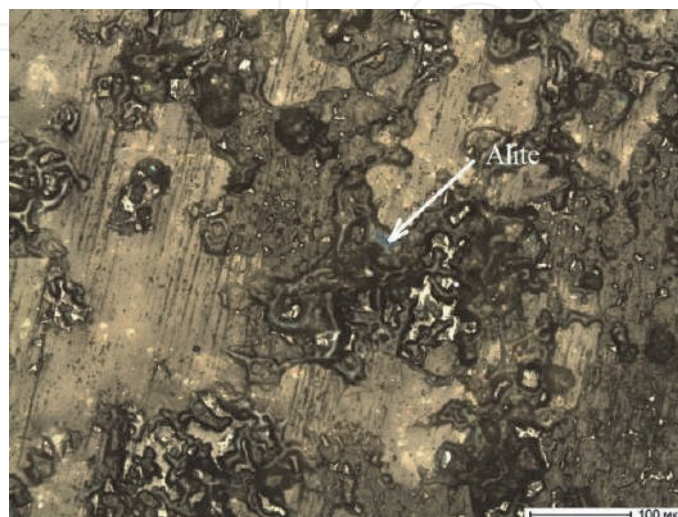


**Figure 9.**

A micrograph of clinker synthesized in accordance with correction calculation No. 2.

| Clinker type  | Composition, % |        | SO <sub>3</sub> , % | S*, m <sup>2</sup> /kg | R008, % | ND, % | Setting time, hour-minute |       |
|---------------|----------------|--------|---------------------|------------------------|---------|-------|---------------------------|-------|
|               | Clinker        | Gypsum |                     |                        |         |       | Initial                   | Final |
| Clinker No. 2 | 100            | 0      | 12.7                | 378                    | 3.1     | 28.3  | 1-50                      | 2-15  |

\*S – Blaine’s specific surface; R008 – residue on the sieve No. 008; ND – normal density.

**Table 12.**

The physical and mechanical properties of Portland cement.

| Clinker type  | Compressive strength, MPa, after, days |      |      |      |
|---------------|--|------|------|------|
|               | 2                                      | 7    | 14   | 28   |
| Clinker No. 2 | 10.1                                   | 14.7 | 20.0 | 44.7 |

**Table 13.**

Portland cement compressive strength.

The quantity of corrective additives depends on the modular characteristics of the synthesized clinker. When limiting the modular characteristics of Portland cement clinker LSF = 0.92–0.98; n = 2.0–3.0; p = 1.7–4.0 the minimum amount of additives equal to 4.0% is introduced with the minimum values of modular characteristics, i.e. LSF = 0.92; n = 2.0; p = 1.7; and with the minimum amount of gypsum introduced, i.e. DS = 0. The maximum amount of corrective additives equal to 23.0% is introduced with the maximum values of modular characteristics, i.e. LSF = 0.98; n = 3.0; p = 4.0 and with the maximum amount of gypsum introduced, i.e. DS = 1.

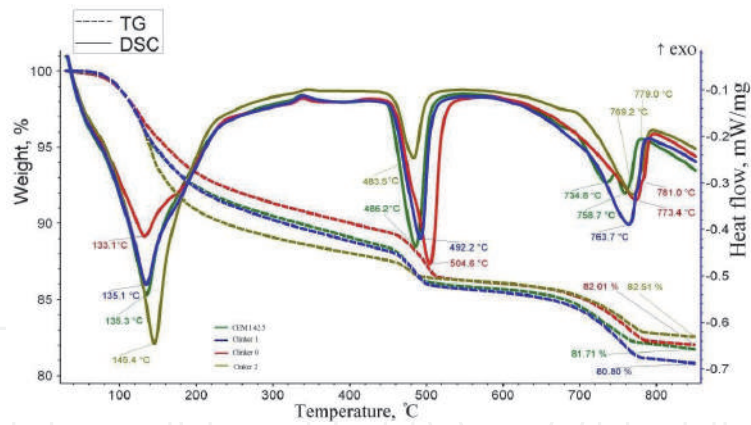


**Figure 10.**  
 Results of comparative thermal analysis (TA) of hydration products.

| Clinker type | The value of the endo effect, J/g | Mass loss, % |
|--------------|-----------------------------------|--------------|
| Clinker 0    | 148.2                             | 17.9         |
| Clinker 1    | 167.0                             | 19.2         |
| Clinker 2    | 180.5                             | 17.5         |
| CEM I 42.5   | 155.0                             | 18.3         |

**Table 14.**  
 Values of the first endo-effect and the total mass loss of samples.

The quantity of clay removed from the raw mix correlates with the amount of mix additives put in the raw mix, i.e. with the same modular characteristics of the clinker the minimum quantity of clay removed corresponds to a minimum quantity of additives and the maximum quantity of clay removed corresponds to the maximum quantity of additives.

At the final stage of investigation comparative thermal analysis (TA) of hydration products was conducted. Results of tests are resulted on **Figure 10**.

The **Table 14** shows the values of the first endo-effect and the total mass loss of samples.

At hydration alite attaches 5 molecules of water, but belite only 2. Due to this difference, the clinker 0 has smallest first endo effect.

## 6. Conclusion

The present study revealed that the  $\text{SO}_3$  negative impact on the Portland cement clinker synthesis, resulted in a  $\text{C}_3\text{S}$  content reduction and the  $\text{C}_2\text{S}$  and  $\text{C}_3\text{A}$  content increasing in the final product. It leads to lowering clinker fire resistance and cement quality due to the thermodynamic preference of the ye'elite  $\text{C}_4\text{A}_3\bar{\text{S}}$  synthesis in the presence  $\text{SO}_3$  and, consequently, the presence of low-basic calcium monoaluminate CA in the synthesized clinker. In the presence of calcium monoaluminate, solid-phase synthesis of high-base  $\text{C}_3\text{A}$  and  $\text{C}_4\text{AF}$  is thermodynamically impossible. As a result, free lime accumulates in the synthesized clinker, which prevents the liquid-phase synthesis of  $\text{C}_3\text{S}$ .

A method for elimination of the  $\text{SO}_3$  negative impact on the Portland cement quality by calculating the raw material mixture composition with a significant amount of  $\text{SO}_3$  has been developed and patented.

## Abbreviations

The following abbreviations are used in this manuscript:

|                   |                                      |
|-------------------|--------------------------------------|
| $C_3S$            | $3CaO \cdot SiO_2$ ;                 |
| $C_2S$            | $2CaO \cdot SiO_2$ ;                 |
| $C_3A$            | $3CaO \cdot Al_2O_3$ ;               |
| $C_4AF$           | $4CaO \cdot Al_2O_3 \cdot Fe_2O_3$ ; |
| $C_3A_3C\bar{S}$  | $3CaO \cdot 3Al_2O_3 \cdot CaSO_4$ ; |
| $2(C_2S)C\bar{S}$ | $2(2CaO \cdot SiO_2) \cdot CaSO_4$ ; |
| $C_{12}A_7$       | $12CaO \cdot 7Al_2O_3$ ;             |
| $CaO_{free}$      | free CaO;                            |
| SC                | Saturation Coefficient;              |
| LSF               | Lime Saturation Factor;              |
| DS                | Degree of Saturation by Sulfate;     |
| LOI               | Loss On Ignition.                    |

## Author details

Oleg Sheshukov\* and Michael Mikheenkov  
Ural Federal University Named after the First President of Russia B.N. Yeltsin,  
Institute of Metallurgy of the Ural Branch of the Russian Academy of Sciences,  
Ekaterinburg, Russian Federation

\*Address all correspondence to: o.j.sheshukov@urfu.ru

## IntechOpen

© 2021 The Author(s). Licensee IntechOpen. This chapter is distributed under the terms of the Creative Commons Attribution License (<http://creativecommons.org/licenses/by/3.0>), which permits unrestricted use, distribution, and reproduction in any medium, provided the original work is properly cited. 

## References

- [1] Factors el Mar Cortada Mut, Linda Kaare Norskov, Peter Glarborg, Kim Dam-Johansen Sulphur release from alternative fuel firing / Maria del Mar Cortada Mut & other // *Global Cement Magazine* 9 (2014) p. 36–41.
- [2] Július Strigáč Effect of Selected Alternative Fuels and Raw Materials on the Cement Clinker Quality/ Strigáč Július // *Journal Of Civil Engineering* Vol. 10, Issue 2, 2015 p. 81–92.
- [3] Ying-Liang Chen, Juu-En Chang, Ming-Sheng Ko Reusing Desulfurization Slag in Cement Clinker Production and the Influence on the Formation of Clinker Phases/ Chen Ying-Liang & other // *Sustainability* 9, 1585 (2017) p.1–14.
- [4] Javed I. Bhatti.; Role of Minor Elements in Cement Manufacture and Use, Portland Cement Association, Skokie, Illinois 1995, p.24–25.
- [5] M. Yamashita, H. Tanaka Low Temperature Burnt Portland Cement Clinker Using Mineralizer/ Yamashita M., Tanaka H. // *Cement Science and Concrete Technology* № 65 (2011) p. 82–87.
- [6] H.F.W. Taylor, *Cement Chemistry*, Academic Press, London, 1990.
- [7] Sayed Horcoss Influence of the clinker  $SO_3$  on the cement characteristics / Horcoss Sayed, Ltief Roger, RizkToufic // *Cement And Concrete Research* 41 (2011). p. 913–919. Available from: <http://www.sciencedirect.com/science/article/pii/S0008884611001268>
- [8] Mieke De Schepper, Philip Van den Heede, Eleni C. Arvaniti, Klaartje De Buysser Sulfates in Completely Recyclable Concrete and the effect of  $CaSO_4$  on the clinker mineralogy/ Schepper De & other // *Construction and Building Materials* 137 (2017) p. 300–306.
- [9] Sayed Horkoss, Roger Lteif, and Toufic Rizk Calculation of the  $C_3A$  Percentage in High Sulfur Clinker / Horcoss Sayed & other // *International Journal of Analytical Chemistry* Volume 2010, Article ID 102146, p. 1–5.
- [10] Laure Pelletier-Chaignat, Frank Winnefeld, Barbara Lothenbach, Gwenn Le Saout Influence of the calcium sulphate source on the hydration mechanism of Portland cement–calcium sulphoaluminate clinker–calcium sulphate binders/ Pelletier-Chaignat Laure & other // *Cement & Concrete Composites* 33 (2011) p. 551–561.
- [11] Donald H. Campbell. *Microscopical Examination and Interpretation of Portland Cement and Clinker* Second Edition/ Published by:Portland Cement Association – USA, 1999. 214 p.
- [12] Babushkin, V.I., Matveev G.M., Mchedlov-Petrosjan, O.M. *Thermodynamics Of Silicates - M: Stroyizdat, 1986.408 p.*
- [13] Kuznezova T.V. *Aluminate and sulfoaluminate cements/ - M.: Stroyizdat, 1986., 208 p.*
- [14] Michael A. Miheenkov Compacting as a way of reception sulfated hydraulic binders/Vestnik MGSU.- – 2011. – № 1 . – p. 131–142
- [15] Patent 2527430 Russian Federation: MPK C04B 7/36. Method for Correcting Composition of Portland Cement Clinker Based on Highe-Sulphate Crude Mixture. Author: Michael A. Miheenkov., Patent Holder: Michael A. Miheenkov. – 2013112990/03; Date of declare. 22.03.2013 ; Date of publication. 27.08.2014. Bulletin. № 24.

[16] Kind V.A. Chemical characteristics of Portland cement/ L.-M. Gosstroyizdat, 1932..

[17] Walter H. Duda Cement.; Data-Book /Internationale Verfahrenstechniken der Zementindustrie 2., Auflage Bauverlag GmbH Wfmbaden and Berlin, 1981, 484 p.

[18] Atakuziev, T.A. Sulfomineral cements on a basis of phosphogypsum/ T.A.Atakuziev, F.M.Mirzoev.: "FAN", 1979. – 152 p.

IntechOpen

## Chapter

# Energy and Economic Comparison of Different Fuels in Cement Production

*Oluwafemi M. Fadayini, Clement Madu, Taiwo T. Oshin, Adekunle A. Obisanya, Gloria O. Ajiboye, Tajudeen O. Ipaye, Taiwo O. Rabi, Joseph T. Akintola, Shola J. Ajayi and Nkechi A. Kingsley*

## Abstract

Cement clinkerisation is the major energy-consuming process in cement manufacturing due to the high-temperature requirement. In this paper, energy data including specific energy consumption, forms, and types of energy used at different units of cement manufacturing processes were analyzed and compared for effectiveness, availability, cost, environmental, and health impact. Data from three different cement industries in Nigeria labeled as A, B, and C were used for the analysis in this study. The results of this research work established that coal is the cheapest energy source but environmental issues exonerate it from being the choice energy source. LPFO and Natural gas give better production output while minimizing pollution and health issues. When benchmarked against each other, Factory B was found to be the most energy-efficient in terms of output and cost of production. Although coal is cheaper compared to fuel oil and supposed to contribute a share of fuel used in cement industries, the industries are moving towards the use of alternative and conventional fuels to reduce environmental pollution. It is therefore recommended that deliberate effort to achieve appreciable energy-efficient levels should be the priorities of the cement industries in Nigeria.

**Keywords:** Cement, Coal, Fuel oil, Natural gas, Energy Consumption, Energy source, Clinkerization

## 1. Introduction

Cement is regarded as a binder, a material useful in building and civil construction that hardens and adheres to other substances to bind them together. Cement is rarely used only, but to bind other building materials such as gravel and sand together. When mixed with fine aggregates, it is used to produce mortar for masonry or with gravel and sand, it produces concrete. Energy consumption in the Industrial sector ranges from 30–70% of the total energy used in some selected countries as previously reported by [1]. The cement sub-sector utilizes nearly 12–15% of entire industrial energy usage [1, 2] due to the high temperatures required in the kilns. Cement is a vital product used in society for constructing

modern infrastructure as well as safe and comfortable buildings. Cement manufacturing is an energy-intensive process due to the high temperature required in the kilns for clinkerization. Energy cost contributes to about 40–50% of cement production cost in Nigeria depending on the production process and type of cement with 1 tonne of cement requiring 60–130 kg of fuel or its equivalent and about 105 kWh of electricity [3].

Fossil fuels like coal, pet coke, fuel oil, and gas are the primary fuels used in the cement kilns. These fuels which exist in solid, gaseous, and liquid also provide most of the global energy needs and demand. Some of these fuels e.g. coal and natural gas are utilized in their natural form while energy resources like petroleum, shale, and bituminous sands require processing, refinement, and distillation to produce consumable fuels.

The conservation of energy is an essential step to take towards overcoming the mounting problems of the worldwide energy crisis and environmental degradation. In particular, developing countries are interested in increasing their awareness of the energy efficiency in power generation and consumption in their countries. However, usually, only limited information/sources on the rational usage of energy are available [4].

The energy source or mix to be implemented will have to meet the varying energy demand of the countries, industry, or organizations as well as improving the security against the energy crisis. Fuel availability, ease of processing and handling, environmental pollution, storage, and cost are some of the factors that determine the selection of fuel [5].

In cement production, the energy use is distributed as 92.7% for pyro-processing, 5.4% for finishing grinding, and 1.9% for raw grinding [6]. The type of fuel used determines the quantity of greenhouse gases (GHG) emission, cement product quality, and cost. Large volumes of CO<sub>2</sub> are emitted during cement production and it is believed that this sector represents 5%–7% of the total CO<sub>2</sub> anthropogenic emissions [7, 8]. Environmental concerns are of great importance since cement and the production of its raw materials are extensively based on fossil fuels.

There are three processes in cement manufacturing plant [9]: raw material mixing, pyroprocessing (burning), and grinding.

*Raw material processing:* this can be the wet process or dry process depending on the method of milling. In the wet process, raw materials other than plaster are crushed to a diameter of approximately 20 mm by a crusher and mixed in an appropriate ratio using an automatic weigh balance. Its particle size is further reduced to finer particles by tube mill of 2–3.5 m diameter and length 10–14 m in the presence of water from a slurry of 35–40% [10]. In the dry process, the raw materials (calcareous and argillaceous) are separately crushed to about 2–5 cm. They are later dried in a cylindrical rotary drier having a diameter of 2 m and a length of about 20 m, pulverized into fine particles, and stored. The pulverized fine raw materials are then mixed automatically in proportions to form a uniform dry mix and sent to a kiln for clinker production where about 80% of the energy used in cement production is consumed [4, 11]. The electrical energy requirement of the dry process is higher compared to the wet process while the thermal energy consumption is very low compared to the wet process. The primary energy consumption in a typical dry process is about 75% fossil fuel and up to 25% electrical energy [1].

The pyroprocessing in the kiln generates about 81% of cement production CO<sub>2</sub> emission; 36.8% from fuel combustion while 46.3% is from pyroprocessing reaction [6]. Hence, the choice of fuel and energy conversion efficiency have a net effect on cement CO<sub>2</sub> emission. The exact consumption of energy in the production of cement varies from one technological approach to another.” The major fuel used in clinker production is coal and petroleum coke but alternate energy source like

biomass, waste heat, fuel oil, solvent, tyres, gas, etc. are becoming attractive in recent years [12]. A considerable amount of energy is consumed in manufacturing cement. Thus, the focus should be centered on energy savings and energy-associated environmental emissions both locally and universally [13–17]. The chief share of the total thermal energy consumption is required by pyro-processing and it accounts for approximately 93–99% of the entire fuel consumption [1]. Though electrical energy is principally used for the operation of the raw materials which accounts for 33% of its consumption, and clinker crushing and grinding equipment which accounts for 38% of its consumption. Electrical energy is needed to operate equipment such as combustion air blowers, kiln motors, and fuel supply, etc. accounting for 22% of its consumption to sustain the pyro-process.

The calorific value of common fuels used in cement production is shown in **Table 1**. Natural gas has the highest energy content followed by fuel oil while coal has the least energy content of the three fuels.

Coal is regarded as the most abundant fossil fuel on earth, with a global recoverable reserve estimated at 216 years [18]. Coal provides 26% of global primary energy consumption and contributes 41% of global electricity generation.

Fuel oil is a distillate or a residue fraction produced from petroleum distillation. It is any liquid from petroleum that is burned in a furnace for heat and power generation. In terms of industrial use of fuel especially in cement kiln firing, heavy fuel oil, or low pour fuel oil (LPFO). Heavy oil is a long residue obtained from the atmospheric distillation column. Heavy fuel oil is used mainly to produce electricity, to fire boiler and furnace in industry, notable the cement, pulp, and paper, and to power large marine and other vessels.

Natural gas is a fossil fuel like oil and coal, thus it is essentially the remains of plants, animals, algae, and microbes that lived millions of years ago. Over the years, natural gas has secured its vital role in every aspect of world development, particularly its role to replace coal and oil with having a high energy content that the two aforementioned.

In Nigeria, cement production has increased exponentially from 2 million tonnes in 2002 to about 17 million in 2011 [19]. Thus, making Nigeria's cement industry contributing about 60% of the West African region's cement output in 2011. Since the sector consumes a considerable amount of energy, it is necessary to identify and reduce energy wastage [20]. Also, the unit fuel cost for cement production in Nigeria is \$30 per tonne which is very high compared to an advanced country like China (\$6 per tonne) thereby contributing to the high cost of unit price cement [21]. The use of energy utilization analysis for energy and financial savings has generated research interest in recent years [22]. Therefore, this research work aims to analyse the cost vis-à-vis the pollution tendencies of each energy source and its consequence on health and the environment from the energy data obtained from the cement industries.

| S/N | Fuel        | Energy Content (MJ/Kg) |
|-----|-------------|------------------------|
| 1   | Coal        | 36.3                   |
| 2   | Natural gas | 54.0                   |
| 3   | Fuel oil    | 45.6                   |

Source: *Engineering ToolBox*, (2008). Fossil and Alternative Fuels Energy Content. [online] Available at: [https://www.engineeringtoolbox.com/fossil-fuels-energy-content-d\\_1298.html](https://www.engineeringtoolbox.com/fossil-fuels-energy-content-d_1298.html) [Accessed: 23/2/2021].

**Table 1.**  
*Energy contents of coal, fuel oil, and natural gas.*

## 2. Methodology

### 2.1 Data collections

Three major Cement producers in Nigeria (Dangote Cement in Obajana, Kogi State; United Cement Company in Calabar, UNICEM - Cross River and Nigerian Cement Company in Nkalagu, NIGERCHEM, Ebonyi State), labeled Factory A, B and C were approached for the Data on energies consumed during cement production and were collected for the analysis.

#### 2.1.1 Calculations involved in the analysis

Specific heat:

The standard or universally accepted specific fuel consumption for clinker production is 720 Kcal/m<sup>3</sup> of clinker from:

$$\frac{\text{Calorific value of gas} \times \text{Total consumed}}{\text{total clinker} \times 1000} = \frac{720\text{Kcal}}{m^3} \quad (1)$$

Let n = 1.

From ideal gas law: PV = nRT

$$R = \frac{P_{act} \times V_{act}}{T_{act}} \text{ at a given temperature and pressure} \quad (2)$$

$$R = \frac{P_o \times V_o}{T_o} \text{ at normal condition (0 °C and 1.0 atm)} \quad (3)$$

Therefore

$$\frac{P_{act} \times V_{act}}{T_{act}} = \frac{P_o \times V_o}{T_o} \quad (4)$$

$$\text{Volumetric flow rate } Q = \frac{V}{t} \quad (5)$$

Substituting Eq. (4) into (1) and simplifying we have

$$Q_o = Q_{act} \times \left[ \frac{P_{act}}{P_o} \right] \times \left[ \frac{T_o}{T_{act}} \right] \quad (6)$$

Where Q<sub>o</sub> = Q<sub>N</sub> = Gas flow rate at normal condition.

Q<sub>act</sub> = measured flow rate in m<sup>3</sup>/hr.

P<sub>act</sub> = P measured + P ambient

P ambient = 1.01325 bar.

P<sub>o</sub> = pressure at normal condition

T<sub>o</sub> = temperature at normal condition

Therefore

$$Q_N = Q_{act} \times \left[ \frac{P_{measured} \times P_{ambient}}{P_o} \right] \times \left[ \frac{T_o}{T_{act}} \right] \left( \frac{Nm^3}{hr} \right) \quad (7)$$

Since we are dealing with volume and not flow rate. Then equation becomes this

$$V_o = V_{act} \times \left[ \frac{T_o}{T_{act}} \right] (Nm^3) \quad (8)$$

$V_o$  = volume at normal condition.

Since all the pressure and temperature are in atmospheric and absolute units. In Eq. (8) the fluid in meter cubic ( $m^3$ ) is converted to Normal cubic meter ( $Nm^3$ ). The reversal of Eq. (8) converts the fluid in Normal cubic meter to meter cubic. Therefore Eq. (8) becomes:

$$V_{act} = V_o \times \left[ \frac{P_o}{P_{act}} \right] \times \left[ \frac{T_{act}}{T_o} \right] (m^3) \quad (9)$$

$V_{act}$  = measured volume in  $m^3$ .

n = number of moles.

R = molal gas constant.

$T_{act}$  = temperature in Kelvin.

$P_{act} = P_{measured} + P_{ambient}$ .

### 2.1.2 Cost analysis

The following cost of material for fuel oil, natural gas, and coal was as obtained [23–25], respectively;

Fuel oil (diesel) = ₦223.740 (\$0.587) per litre.

Natural gas = \$2.76 per 1000  $ft^3$ .

Coal = \$68.9 per tons.

The calculated cost in **Table 2** is subject to some conversions as the consumption of coal, fuel, and energy is given in tonnes. The cost for natural gas is given in  $\$/ft^3$  and the cost of fuel oil is given in \$ per liters. For the two cases where volume is used, the quantity consumed is converted from tonnes to  $ft^3$  and liters for natural gas and fuel oil, respectively.

Density of fuel oil (diesel) = 0.85 kg/litre.

Density of natural gas = 0.68  $kg/m^3$ .

Density of coal = 1506  $kg/m^3$ .

1 tonnes = 1,000 kg.

1  $m^3 = 35.315 ft^3$

$$volume = \frac{mass}{density} \quad (10)$$

## 3. Results

### 3.1 Flue gas composition

**Table 2** shows the various proportions of flue gases in coal, fuel oil, and natural gas (**Figure 1**).

## 4. Discussion of results

From the specific heat of consumption point of view, it is observed that of the three different cement companies that were used for analysis; the specific heat of

| SN | Factory | COAL        |            |                          |          | FUEL        |            |                          |                        | NATURAL GAS |            |                          |            |
|----|---------|-------------|------------|--------------------------|----------|-------------|------------|--------------------------|------------------------|-------------|------------|--------------------------|------------|
|    |         | Prod., tons | Total Fuel | C <sub>P</sub> , Kcal/kg | Cost, \$ | Prod., tons | Total Fuel | C <sub>P</sub> , Kcal/kg | Cost, \$               | Prod., tons | Total Fuel | C <sub>P</sub> , Kcal/kg | Cost, \$   |
| 1  | A       | 6,000       | 720        | 600                      | 49,608   | 6,014       | 428,755    | 697                      | 2.96 x 10 <sup>8</sup> | 6,081       | 470,470    | 698                      | 67,435,924 |
|    |         | 6,088       | 735        | 604                      | 50,641.5 | 6,013       | 421,850    | 676                      | 2.91 x 10 <sup>8</sup> | 6,095       | 466,260    | 690                      | 66,832,474 |
|    |         | 6,148       | 745        | 606                      | 51,330.5 | 6,074       | 425,987    | 686                      | 2.94 x 10 <sup>8</sup> | 6,168       | 460,000    | 673                      | 65,935,182 |
|    |         | 6,074       | 725        | 597                      | 49,952.5 | 6,148       | 424,586    | 675                      | 2.93 x 10 <sup>8</sup> | 6,081       | 471,363    | 699                      | 67,563,925 |
| 2  | B       | 4,600       | 595        | 647                      | 40,995.5 | 5,028       | 428,577    | 834                      | 2.96 x 10 <sup>8</sup> | 4,074       | 313,647    | 694                      | 44,957,331 |
|    |         | 4,720       | 608        | 644                      | 41,891.2 | 5,145       | 412,580    | 784                      | 2.85 x 10 <sup>8</sup> | 3,563       | 310,840    | 787                      | 44,554,983 |
|    |         | 4,175       | 540        | 646                      | 37,206   | 5,111       | 417,255    | 798                      | 2.88 x 10 <sup>8</sup> | 3,612       | 306,666    | 766                      | 43,956,693 |
|    |         | 4,834       | 621        | 642                      | 42,786.9 | 5,273       | 435,674    | 808                      | 3.01 x 10 <sup>8</sup> | 3,554       | 314,242    | 798                      | 45,042,616 |
| 3  | C       | 5,125       | 612        | 597                      | 42,166.8 | 5,412       | 385,789    | 697                      | 2.65 x 10 <sup>8</sup> | 3,798       | 282,283    | 670                      | 40,461,698 |
|    |         | 5,175       | 625        | 604                      | 43,062.5 | 5,466       | 383,298    | 689                      | 2.65 x 10 <sup>8</sup> | 3,908       | 276,000    | 637                      | 39,561,109 |
|    |         | 5,164       | 616        | 596                      | 42,442.5 | 5,533       | 382,037    | 675                      | 2.64 x 10 <sup>8</sup> | 3,807       | 279,756    | 662                      | 40,099,485 |

*Prod = 24 hours Production in tons; C<sub>P</sub> = Specific heat, Kcal/kg; Total fuel = Total fuel consumed during the 24 hours of production, tonnes.*

**Table 2.**  
Calculated specific heat consumption and cost for the different fuel.

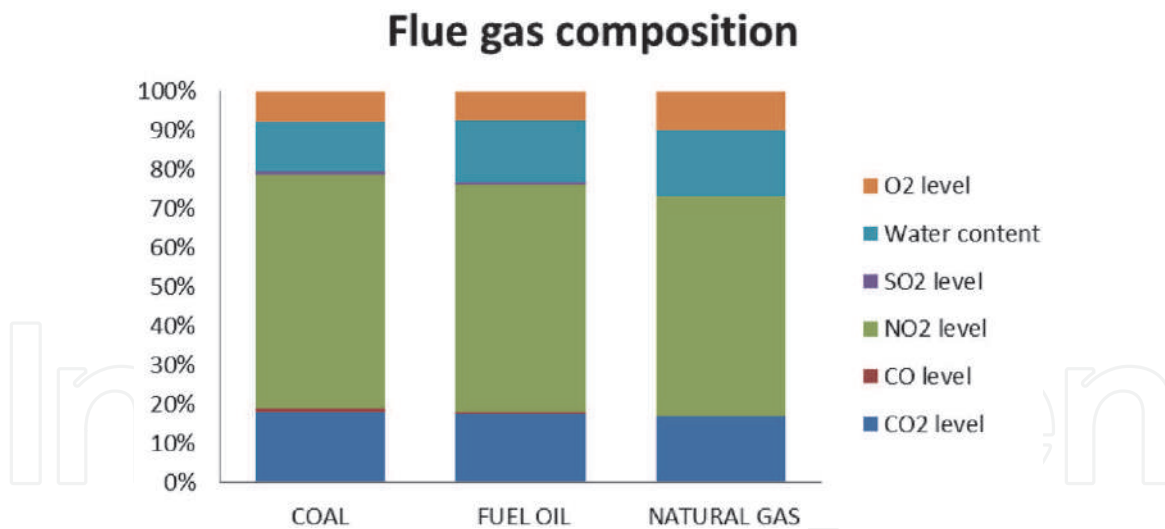


**Figure 1.**  
 Flue gas from Coal, Fuel oil, and Natural gas from gas analyses.

consumption of coal was less compared to that of fuel oil and natural gas (**Table 2**). This indicates that coal, as a good source of energy for firing in the clinker considering its high calorific value. On the other hand, the cost analysis revealed coal as the cheapest energy used by these cement companies as shown in **Table 2**, that is, 1 m<sup>3</sup> of coal was consumed at \$103.766. For natural gas, 1 m<sup>3</sup> of it was consumed at \$9.747 while 1 m<sup>3</sup> of LPFO was consumed at \$586.8513.

Natural gas is the most readily available, and highly economical source of energy in use for the production of cement, compared to coal and fuel oil. Related results were reported by Ohunakin et al., [3] for Energy and Cost Analysis of Cement Production Using the Wet and Dry Processes in Nigeria. Based on the flue gases produced from these three sources of energy at Dangote cement (**Table 3**), Sulphur oxides emissions are relatively higher in coal and fuel oil than in natural gas. For carbon monoxide emission, this is high in coal followed by fuel oil while it is low in natural gas. Nitrogen oxide emissions are high in coal and fuel oil compared to natural gas. Also, Carbon Dioxide emission is high in coal and fuel oil compared to natural gas. In a similar study, Worrell et al., [26] report that fuels like coal and coke contribute to an increase in specific carbon dioxide emissions. Similarly, the Oxygen content is high in natural gas compared to coal and fuel oil. Based on the flue gases, natural gas presents itself as the most efficient and the most environmentally friendly source of energy.

| DANGOTE          | FLUE GAS (%) (From Gas Analyzer) |          |             |
|------------------|----------------------------------|----------|-------------|
| Compound         | Coal                             | Fuel Oil | Natural Gas |
| CO <sub>2</sub>  | 18.01                            | 17.73    | 17.02       |
| CO               | 0.89                             | 0.10     | 0.002       |
| H <sub>2</sub> O | 12.80                            | 15.51    | 16.71       |
| NO <sub>2</sub>  | 59.78                            | 58.01    | 55.85       |
| SO <sub>2</sub>  | 0.82                             | 0.92     | 0.05        |
| CH <sub>4</sub>  | 0.00                             | 0.00     | 0.00        |
| O <sub>2</sub>   | 7.70                             | 7.67     | 9.90        |

**Table 3.**  
 Comparison of flue gas from coal, fuel oil, and natural gas.

## **5. Conclusion**

Although coal gave a cheaper consumption cost compared to fuel oil, for the production of cement, as expected, which could be used as an immediate substitute for natural gas, if peradventure its unavailability arises. Nevertheless, the environmental issues presented from its use as an energy source cannot be ignored. The LPFO (fuel oil) is quite expensive and would unavoidable impact on the cost of the final product. Benchmarking these three factories against each other, the cheapest energy consumption cost per ton production of cement was from Factory B while Factory A was the most expensive – for all three energy sources under investigation. From the analysis of the work, natural gas is one of the fossil fuels used in the production of cement. It is the cheapest amongst the three-fuel used in the production of cement and readily available. Also, natural gas emits lesser greenhouse gases to the environment, thereby lowering its effect on plant and animal health. Coal which is a close substitute is unavailable due to the closing down of Nigeria's coal mine and it poses too much threat to the environment and the health of plants and animals. Fuel oil is also available but as of now it is the most expensive fuel used in Nigerian cement industries and it also poses a high threat to the environment and life.

## **6. Recommendations**

Energy sources have a direct impact on the market price of cement, the environment, and human health. Natural gas is an available energy source in Nigeria, and more economical and environmentally friendly compared to coal and fuel oil. It is therefore recommended - to cut down energy costs, guarantee power supply to the power plant, and minimize the emission of threats caused by cement industries to the environment. Factory B was most energy-efficient and a closer understanding of their process should be considered by Factory A and C. The unit cost of fuel oil component, the commonly used energy source in cement production in Nigeria is very high, over \$15 as against \$6 in China [3]. This is responsible for the high cost of cement in Nigeria. Thus, the need for an energy-efficient production process is recommended.

### **Conflict of interest**

There is no conflict of interest associated with this work.

IntechOpen

## Author details

Oluwafemi M. Fadayini<sup>1\*</sup>, Clement Madu<sup>1</sup>, Taiwo T. Oshin<sup>2</sup>,  
Adekunle A. Obisanya<sup>3</sup>, Gloria O. Ajiboye<sup>2</sup>, Tajudeen O. Ipaye<sup>3</sup>, Taiwo O. Rabi<sup>4</sup>,  
Joseph T. Akintola<sup>1</sup>, Shola J. Ajayi<sup>1</sup> and Nkechi A. Kingsley<sup>1</sup>

1 Department of Chemical Engineering, Lagos State Polytechnic, Ikorodu, Lagos, Nigeria

2 Department of Chemical Science, School of Pure and Applied Sciences, Lagos State Polytechnic, Ikorodu, Nigeria

3 Department of Chemical Engineering, Yaba College of Technology, Yaba, Lagos, Nigeria

4 Department of Civil Engineering, Lagos State Polytechnic, Ikorodu, Lagos, Nigeria

5 Department of Mechanical Engineering, Lagos State Polytechnic, Ikorodu, Lagos, Nigeria

\*Address all correspondence to: [olufeday@gmail.com](mailto:olufeday@gmail.com);  
[fadayini.o@mylaspotech.edu.ng](mailto:fadayini.o@mylaspotech.edu.ng)

## IntechOpen

© 2021 The Author(s). Licensee IntechOpen. This chapter is distributed under the terms of the Creative Commons Attribution License (<http://creativecommons.org/licenses/by/3.0>), which permits unrestricted use, distribution, and reproduction in any medium, provided the original work is properly cited. 

## References

- [1] N. A. Madlool, R. Saidur, M. S. Hossain, and N. A. Rahim, "A critical review on energy use and savings in the cement industries," *Renew. Sustain. Energy Rev.*, vol. 15, no. 4, pp. 2042–2060, 2011, Accessed: Nov. 08, 2020. [Online]. Available: <https://ideas.repec.org/a/eee/rensus/v15y2011i4p2042-2060.html>.
- [2] J. P. John, "Parametric Studies of Cement Production Processes," *J. Energy*, vol. 2020, 2020, doi: 10.1155/2020/4289043.
- [3] O. S. Ohunakin, O. R. Leramo, O. A. Abidakun, M. K. Odunfa, and O. B. Bafuwa, "Energy and Cost Analysis of Cement Production Using the Wet and Dry Processes in Nigeria," *Energy Power Eng.*, vol. 05, no. 09, pp. 537–550, 2013, doi: 10.4236/epe.2013.59059.
- [4] C. Galitsky and L. Price, "Opportunities for Improving Energy Efficiency, Reducing Pollution and Increasing Economic Output in Chinese Cement Kilns," *ACEEE 2007 Summer Study Energy Effic. Ind.*, pp. 1–12, 2007.
- [5] P. Oladunjoye, "Nigeria: Cement Production And Survival of the Construction Industry - allAfrica.com," *Daily Independent*, Jun. 04, 2011. <https://allafrica.com/stories/201106061192.html> (accessed Nov. 08, 2020).
- [6] W. T. Choate, "Energy and Emission Reduction Opportunities for the Cement Industry," *Energy Effic. Renew. Energy*, pp. 1–41, 2003.
- [7] M. Schneider, M. Romer, M. Tschudin, and H. Bolio, "Sustainable cement production-present and future," *Cement and Concrete Research*, vol. 41, no. 7. Elsevier Ltd, pp. 642–650, 2011, doi: 10.1016/j.cemconres.2011.03.019.
- [8] M. G. Rasul, W. Widiyanto, and B. Mohanty, "Assessment of the thermal performance and energy conservation opportunities of a cement industry in Indonesia," *Appl. Therm. Eng.*, vol. 25, no. 17–18, pp. 2950–2965, 2005, doi: 10.1016/j.applthermaleng.2005.03.003.
- [9] P. A. Alsop, *The Cement Plant Operations Handbook*, Third. Portsmouth: David Hargreaves, International Cement Review, 2001.
- [10] Portland Cement Association, "Report on Sustainable Manufacturing," 2006. [Online]. Available: [www.cement.org/smreport11](http://www.cement.org/smreport11).
- [11] R. G. Bond and C. P. Straub, *CRC handbook of environmental control*, vol. 4. Cleveland: CRC Press, 1974.
- [12] WSP Parson Brinkerhoff and DNV GL, "Industrial Decarbonisation & Energy Efficiency Roadmaps to 2050: Cement," 2015.
- [13] Engin & V. Ari, Energy auditing and recovery for dry type cement rotary kiln systems. *Energy Conversion and Management*, 46, 2005
- [14] D. Gielen, & P. Taylor, Indicators for industrial energy efficiency in India. *Energy*, 34, 2009
- [15] C. Sheinbaum, & I. Ozawa, Energy use and CO<sub>2</sub> emissions for Mexico's cement industry. *Energy* 23(9), 725–32, 1998
- [16] J. Soares, & M. Tolmasquim, Energy efficiency and reduction of CO<sub>2</sub> emissions through 2015. *Mitigation and Adaptation Strategies for Global Change*, 5, 297–318, 2000
- [17] E. Worrell, & N. Martin, Potentials for energy efficiency improvement in the US cement industry. *Energy*, 25, 189–214, 2000
- [18] IEA (2004), *Coal Information 2004*, OECD Publishing, Paris, <https://doi.org/10.1787/coal-2004-en>.

[19] Olayinka S. Ohunakin, Oluwafemi R. Leramo, Olatunde A. Abidakun, Moradeyo K. Odunfa, Oluwafemi B. Bafuwa, 2013, "Energy and Cost Analysis of Cement Production Using the Wet and Dry Processes in Nigeria", *Energy and Power Engineering*, 2013, 5, 537-550

[20] N. A. Madlool, R. Saidura, M. S. Hossaina, and N. A. Madloo Rahim, "A Critical Review on Energy Use and Savings in the Cement Industries," *Renewable and energy Reviews*, Vol. 15, No. 4, 2011, pp. 2042-20 <http://dx.doi.org/10.1016/j.rser.2011.01.005>

[21] <http://www.nigerianbestforum.com/blog/?p=59984>

[22] A. Avami and S. Sattar, "Energy Conservation Opportunities: Cement Industries in Iran," *International Journal of Energy*, Vol. 3, 2007, pp. 101-110.

[23] [globalpetrolprices.com](https://www.globalpetrolprices.com/Nigeria/diesel_prices/). (2021, January 15). *Nigeria Diesel Prices, liter, 11 - Jan - 2021*. Retrieved from [GlobalPetrolPrices.com](https://www.globalpetrolprices.com/Nigeria/diesel_prices/): [https://www.globalpetrolprices.com/Nigeria/diesel\\_prices/](https://www.globalpetrolprices.com/Nigeria/diesel_prices/)

[24] Market Insider. (2021, January 15). *Natural Gas (Henry Hub)*. Retrieved from Market Insider: <https://markets.businessinsider.com/commodities/natural-gas-price>

[25] Market Insider. (2021, January 15). *Coal*. Retrieved from Market Insider: <https://markets.businessinsider.com/commodities/coal-price>

[26] Worrell, K. Kermeli, & C. Galitsky, *Energy Efficiency Improvement and Cost Saving Opportunities for Cement Making*. Utrecht, United states ENERGY STAR, 2013